COPPE
Instituto Alberto Luiz Coimbra de Pós-Graduação e Pesquisa de Engenharia
UFRJ

VELOCITY FREE FEEDBACK CONTROL VIA VARIABLE HIGH GAIN OBSERVER OF PROSTHETIC LEG TESTING ROBOTS: A TRADE-OFF BETWEEN TRACKING ACCURACY AND CONTROL NOISE

Ignácio de Azambuja Midosi Ricart

Dissertação de Mestrado apresentada ao Programa de Pós-graduação em Engenharia Elétrica, COPPE, da Universidade Federal do Rio de Janeiro, como parte dos requisitos necessários à obtenção do título de Mestre em Engenharia Elétrica.

Orientador: Alessandro Jacoud Peixoto

Rio de Janeiro
Março de 2020

VELOCITY FREE FEEDBACK CONTROL VIA VARIABLE HIGH GAIN OBSERVER OF PROSTHETIC LEG TESTING ROBOTS: A TRADE-OFF BETWEEN TRACKING ACCURACY AND CONTROL NOISE

Ignácio de Azambuja Midosi Ricart

DISSERTAÇÃO SUBMETIDA AO CORPO DOCENTE DO INSTITUTO ALBERTO LUIZ COIMBRA DE PÓS-GRADUAÇÃO E PESQUISA DE ENGENHARIA (COPPE) DA UNIVERSIDADE FEDERAL DO RIO DE JANEIRO COMO PARTE DOS REQUISITOS NECESSÁRIOS PARA A OBTENÇÃO DO GRAU DE MESTRE EM CIÊNCIAS EM ENGENHARIA ELÉTRICA.

Orientador: Alessandro Jacoud Peixoto

Aprovada por: Prof. Eduardo Vieira Leão Nunes, D.Sc.

Prof. Carlos Julio Tierra Criollo, D.Sc.

Prof. Alessandro Jacoud Peixoto, D.Sc.

RIO DE JANEIRO, RJ – BRASIL
MARÇO DE 2020

Ricart, Ignácio de Azambuja Midosi

Velocity free Feedback Control via Variable High Gain Observer of Prosthetic Leg Testing Robots: A Trade-off Between Tracking Accuracy and Control Noise/Ignácio de Azambuja Midosi Ricart. – Rio de Janeiro: UFRJ/COPPE, 2020.

XVI, 93 p.: il.; 29, 7cm.

Orientador: Alessandro Jacoud Peixoto

Dissertação (mestrado) – UFRJ/COPPE/Programa de Engenharia Elétrica, 2020.

Referências Bibliográficas: p. 87 – 93.

1. Prosthesis Test Robot. 2. HGO. 3. PID. I. Peixoto, Alessandro Jacoud. II. Universidade Federal do Rio de Janeiro, COPPE, Programa de Engenharia Elétrica. III. Título.

"Yesterday is history, tomorrow is
a mystery, and today is a gift...
that's why they call it present." -
Master Oogway

Agradecimentos

Gostaria de agradecer ao apoio incondicional de meus pais, e à paciência do meu orientador por ter encarado essa jornada comigo. João, Alex, Halfeld, Matheus, amigos do Lead, amigos do Labcon, Dudu Baleia. Obrigado a todos que estiveram presentes em minha vida, pois me ajudaram a chegar onde estou.

Resumo da Dissertação apresentada à COPPE/UFRJ como parte dos requisitos necessários para a obtenção do grau de Mestre em Ciências (M.Sc.)

CONTROLE COM REALIMENTAÇÃO DE SAÍDA VIA OBSERVADOR DE ALTO GANHO VARIÁVEL DE ROBÔ PARA TESTE DE PRÓTESES: UMA RELAÇÃO DE COMPROMISSO ENTRE ACURÁCIA DE RASTREAMENTO E RUÍDO NO SINAL DE CONTROLE

Ignácio de Azambuja Midosi Ricart

Março/2020

Orientador: Alessandro Jacoud Peixoto

Programa: Engenharia Elétrica

Este trabalho trata da modelagem e implementação de um controle e um observador em um robô de testes para próteses simulado composto por quatro juntas: deslocamento vertical do quadril, movimento de extensão e flexão do quadril, extensão e flexão do joelho e movimento de dorsiflexão e plantarflexão do tornozelo. O modelo dinâmico completo é apresentado e um modelo simplificado é utilizado na avaliação do controlador/observador. Inicialmente, um controlador com realimentação total de estados é implementado utilizando torque computado e PID, após isso um observador the alto ganho (HGO) é projetado para estimar os estados do dispositivo. Aqui é proposto uma implementação de HGO para estimar a velocidade das juntas através de um observador com alto ganho variante no tempo sintetizado a partir de sinais medidos e desenolvido para reduzir a quantidade de ruído presente no sinal de controle dos motores e manter um erro de rastreamento aceitável. Simulações são realizadas para avaliar o desempenho entre utilizar observador com alto ganho fixo ou o variável proposto. A análise de robustez do controle em malha fechada é realizada através de simulações numéricas considerando a presença de ruído e incerteza paramétrica.

Abstract of Dissertation presented to COPPE/UFRJ as a partial fulfillment of the requirements for the degree of Master of Science (M.Sc.)

VELOCITY FREE FEEDBACK CONTROL VIA VARIABLE HIGH GAIN OBSERVER OF PROSTHETIC LEG TESTING ROBOTS: A TRADE-OFF BETWEEN TRACKING ACCURACY AND CONTROL NOISE

Ignácio de Azambuja Midosi Ricart

March/2020

Advisor: Alessandro Jacoud Peixoto

Department: Electrical Engineering

This work addresses the modeling, state estimation, and control of a robot/prosthesis system with four joints: vertical hip prismatic joint, thigh, knee, and ankle rotational joints. The full dynamic model is provided, and a simplified version is considered for control/estimator evaluation. Initially, a full-state feedback scheme is implemented using computed torque plus a PID controller, and then a high gain observer is designed to estimate the system states. We propose the implementation of a high gain observer (HGO) to estimate the prosthesis joint velocities with a time-varying HGO gain synthesized from measurable signals designed to reduce the amount of noise in the control effort while keeping an acceptable tracking error transient performance. Simulations are conducted to evaluate the performance using fixed HGO gain in comparison with the proposed variable HGO approach, in the presence of noise and parametric uncertainties.

Contents

List of Figures

List of Tables

Chapter 1

Introduction

This chapter shows relevant information found in the literature regarding the human gait cycle, prosthesis technologies, control architectures, and observers for nonlinear systems. Initially, phases and periods that form one gait cycle are presented, then prostheses and their types are shown along with their pros and cons. As some kinds of prosthesis require controllers, attention is also given to describing to the reader the control architectures and laws implemented according to the literature, as well as the prosthetic velocity and ground force reaction estimations and state observer's techniques applied to nonlinear systems in general. This chapter ends with the author's motivation to develop this work and the main objective of this Dissertation.

1.1 Human Gait Cycle

To better understand prosthesis usage and all the upcoming content, it is essential to understand the main task that a prosthesis must perform: the walk/gait. Having this knowledge, one may design hardware and control algorithms taking into consideration the mechanical characteristics and details of the gait.

Walking is a natural way of moving our body from one place to another by performing a sequence of movements from our limbs [1]. This series of actions is also known as gait and has a customary rate of 80m/min. There are three main categorizations: whether there is contact with the ground or not, the number of parts touching the ground, or the events' functional meaning in a gait cycle.

When performing a gait cycle, one may refer to it as stride, which is a composition of two steps. In the gait cycle, there is a period in which the foot is on the ground, called stance phase, and another where the foot is in the air for limb advancement, also known as swing phase. Both lower limbs alternate their roles between stance and swing. Table 1.1 (obtained from [1]) shows the contact duration from each of these periods within a gait, where the stance accounts for 60% of the gait cycle, while 40% is the swing [1].

Floor Contact Periods		
Stance		60%
Initial Double Stance	10%	
Single Limb Support	40%	
Terminal Double Stance	10%	
Swing		40%

Table 1.1: Duration from each period during a gait cycle. This values change according to the person's speed. Walking faster lengthens single stance and shortens the two double stance intervals.

Floor Contact Periods			
Stance			50%
Weight Acceptance		10%	
Initial Contact	0-2%		
Loading Response	0-10%		
Single Limb Support		40%	
Mid Stance	10-30%		
Terminal Stance	30-50%		
Pre-Swing + Swing			50%
Limb Advancement		50%	
Pre-Swing	50-60%		
Initial Swing	50-73%		
Mid Swing	73-87%		
Terminal Swing	87-100%		

Table 1.2: Duration from each period during a gait cycle according to functional phases of a gait cycle

Another way to categorize the gait phases is by identifying the number of parts touching the ground. In this approach, the stance involves periods in which the two feet are on the ground (start and end of stance phase) and the part in which there is only one foot in contact with the ground (single-limb support or single stance) [1]. While one limb is in the single-limb support, the other is in the swing phase. Table 1.1 (obtained from [1]) illustrates the duration from each period in a gait cycle.

The other classification separates into eight functional phases from the gait cycle so that the movement performs three basic tasks: weight acceptance, single limb support, and limb advancement [1].

Weight acceptance involves the initial contact and the loading response phases. This task is responsible for shock absorption, initial limb stabilization, and preservation of the movement progression.

There are mid-stance and terminal stance in the single limb support task. During this task, one limb is responsible for lifting the whole body weight. The progression over the stationary foot along with leg and trunk stabilization happens during mid-stance.

Then, the terminal stance phase keeps the movement progression of the body beyond the supporting foot.

Finally, limb advancement encompasses the entire swing phase (pre, initial, mid, and terminal swing). There is a preparatory phase that begins with the initial contact from the opposite limb (contralateral foot) and ends with ipsilateral toe-off called pre-swing. The ankle plantarflexion in this phase generates about 85% of the total energy generated during the gait cycle [2].

Amputees can only perform the pre-swing phase properly when using an active prosthesis, as this requires net power injection. The literature describes the ankle joint requirements to complete this phase adequately [1], which allows the swing phase to use the whole body momentum. A direct consequence of a proper pre-swing stage is the increase in gait efficiency, as the entire leg swing relies on a passive movement of letting the leg free to move.

The initial swing begins when lifting the foot of the floor (via knee flexion) and ends when the ipsilateral foot is opposite to the stance foot. Then, the mid-swing ends when the limb is forward, and the tibia is vertical. The terminal swing ends with the leg set for the stance phase, and then the foot strikes the floor.

All these phases compose one gait cycle, which is efficiently performed by healthy bodies unconsciously. The human body uses minimal joint movements to optimize the walking process and expand the minimum metabolic energy as possible.

There are studies to obtain this gait data using motion-capture systems [3][4]. With this information, it is possible to evaluate human gait, assess, and treat individuals with conditions affecting their ability to walk, improve a high-performance athlete's technique.

According to [5], the root-mean-square (RMS) standard deviation over the stride is 1.5, 1.9, and 1.8 degrees in the ankle, knee, and at the hip, respectively. This data was obtained after nine repeat trials of the same subject over three separate days. This data is necessary in this dissertation to set "acceptable" RMS tracking errors, as these values are usually hard to obtain in the literature. Despite performing tests with few subjects, these results are used to evaluate prosthesis tracking performance [6][7].

A study made by [3] with 28 subjects running at three different speeds, gives some useful information to this dissertation about desired contour conditions: (i) 150 Hz sample rate for kinematics acquisition, (ii) raw marker-trajectory data are filtered using a fourth-order, low-pass Butterworth filter with a cut-off frequency of 10 Hz. Then the maximum angle from each joint (hip, knee, and ankle) movement (flexion/extension or plantarflexion/dorsiflexion) is displayed in terms of the mean value and the standard deviation. The lowest standard deviation is 2.49 degrees in the maximum ankle dorsiflexion angle. With this information, it is possible to define the desired performance regarding tracking and estimation implemented in the prosthesis. Other studies use root-mean-square-error to evaluate algorithms and techniques performance in gait analysis [4] [8] [9]. The joints

hip and knee extension/flexion obtained, and ankle plantarflexion/dorsiflexion, show an average standard deviation of 12.9, 11.5, and 7.2 degrees, respectively. This data was obtained with more than 100 subjects and using 150Hz acquisition rate. This information may be useful for validating the reference signal and defining the desired performance.

1.2 Prosthesis Technologies

Due to vascular disease (54%), including diabetes and peripheral arterial disease, trauma (45%), cancer (less than 2%), and several other reasons [10], lower limb amputations are necessary. Nearly 2 million people are living with limb loss in the United States, and there are more than 30 million worldwide [11]. Using prosthesis may be a way to allow them to maintain their activities of daily livings (ADLs) and have the mobility partially/wholly restored.

The lower limb amputation could be at the foot, including toes or only partially, at the ankle (ankle disarticulation), below the knee (transtibial), at the patella (knee disarticulation), above the knee (transfemoral) or at the hip (hip disarticulation). Depending on which residual limb remains, mobility could be restored by using an adequate technical solution.

The solution could be a prosthetic foot or, in a worst-case scenario, the combination of prosthetic foot/ankle, shin/pylon, prosthetic knee, and a socket interfacing the residual limb with the prosthetic leg. In some cases, it is also necessary a hip replacement beyond the whole prosthetic leg.

There are three categories for currently available lower-limb prostheses: purely passive, semi-active, and active [12].

Purely passive prosthesis relies on locking mechanisms and hydraulic/pneumatic cylinders with static damping parameters to enable a softer movement and contact with the ground. They have a robust design and low up-front cost. However, they cannot generate net power and don't adapt autonomously to the user's changing needs. Due to their simplicity, they also don't provide sensory feedback regarding states of the limb and the device [13].

Amputees using passive prostheses expend up to 60% more metabolic energy than healthy subjects [14] and three times more hip power/torque in the affected side, presumably due to the lack of powered joints [15]. The passive mechanism works limiting knee angular velocity in the early and the late swing phase [16] and also during weight acceptance.

Semi-active prostheses manipulate the joint position by modifying the energy dissipation properties according to the estimated current gait cycle and velocity. It changes the damping effect parameter via hydraulic/pneumatic cylinders according to the device's sensors, such as knee flexion and extension angle or accelerometer [17] [18] [19], improv-

ing the knee stability and adapting to different walking speeds [20]. This system requires the use of microprocessors due to signal processing algorithms and the amount of data gathered by sensors.

When realizing more complex tasks such as walking uphill, it is crucial to generate net power in prosthetic joints through DC electrical motors, pneumatic or hydraulic actuators [21], [22], [23]. The active prosthesis provides a way to accomplish these complex tasks and also enhances performance. This improvement occurs due to a net power injection in the ankle joint during the pre-swing phase; this allows a more efficient movement progression and decreases the energy cost of walking and gait asymmetries.

The work in [2] presents the relevance of the ankle in a gait cycle and displays the prosthetic ankle evolution, from passive to an active prosthesis. The author evaluates the metabolic costs and biomechanical properties of the ankle prosthesis. Later he shows that, by the time, pneumatically and electrically driven devices provided from 100 to 200 Nm torque output and established an ankle range of motion of 30 degrees. The work then concludes that active components are necessary due to high ankle moments in the late stance phase and enhance the patient's gait pattern while also decreasing the metabolic energy expenditure.

Studies made in [2] and [23] about prosthesis technology evolution compares the pros and cons. They point out that the main concerns regarding prostheses are safety and seamless integration of human-device.

1.3 Prosthesis Controllers

Embedded systems are the core components under active prosthesis development. They enable the amputee to perform the required ADLs via control algorithms that send information to the actuators based on measured data from the user, device, or environment. This section focus on ways to categorize the controllers implemented by the embedded computers for a lower-limb prosthesis.

One way to categorize control is based on hierarchy [24][13], which resembles the structure and functionality of the human central nervous systems. The controller architecture combines three layers: High, mid, and low level.

At a high level, the detection of locomotive intent occurs based on signals from the user, device, and the environment. The mid-level controller translates the user's motion intention to a desired prosthesis' state, which is used by the low-level layer to track this desired state. It implements a control law that minimizes the error between the current and the desired joint states.

The high-level control is responsible for detecting an activity intention, ideally without the user's conscious input, and switching between mid-level controllers to perform a task. When executing cyclical/repetitive tasks, there are two ways to define/create the criteria:

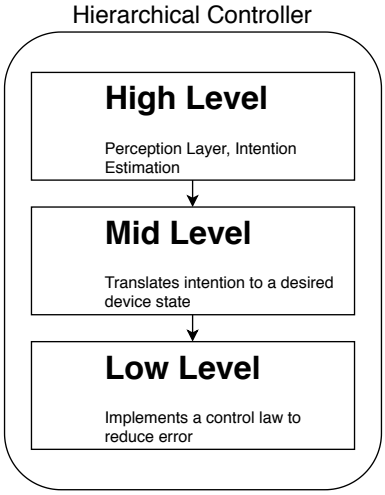

Figure 1.1: Hierarchical Control Framework.

heuristic or automated. The heuristic approach requires hard-coded definitions of possible gait modes and a set of rules to indicate gait mode transition. (i) It initially detects the current system's states, (ii) checks the possible gait mode transitions, (iii) evaluate the rules set with the data acquired from user, device, and environment, (iv) and then changes the current gait mode triggering mid-level controllers. The main methods used to identify mode transitions heuristically are Finite State Machines (FSM)[25][26][27] and decision trees[28]. These methods are simple to implement; however, defining the rules may be tricky depending on the number of desired modes.

The automated approach is a way to avoid setting/defining manually the rules and possible gait modes described in steps (ii) and (iii). The classifiers used in prosthesis are Naive Bayes, Linear or Quadratic Discriminant Analysis, Gaussian Mixture Models, Support Vector Machine, Dynamic Bayesian Networks, and Artificial Neural Networks [13]. The rules used to trigger transitions could be based on foot angle change, indicating a transition from level walking to stair ascent, or differences in ground reaction forces, indicating a shift from walking to running. In addition to the device's states, one may also use physiological signals to compose the rules. This data from surface electromyogram (EMG) could be used alone or combined with electromechanical states from the prosthesis.

The drawback of automated rule-based is the effort of an adequately classified training data and the general necessity of the user's training data, which may be difficult or even impossible to obtain.

The approaches so far do not use the physiological signal to control the prosthesis directly. They only serve as a way to trigger gait mode transitions. The direct volitional control allows the user to consciously modulate the input signal to the device, which is useful on non-cyclical or irregular tasks such as walking in a crowd or on rough terrain or execute non-locomotive tasks (e.g., leg repositioning). This high-level control may be

confused with the mid-layer, but the main difference is that in this top layer, the output is a mode/user intention, the lowest layer output is an error value between the desired and current states.

Some critical aspects of the high-level controller are classification latency and misclassification. Sometimes this layer may only trigger the mid-level controller on initial gait phases, and this may happen during the transition from walking and descending a stair, which could result in an accident. When developing this controller, it is important to take into account the time necessary to perceive a gait mode transition. Another problem is the misclassification. However, this situation may be handled to the mid-level layer, which will somehow indicate that the states are not matching with the desired intention.

The second controller layer is responsible for converting an estimated locomotive intent to a desired device state for the low-level controller to track. As the low-level controller handles one joint actuation, the mid-layer is also responsible for coordinating the control between multiple actuated joints. Sometimes misclassification from the high-level controller may occur, so it is essential also to indicate when the errors are with a different profile than the expected.

In this layer, the control implementations may depend or not on gait information. Thus, they are categorized as non-phase or phase-based. Complementary Limb Motion Estimation (CLME) is one approach that does not depend on gait information. It infers the intended motion based on the residual limb movements, such as those from arms, upper body, and the residual leg limb. It then maps this to a reference trajectory, which is used by the low-level controller.

Among the phase-based techniques, the Finite State Controller (FSC) is the most used. It decomposes the gait cycle into an arbitrary number of distinct phases, such as the ones described in Section 1.1 [29][30]. The information used to differentiate between aspects usually is based on foot contact event, and joint velocities [13], but many others could be deployed. Each phase has its control parameters and objectives (e.g., track position or impedance). In most of the referenced FSCs implementations, these parameters are set heuristically and user-specific, meaning that each patient should pass through experiments to fine-tune its device [13]. Thankfully, techniques to overcome this step have been proposed by automatically setting these parameters[30].

Another approach, called Normalized Trajectory Control, involves adapting a nonspecific joint trajectory to match the user's pace and anthropomorphic characteristics. This trajectory is the result of previously recorded paths from many human gait cycles. It may also be referred to as "dynamic pace control" and uses Fast-Fourier Transform (FFT) coefficients to fit the trajectory. The output from this control is usually a desired joint position.

The echo control is also a phase-based controller. This method uses a master-slave principle, in which the abled leg is a master that has to be followed by the slave (prosthetic

leg). This control assumes movement symmetry, and sometimes a time delay is necessary to reproduce the abled leg motion. When executing a sit-to-stand sequence, the slave must follow the master instantly. When the system is set to some other modes (e.g., as "walk"), the slave must perform a delayed motion from the master's. Some drawbacks of this method are that the slave also reproduces undesired movements from the master. The echo control is also a problem for the high-level control because it can only change the gait mode at the beginning of the stride.

All the algorithms implemented by the mid-level controller output a device state, which has to be tracked by the low-level controller. This state may be comprised of a combination of joint position, velocities, and torques. Controlling the position or speed of the device shows great performance when the desired trajectory and perturbations/interaction forces are well characterized. Torque control is possible when the output mechanical impedance of the actuator is low relative to the load. This method is useful when handling interaction forces, which causes a more natural behavior between the prosthesis and the user.

Most of the works regarding prosthesis use impedance control for knee and ankle joints, while using position control for the hip joint. When using FSC in a mid-level controller, one may implement different low-level controls in the same joint, depending on the gait phase [29].

Another way to categorize control is to divide how the embedded microprocessor interacts with the user's will (in the form of neural signal) [23]. This approach suggests two control classes: Computationally intrinsic control (CIC) and Extrinsic interactive control (IEC).

CIC stands for a microprocessor system with its sensors and actuators and not interacting with the amputee directly. Therefore, any inconsistency between the desired user movement and the prosthesis may lead to a fall of something worst. Devices implementing CIC are then responsible for generating the desired gait pattern and also identify the current user's state, such as walking, running, or climbing upstairs to provide safety during ADLs. [23][31][6]

Some examples of computationally intrinsic control are muscle reflex control, finite state machine impedance control [21][31][25], phase plane control, echo control and complementary limb motion estimation [32].

IEC relies on human efferent signal measurements such as muscle activities acquired via EMG sensors, pattern recognition systems, and cortical or peripheral nerve feedback. This control model should also provide feedback information to the brain via afferent communication (haptic).

Some examples of IEC are control based on residual joints, segments, or organs such as EMG or surface EMG based control, neuromuscular mechanism fusion, and agonist-antagonist myoneural interface signal control [33].

Researches from [23] also showed that most active and semi-active prostheses, by the time, implemented computationally intrinsic control. They rely on measurements mainly provided by rotary encoders, force sensors, and strain gauges. The actuators were mostly hydraulic valves, pneumatic pistons, or electromechanical actuators (DC motor).

1.4 Prosthetic Velocity and Ground Force Reaction Estimations

In general, numerical approaches for velocity estimations are implemented via state observers or derivative filters, like a lead filter. However, the noise attenuation is a well-known challenge in those cases. In this direction, state estimation using Kalman Filter, Sliding Mode Observer (SMO), and High-gain Observer (HGO) are promising approaches.

The Kalman Filter approaches consider output noise e have many works regarding prosthetic tracking performance. Researches from [6] and [9] designed Extended Kalman Filters (EKF) and Unscented Kalman Filters (UKF) to estimate joint position, velocities and ground reaction forces (GRF). These estimations are used in a test robot for prosthesis parameter identification and also for real prosthesis control. Later, [34] compared four robust model reference adaptive impedance (RMAI) observer/controllers. For this work, GRFs estimations were obtained via SMO, Adaptive observer, EKF, and UKF in the presence of parametric uncertainty (30%).

In the absence of measurement noise, a high-gain observer is known as a robust technique for estimating derivatives of the output signal, while achieving fast convergence [35]. The study of HGO in nonlinear feedback control started in the late 1980s with works from [36], [37], and [38]. [39] started one of the study schools, which then covered a broad class of nonlinear systems and obtained global results under global growth conditions. These investigations propose fixed HGO gains for state estimation in the presence of parametric error. However, no consideration of noise is made.

The HGO peaking phenomenon was initially showed in [40] and [41]. Later [42] brought attention to the fact that the peaking could cause a finite escape time. The proposed solution was to use a globally bounded function of the state estimates as control. This control saturates during the peaking phenomenon, and as this dynamic is faster than the plants, the actual observed stated would still be closer to its initial value. In [43], an adaptive output feedback controller for rigid robots using HGO was proposed. It was possible to recover the performance achieved under state feedback control asymptotically, while also overcoming the peaking phenomenon using the saturation on the torque inputs.

Output-feedback control strategies using HGOs [44] represent an important design class, in particular, the schemes based on time-varying techniques (HGO with variable

gain) [45], [46], [47] ,[48], [49]. In [50], [51], an output-feedback sliding-mode control design has been proposed for arbitrary relative degree uncertain systems, where the class of plants encompasses time-varying minimum-phase nonlinear plants, affine in control, transformable to a normal form and for which a norm state estimator can be implemented. The main objective in [50] was to use a dynamic observer gain in order to obtain global results without invoking global Lipschitz-like restrictions.

The problem of measurement noise is addressed by some works that also propose HGO variable gains. A work [52] showed that one might decrease steady-state estimation error using a high gain to attenuate the effects o modeling uncertainty. However, the error also has a component due to measurement noise, which is amplified when increasing the observer gain. One approach to overcome this trade-off constraint was to design a nonlinear gain structure with different gains during transient and steady-state response [53].

In [52], a switched observer gain technique was proposed. The idea is to use a high gain when the estimation error is mostly increasing the observation accuracy. However, it is susceptible to more significant measurement noise errors. When dealing with low output error, the gain switches to a smaller value to balance the error. The problem of measurement noise on a discretized system composed by controller and HGO has also already been addressed [54].

Despite this researches about the trade-off constraints, [55] confirmed that this sort of compromise does not exist when the main goal is the system tracking accuracy. The results were verified for linear systems; an analysis in nonlinear ones was left as future work.

1.5 Motivation

Moved by research conducted at Ohio State University regarding prosthesis [31], this work started as a way to implement in a simulated environment the dynamics and control of a device, which always was of great interest to the author, a prosthesis. The author used results by Dan Simon as a guideline through his research. By the time the solution was a three degree-of-freedom prosthesis test robot. This system is useful to evaluate and compare prosthesis prototypes because it has improved repeatability when compared to human trials, and embedding sensors is also easier than in human trials. This method may accelerate the development of new prosthesis concepts and control algorithms [56].

The test robot depicted in Figure 1.2 is composed of a prismatic joint emulating vertical hip displacement, a revolute joint serving as hip flexion/extension joint, and a transfemoral prosthesis attached to it [56]. In [56], a robust controller for motion tracking was developed and compared with a decoupled sliding mode controller. The control achieved a good tracking of hip vertical displacement (1.75 mm of root-mean-square-error) and hip

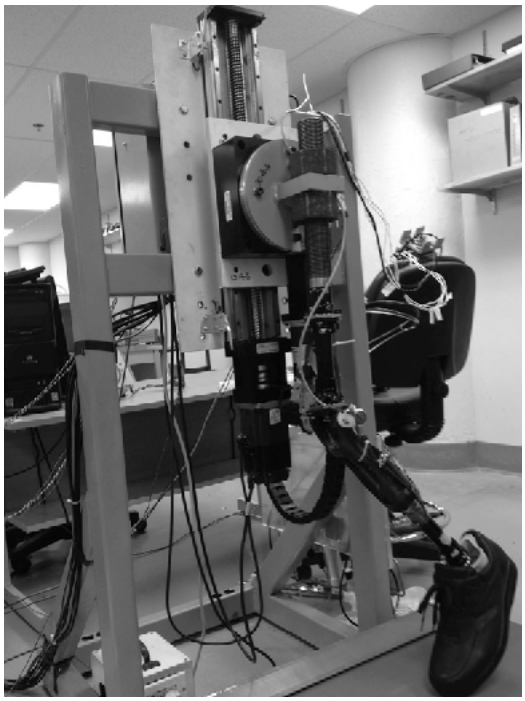

Figure 1.2: Motivational example.

Parameter	Description	Nominal value	Units
m_1	Mass of link 1	40.5969	kg
m_2	Mass of link 2	8.5731	kg
m_3	Mass of link 3	2.29	kg
l_2	Thigh length	0.425	m
l_3	Length of knee joint to bottom of shoe	0.527	m
c_2	Center of mass on thigh	0.09	m
c_3	Center of mass on shank	0.32	m
f	Sliding friction in link 1	83.33	N
b	Rotary actuator damping	9.75	N m s
I_{2z}	Rotary inertia of link 2	0.138	kg/m^2
I_{3z}	Rotary inertia of link 3	0.0618	kg/m^2
g	Acceleration of gravity	9.81	m/s^2

Figure 1.3: Test robot parameters used for simulations and experiments in Cleveland.

flexion/extension (2.6 deg of RMSE). Then, works regarding the position, velocity, and ground reaction force estimations were done considering a different number of sensors (from 4 to 2) [6][9]. In these works, the estimation converges to the true states before 50ms and shows an RMS estimation error of 0.003m, 0.002 rad, 0.003 rad, and 0.005 rad for hip, thigh, knee, and ankle joints respectively.

Later, in [7], they compared and tested two robust model reference adaptive impedance controllers for a three degrees-of-freedom (3DOF) powered prosthesis/test robot. The control magnitudes were similar to abled-bodied averaged hip force (-800 to 200 N), thigh torque (-50 to 100 Nm), and knee torque (-50 to 50 N.m) [5][57][58]. Figure 1.3 shows experimental parameters from [7].

A solution using a high gain observer is proposed in this work to simulate the test robot

and add a contribution to the research community. This designed observer gain deals with effort noise measurement while trying to assure an acceptable tracking performance. This method is an alternative to a Kalman Filter approach, which does not explicitly handles noise in the effort signal.

1.6 Objective

In this thesis, considering that a robot/prosthesis system has parametric uncertainties and angle measurement is subject to noise, a time-varying HGO design is proposed, similar to [50]. This variable gain approach is different from most of the existing techniques, where the HGO gain is updated either solving a Riccati equation [45][59][60] or via functions based on measurable signals and norm domination techniques [48], [59], [61] and [50].

While estimating in real-time the noise energy presented in the control effort, an adaptation law changes the observer gain to achieve an acceptable trade-off between control signal noise and tracking performance. It is important to note that, although global results are not pursued, the proposed technique is easily applicable to practical scenarios, given that bounds for the system states are known a priori.

Although the literature uses mainly impedance control in low-level control law, a proportional-integral-derivative (PID) conventional control with feedback linearization is developed in order to make a robotic prosthetic leg follow the desired walking pattern. The trajectory was obtained from human gait analysis and could be seen as a normalized trajectory control in the mid-level.

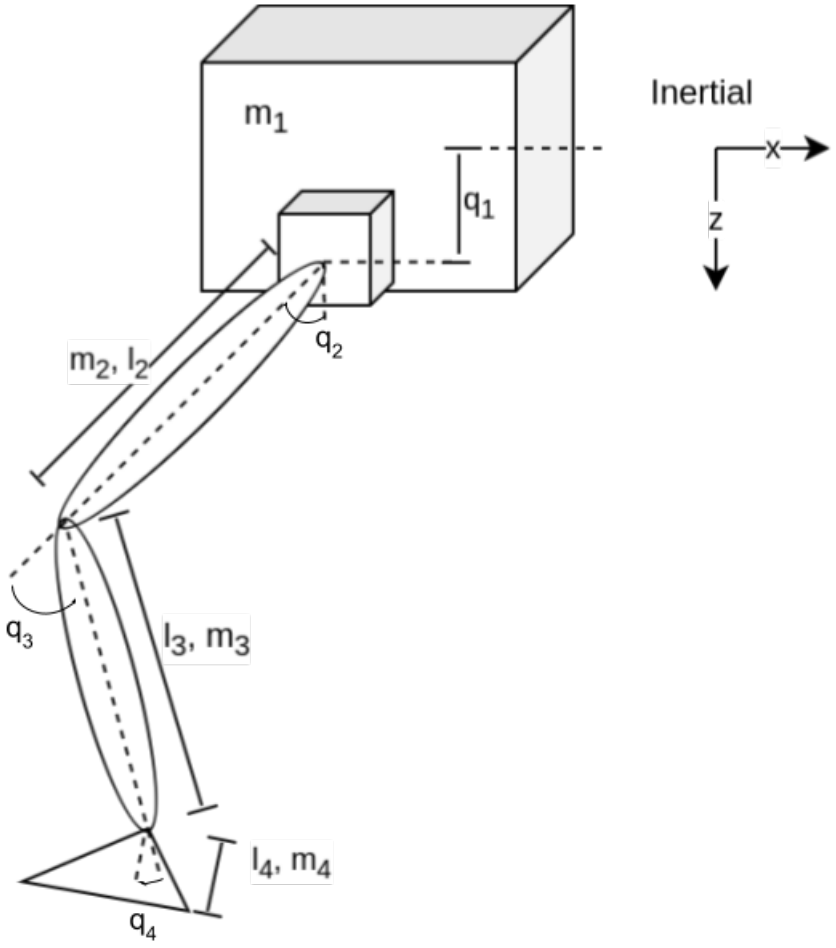

Figure 1.4: Coordinate frames used to represent the prosthesis model and calculate kinematics and dynamics along the sagittal plane.

The proposed approach is verified in a simulation environment with a 4-link robot/prosthesis system (PRRR), with parameters extracted from [31] and motion limited to the sagittal plane, as depicted in Fig. 1.4.

1.7 Contributions

Motivated by prosthetic technologies, this work tried to simulate a prosthetic robot dynamic in a closed-loop system considering the presence of parametric uncertainties and noise perturbation. Because of that, the important contributions presented in this thesis are:

1. A prosthesis simplified model developed and validated using Recursive Newton Euler and Lagrange;

2. A realistic tuning of PID controller for prosthetic control in the presence of parametric uncertainties and noise;

3. The main contribution is the design of a variable high gain observer, from a practical point of view, as a function of the tracking error and the amount of noise in the control effort. Leading to a publication [62].

1.8 Notation and Terminology

The 2-norm (Euclidean) of a vector x and the corresponding induced norm of a matrix A are denoted by $|x|$ and $|A|$, respectively. The symbol $\lambda[A]$ denotes the spectrum of A and $\lambda_m[A] = -\max_i\{Re\{\lambda[A]\}\}$.

The $\mathscr{L}_{\infty e}$ norm of a signal $x(t) \in \mathbb{R}^n$ is defined as $\|x_t\| := \sup_{0\leq\tau\leq t} |x(\tau)|$.

The symbol "s" represents either the Laplace variable or the differential operator "d/dt", according to the context.

As in [63] the output y of a linear time invariant (LTI) system with transfer function $H(s)$ and input u is given by $y = H(s)u$. Convolution operations $h(t) * u(t)$, with $h(t)$ being the impulse response from $H(s)$, will be eventually written, for simplicity, as $H(s) * u$.

Classes of $\mathscr{K}, \mathscr{K}_\infty$ functions are defined according to [64, p. 144]. ISS, OSS and IOSS mean Input-State-Stable (or Stability), Output-State-Stable (or Stability) and Input-Output-State-Stable, respectively [65].

The symbol π denotes class-$\mathscr{KL}$ functions. Eventually, we denote by $\pi(t)$ any exponentially decreasing signal, i.e., a signal satisfying $|\pi(t)| \leq \Pi(t)$, where $\Pi(t) := Re^{-\lambda t}$, $\forall t$, for some scalars $R, \lambda > 0$.

Chapter 2

Prosthesis Modelling and Problem Formulation

In this work, the considered prosthesis is a robot manipulator (a PRRR) kinematic chain composed of four actuated joints and an attached foot as end-effector. The first two joints correspond to the hip vertical displacement and flexion/extension, respectively. The two subsequent represent to the knee and ankle joints.

The hip vertical displacement occurs along an axis perpendicular to the ground. It refers to an inertial base, instead of being modeled as the obliquity between one anterior superior iliac spine and the other. The first joint is a prismatic joint (linear actuator), while the others are revolute joints. For simplicity, the whole system analysis occurs only in the sagittal plane.

The simulation scenario is composed by a four-link suspended prosthetic leg with sensors, a controller, and a reference signal generator. There is no contact with the ground, which can cause divergence from the force/torque input signal found in the literature.

The next section formulates the problem that is addressed to the control. It considers what data is necessary and available to fulfill the required task.

This chapter presents a prosthesis model considering the plant dynamics and later propose a simplified model, which is used throughout this work. The last section addresses the problem formulation.

2.1 System Model

The dynamics of the prosthetic system is obtained via Lagrange formulation applied to a 4-link rigid body robot with prismatic-revolute-revolute-revolute (PRRR) configuration. Following the notation in [31], [66] and [6], the dynamic equation is given by:

$$D(q)\ddot{q} + C(q,\dot{q})\dot{q} + B(q,\dot{q}) + P(\dot{q}) + J_e^T F_e + G(q) = F_a\,, \tag{2.1}$$

where q represents the vector of joints positions (q_1 represents the hip vertical displacement, q_2 is the thigh angle, q_3 is the knee angle and q_4 represents ankle angle), $D(q)$ is the inertia matrix, $C(q,\dot{q})$ is a matrix accounting for centripetal and Coriolis effects, $B(q,\dot{q})$ is the joints damper nonlinear matrix, J_e is the kinematic Jacobian relative to the point of application of external forces F_e, $G(q)$ is the vector of gravitational forces, and F_a is the torque/force produced by the actuators. The term $P(\dot{q})$ explicitly represents the Coulomb friction as in [67]. Note that, inertial and frictional effects in the actuators can be included in this model.

To establish a basis for dynamic model derivations and to verify the leg geometry during simulations, the set of reference frames used for forward kinematics problems are the same as the ones assigned in Fig. 1.4 [31].

The analytical Lagrange approach is known for not being computationally efficient when calculating inertia $D(q)$, Coriolis $C(q,\dot{q})$ and gravity $G(q)$ terms [68]. Because of that, the standard Newton-Euler approach has been implemented in simulation environment with the plant parameters extracted from [31], [6] and [66].

The matrix/vector terms from inertia $D(q)$, Coriolis $C(q,\dot{q})$ and gravity $G(q)$ are given as functions of q, $\dot{q}$ and Θ.

In [68], the Lagrangian formulation is explained, and how $D(q)$, $C(q,\dot{q})$ and $G(q)$ are obtained. For implementation purposes, some plant parameters are separated according to the results obtained in the previous matrices. These terms are represented inside the vector Θ, which is given by.

$$
\begin{aligned}
\Theta_1 &= m_1 + m_2 + m_3 + m_4 \\
\Theta_2 &= c_2 m_2 + l_2 m_3 + l_2 m_4 \\
\Theta_3 &= c_4 m_4 \\
\Theta_4 &= c_3 m_3 + l_3 m_4 \\
\Theta_5 &= I_{2z} + I_{3z} + I_{4z} + c_2^2 m_2 + c_3^2 m_3 + c_4^2 m_4 + l_2^2 m_3 + l_2^2 m_4 + l_3^2 m_4 \\
\Theta_6 &= c_4 l_2 m_4 \\
\Theta_7 &= c_3 l_2 m_3 + c_2 l_3 m_4 \\
\Theta_8 &= c_4 l_3 m_4 \\
\Theta_9 &= c_3^2 m_3 + c_4^2 m_4 + l_3^2 m_4 + I_{3z} + I_{4z} \\
\Theta_{10} &= c_4^2 m_4 + I_{4z}
\end{aligned}
$$

Then $D(q)$, $C(q,\dot{q})$ and $G(q)$ are given by:

$$
\begin{aligned}
D(1,1) =& \Theta_1 \\
D(1,2) =& \Theta_2 cos(q_2) + \Theta_3 cos(q_2+q_3+q_4) + \Theta_4 cos(q_2+q_3) \\
D(1,3) =& \Theta_3 cos(q_2+q_3+q_4) + \Theta_4 cos(q_2+q_3) \\
D(1,4) =& \Theta_3 cos(q_2+q_3+q_4) \\
D(2,1) =& D(1,2) \\
D(2,2) =& \Theta_5 + 2\Theta_6 cos(q_3+q_4) + 2\Theta_7 cos(q_3) + 2\Theta_8 cos(q_4) \\
D(2,3) =& \Theta_9 + \Theta_7 cos(q_3) + 2\Theta_8 cos(q_4) + \Theta_6 cos(q_3+q_4) \\
D(2,4) =& \Theta_{10} + \Theta_6 cos(q_3+q_4) + \Theta_8 cos(q_4) \\
D(3,1) =& D(1,3) \\
D(3,2) =& D(2,3) \\
D(3,3) =& \Theta_9 + 2\Theta_8 cos(q_4) \\
D(3,4) =& \Theta_{10} + \Theta_8 cos(q_4) \\
D(4,1) =& D(1,4) \\
D(4,2) =& D(2,4) \\
D(4,3) =& D(3,4) \\
D(4,4) =& \Theta_{10}
\end{aligned}
$$

$$
\begin{aligned}
C(1,1) =& 0 \\
C(1,2) =& -\dot{q_3}(\Theta_3 sin(q_2+q_3+q_4)+\Theta_4 sin(q_2+q_3)) \\
& -\dot{q_2}(\Theta_2 sin(q_2)+\Theta_3 sin(q_2+q_3+q_4)+\Theta_4 sin(q_2+q_3) \\
& -\dot{q_4}\Theta_3 sin(q_2+q_3+q_4) \\
C(1,3) =& -\dot{q_2}(\Theta_3 sin(q_2+q_3+q_4)+\Theta_4 sin(q_2+q_3)) \\
& -\dot{q_3}(\Theta_3 sin(q_2+q_3+q_4)+\Theta_4 sin(q_2+q_3) \\
& -\dot{q_4}\Theta_3 sin(q_2+q_3+q_4) \\
C(1,4) =& -\dot{q_2}\Theta_3 sin(q_2+q_3+q_4) \\
& -\dot{q_3}\Theta_3 sin(q_2+q_3+q_4) \\
& -\dot{q_4}\Theta_3 sin(q_2+q_3+q_4) \\
C(2,1) =& 0 \\
C(2,2) =& -\dot{q_3}(\Theta_6 sin(q_3+q_4)+\Theta_7 sin(q_3)) \\
& -\dot{q_4}(\Theta_6 sin(q_3+q_4)+\Theta_8 sin(q_4)) \\
C(2,3) =& -\dot{q_2}(\Theta_6 sin(q_3+q_4)+\Theta_7 sin(q_3)) \\
& -\dot{q_3}(\Theta_6 sin(q_3+q_4)+\Theta_7 sin(q_3)) \\
& -\dot{q_4}(\Theta_6 sin(q_3+q_4)+\Theta_8 sin(q_4)) \\
C(2,4) =& -\dot{q_2}(\Theta_6 sin(q_3+q_4)+\Theta_8 sin(q_4)) \\
& -\dot{q_3}(\Theta_6 sin(q_3+q_4)+\Theta_8 sin(q_4)) \\
& -\dot{q_4}(\Theta_6 sin(q_3+q_4)+\Theta_8 sin(q_4)) \\
C(3,1) =& 0 \\
C(3,2) =& \dot{q_2}(\Theta_6 sin(q_3+q_4)+\Theta_7 sin(q_3)) \\
& -\dot{q_4}(\Theta_8 sin(q_4)) \\
C(3,3) =& -\dot{q_4}(\Theta_8 sin(q_4)) \\
C(3,4) =& -\dot{q_2}(\Theta_8 sin(q_4)) \\
& -\dot{q_3}(\Theta_8 sin(q_4)) \\
& -\dot{q_4}(\Theta_8 sin(q_4)) \\
C(4,1) =& 0 \\
C(4,2) =& \dot{q_2}(\Theta_6 sin(q_3+q_4)+\Theta_8 sin(q_4)) \\
& +\dot{q_3}(\Theta_8 sin(q_4)) \\
C(4,3) =& \dot{q_2}(\Theta_8 sin(q_4)) \\
& +\dot{q_3}(\Theta_8 sin(q_4)) \\
C(4,4) =& 0
\end{aligned}
$$

$$
\begin{aligned}
G(1) &= -g\Theta_1 \\
G(2) &= -g(\Theta_2 cos(q_2) + \Theta_3 cos(q_2+q_3+q_4) + \Theta_4 cos(q_2+q_3)) \\
G(3) &= -g(\Theta_3 cos(q_2+q_3+q_4) + \Theta_4 cos(q_2+q_3)) \\
G(4) &= -g\Theta_3 cos(q_2+q_3+q_4)
\end{aligned}
$$

2.1.1 A Simplified Model

In order to illustrate the observer design proposed in this work, consider a simplified version of the machine/prosthesis system (2.2) where no external forces are considered ($F_e \equiv 0$), the specific leg prosthesis damping matrix is disregarded ($B(q,\dot{q}) \equiv 0$) and the Coulomb friction is neglected ($P(\dot{q}) \equiv 0$). In this case, the machine/prosthesis system is described by:

$$D(q)\ddot{q} + C(q,\dot{q})\dot{q} + G(q) = F_a\,. \tag{2.2}$$

Where $D(q), C(q,\dot{q})$ and $G(q)$ are supposed to be uncertain, but the corresponding nominal matrices $D_n(q), C_n(q,\dot{q})$ and $G_n(q)$ are assumed to be known. In particular, the inertia matrix $D(q)$ which is invertible, since $D(q) = D^T(q)$ is strictly positive defined.

Introducing the variables $x_1 := q \in \mathbb{R}^4$ and $x_2 := \dot{q} \in \mathbb{R}^4$, the model (2.2) can be rewritten in the state-space form as:

$$
\begin{aligned}
\dot{x}_1 &= x_2\,, \\
\dot{x}_2 &= k_p(x,t)\,[u + d(x,t)]\,, \quad u := F_a \in \mathbb{R}^{4\times 1}\,, \\
y &= x_1\,,
\end{aligned}
\tag{2.3}
$$

or, equivalently,

$$
\begin{aligned}
\dot{x} &= A_\rho x + B_\rho k_p(x,t)[u + d(x,t)]\,, \\
y &= C_\rho x\,,
\end{aligned}
\tag{2.4}
$$

where $x = \begin{bmatrix} x_1 & x_2 \end{bmatrix}^T$ is the state vector, $k_p(x,t) = D(x_1)^{-1} \in \mathbb{R}^{4\times 4}$, $d(x,t) := -C(x_1,x_2)x_2 - g(x_1) \in \mathbb{R}^{4\times 1}$, $C_\rho = \begin{bmatrix} I_{4\times 4} & 0_{4\times 4} \end{bmatrix} \in \mathbb{R}^{4\times 8}$, and the pair (A_ρ, B_ρ) is in Brunovskys canonical controllable form:

$$A_\rho = \begin{bmatrix} 0_{4\times 4} & I_{4\times 4} \\ 0_{4\times 4} & 0_{4\times 4} \end{bmatrix} \in \mathbb{R}^{8\times 8}\,, \tag{2.5}$$

and

$$B_p = \begin{bmatrix} 0_{4\times4} & I_{4\times4} \end{bmatrix}^T \in \mathbb{R}^{8\times4}. \tag{2.6}$$

For each solution of (2.4) there exists a maximal time interval of definition given by $[0, t_M)$, where t_M may be finite or infinite. Thus, finite-time escape is not precluded, *a priori*.

Prosthesis Parameters and Simulation

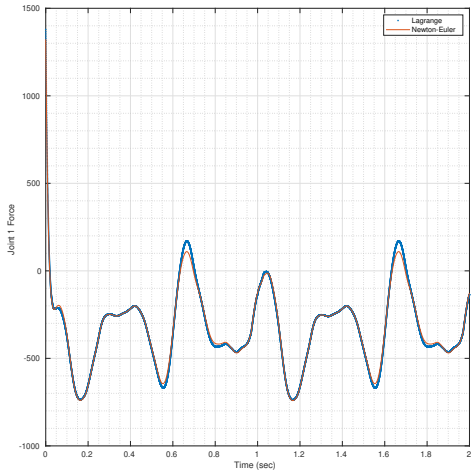

Figure 2.1: Plant model comparison between Recursive Newton-Euler and Lagrange approach for hip vertical displacement joint.

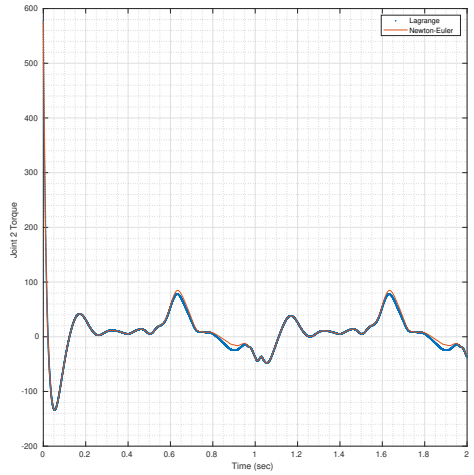

Figure 2.2: Plant model comparison between Recursive Newton-Euler and Lagrange approach for hip flexion/extension.

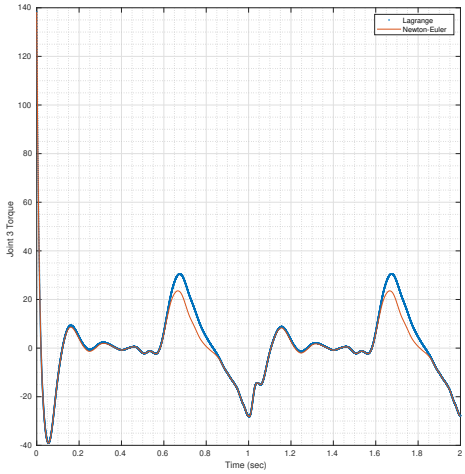

Figure 2.3: Plant model comparison between Recursive Newton-Euler and Lagrange approach for knee flexion/extension.

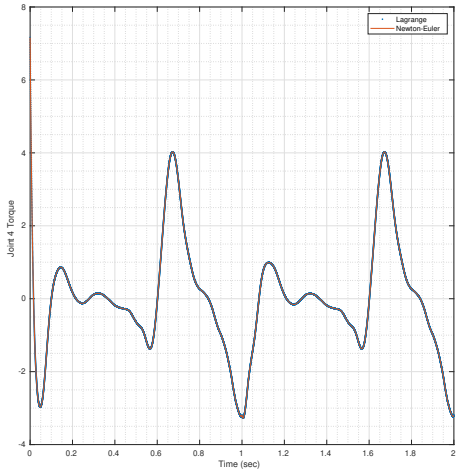

Figure 2.4: Plant model comparison between Recursive Newton-Euler and Lagrange approach ankle plantarflexion/dorsiflexion.

The Figures 2.1-2.4 illustrates that both Lagrangian formulation and the Recursive Newton-Euler approach present close joint torques. However, there are some differences which produce different results as depicted in Figure 2.3. In this simulation, the system is in a closed-loop with PID and computed torque controller, responsible for cancelling non-linearities. Additionally ,the prostheses follows a reference trajectory.

The Lagrangian formulation follows (2.2) and the matrices are given by the terms mentioned earlier in this chapter. The Recursive Newton-Euler approach calculates a resulting plant torque.

Parameter	Value	Unit
m_1	21.29	Kg
m_2	8.57	Kg
m_3	2.29	Kg
m_4	1	Kg
I_1	0	Kg-m^2
I_2	0.435	Kg-m^2
I_3	0.062	Kg-m^2
I_4	0.018	Kg-m^2
l_1	0	m
l_2	0.5	m
l_3	0.4	m
l_4	0.1	m
c_1	0	m
c_2	0.25	m
c_3	0.2	m
c_4	0.05	m
g	9.81	m/s^2

Table 2.1: Parameters from prosthetic leg used in simulation.

Joint	Axis
h_1	z
h_2	-y
h_3	-y
h_4	-y

Table 2.2: Joint axis in prosthesis model.

The prosthesis parameters necessary to calculate the rigid body dynamics are shown in Table 2.1. They are (i) link mass m_i, (ii) inertia I_i in rotation axis, (iii) link length l_i, (iv) link center of gravity c_i , and (v) rotation axis h_i. Table 2.1 shows the parameters' values and Figure 2.5 shows the simulated implementation of the robot.

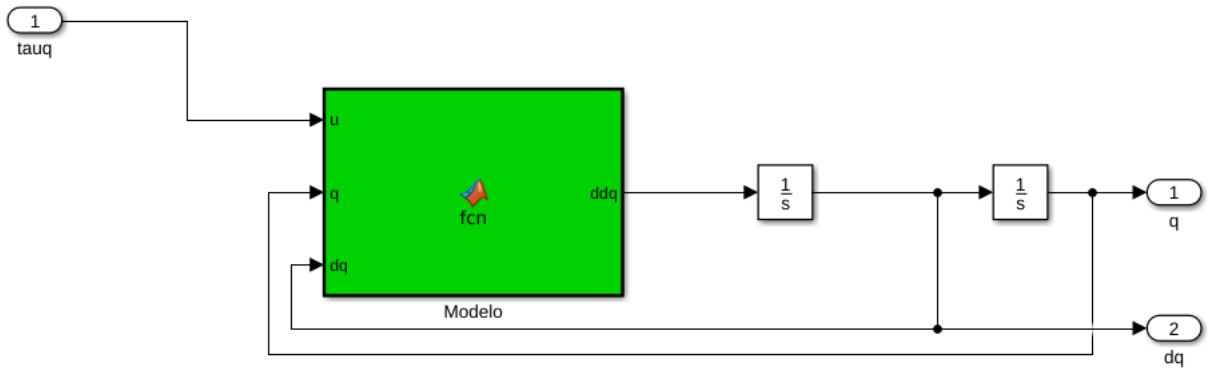

Figure 2.5: Robotic model plant diagram used in simulation.

2.2 Problem Formulation

The control objective is to design a control signal using only output information (only the joints position q) which drives the tracking error to zero or to a small vicinity of zero (practical tracking), while assuring boundedness of all closed-loop signals. The tracking error is defined as

$$e(t) := q_d - q = q_d - x_1 \tag{2.7}$$

where the last equality comes from the plant state representation (2.3)

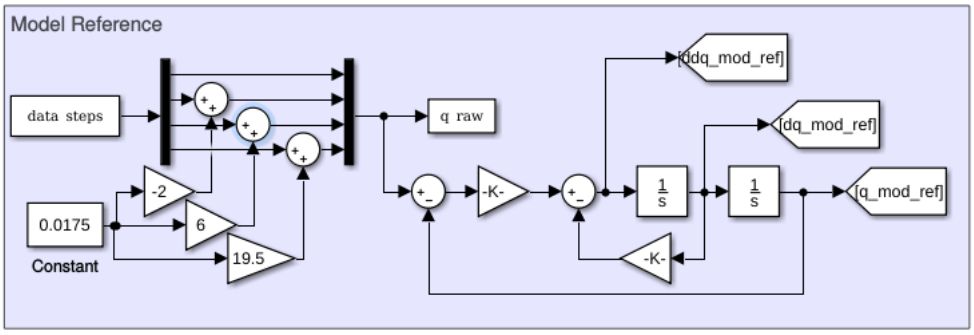

Figure 2.6: Model reference block implementation in simulation environment.

The reference signal q_d is a bounded time series signal obtained from a data set of healthy people walking on level ground acquired for human gait analysis [69]. However, the joint angles have a little offset compared to a normative gait curve from Brazilian subjects. During the simulation, hard-coded gains add a compensating offset to overcome this problem, as depicted in Fig. 2.6.

Another problem arises from the obtained data; the start and end joint angles don't match. In the case of reproducing movements with more than one gait cycle, there would be a discontinuous value between the end of one gait and the start of the next. To overcome

this problem, a moving average filter is added to the system.

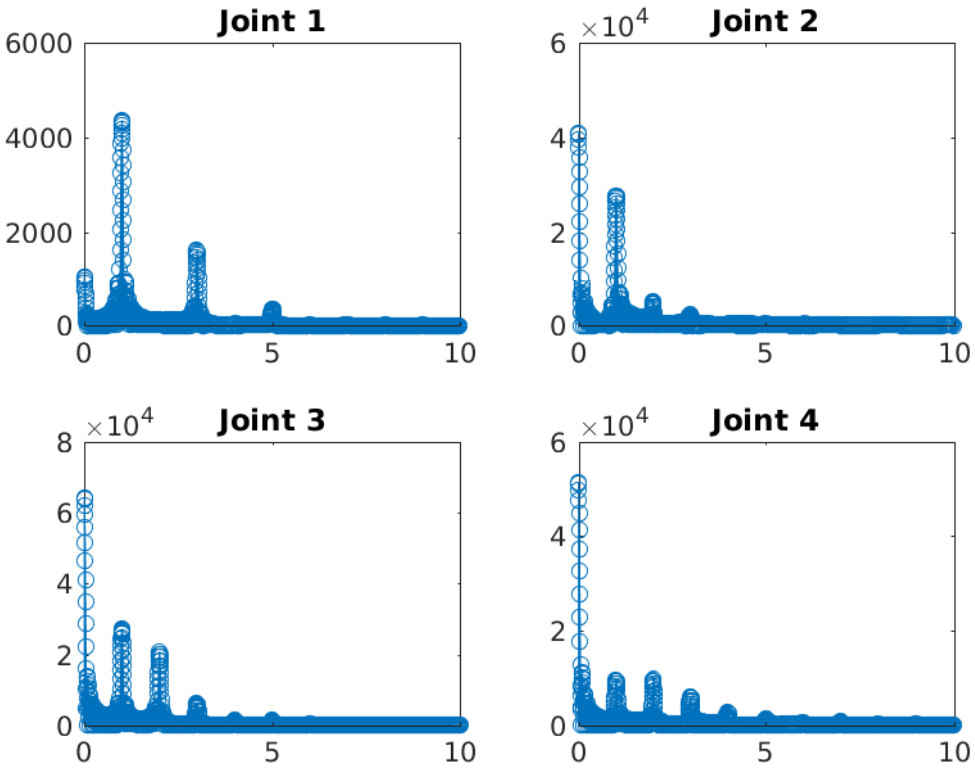

Figure 2.7: Human gait spectrum according for each joint.

The data obtained from human gait analysis usually have an acquisition sample rate of 100Hz, and most human gait spectrum information is below 5Hz, according to Fig. 2.7. This data may be valuable when designing a solution to filter measurement noise. For example, in [3], the raw marker-trajectory data and GRF data were filtered using a fourth-order, low-pass Butterworth filter with a cut-off frequency of 10 Hz.

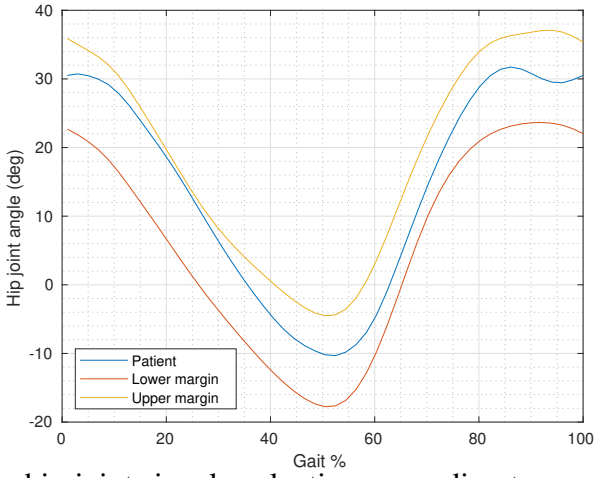

Figure 2.8: Reference hip joint signal evaluation, according to normalized data obtained from Biocinetica.

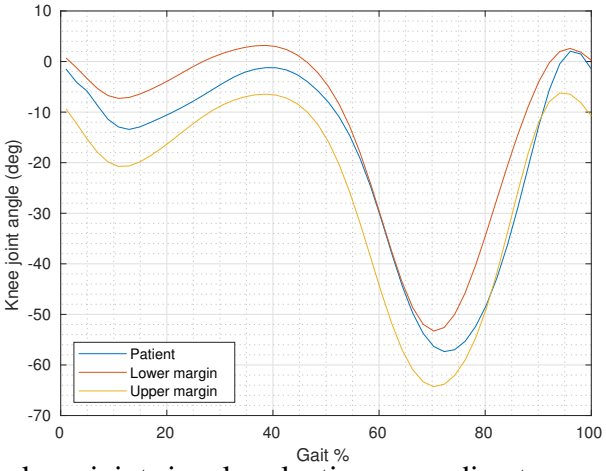

Figure 2.9: Reference knee joint signal evaluation, according to normalized data obtained from Biocinetica.

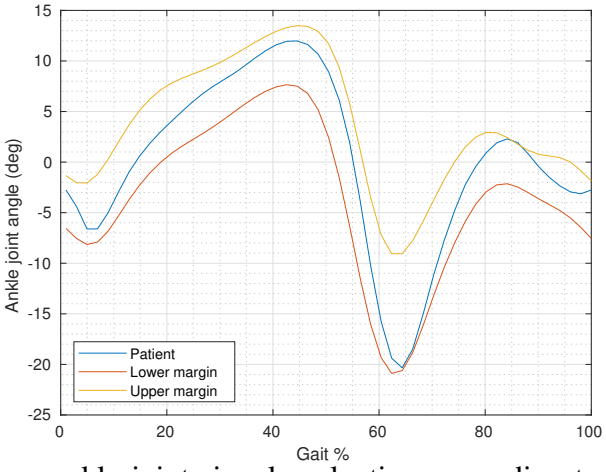

Figure 2.10: Reference ankle joint signal evaluation, according to normalized data obtained from Biocinetica.

Figures 2.8, 2.9, and 2.10 show the results from the signal conditioning. The blue signal represents a patient or an average from patients extracted from [69], and red and yellow set the normative boundaries from human gait.

For this work, a filter (also referred to as **model reference**) has been designed to provide the reference trajectory as a filtered version of the conditioned human gait angles q_d from [69], and also the time-varying derivatives $\dot{q}_d$ and $\ddot{q}_d$. These derivatives help the control law to achieve better performance in the PID control. Figure 2.11 depicts the raw signal along with the filter's output. The difference between them is a delay in every joint, which wouldn't compromise the human gait performance. This filter is obtained implementing the following transfer function:

$$H(s) = \frac{\omega_n^2}{s^2 + 2\xi\,\omega_n + \omega_n^2}, \tag{2.8}$$

which is also illustrated as a block diagram in Fig. 2.6. The parameters used are: $\omega_n = 40\,rad/s$ and $\xi = 0.7$.

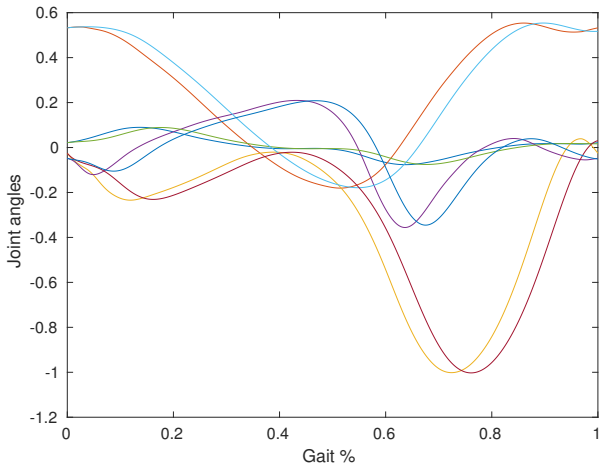

Figure 2.11: Reference signal and filtered reference signal.

The next sections focus on the controller design to achieve a low tracking error and its implementations. The first approach is the state feedback control, where all necessary states are available.

The control via state feedback is feasible in ideal cases where all the required sensors are present in the system, and thus all states are available for the controller as system output. In the present case, this means a prosthetic leg with rotary/linear encoders and tachometers. They are responsible for acquiring joint displacement and joint velocities, respectively. Initially, all measurements are used without the presence of noise and parametric uncertainties. In another section, these perturbations are added to the system to compare the tracking efficiency.

Later, another scenario is presented, where only some measurements are available and state estimations are necessary. This means that the 4DOF robots/prosthesis system would encompass rotary/linear encoders, for position measurements, and an observer calculates the joint velocities. In addition, noise and parametric uncertainties are also considered.

We propose an scheme to estimate the prosthesis velocity based on a time-varying observer gain synthesized from measurable signals. It is designed to reduce the amount of noise in the control effort while keeping an acceptable tracking error transient performance. Numerical simulations analyze the robustness of the closed-loop control.

Chapter 3

State Feedback Control

In an active prosthesis, the embedded system is responsible for using sensors measurements and a tracking objective to execute a joint control. The tracking could be of an impedance profile, a torque profile, or a joint position. This signal depends on the mid-level control implemented on the prosthesis, and in the present case, the reference signal is a set of joint positions, which are tracked by the controller.

This chapter presents the proportional-integral-derivative controller using computed torque, and feed-forward to control the 4DOF robot. Additionally, all the plant states are available as outputs.

The objective of the controller, in this chapter, is to track realistic motion profiles $q_d(t)$ provided by the second-order filter (2.8). Knowing that all required sensors are present, and thus, all the required states are available, in a model given as:

$$\dot{x}_1 = x_2\,, \tag{3.1a}$$

$$\dot{x}_2 = k_p(x,t)\left[u + d(x,t)\right], \quad u := F_a \in \mathbb{R}^{4\times 1}\,, \tag{3.1b}$$

$$y = x_1\,. \tag{3.1c}$$

where $k_p(x,t) = D(x_1)^{-1} \in \mathbb{R}^{4\times 4}$, $d(x,t) := -C(x_1,x_2)x_2 - G(x_1) \in \mathbb{R}^{4\times 1}$, and $C_\rho = \begin{bmatrix} I_{4\times 4} & 0_{4\times 4} \end{bmatrix} \in \mathbb{R}^{4\times 8}$.

3.1 Computed Torque with PID Feedback Components (CTPID)

3.1.1 PID Control

PID control theory is one of the most basic and yet extensively discussed topics in control literature, and PID controllers are the most common type of controller used in industry.

They are suitable for solving a great variety of control problems, even for controlling certain classes of non-linear systems.

The motivation for testing PID control comes from the fact that the inherent non-linearities in a system's dynamic equation such as a robot manipulator can be viewed as input disturbances in an equivalent linear dynamic model in the joint space.

This type of decentralized control is specially suited for low speed/acceleration operations and for manipulators equipped with high reduction ratio gears [68], because high speeds/accelerations and low reduction ratio gears increase the amplitude of the signals associated to the non-linearities of the system.

Taking the input u of the system, the general PID control law can be written as:

$$u = K_p e(t) + K_d \dot{e}(t) + K_i \int_0^t e(t)\, dt\,, \tag{3.2}$$

where $e = q_d - q$ is the error in the joint angles.

3.1.2 Computed Torque Control with Integral Term

The computed torque framework is based on the complete cancellation of all non-linearities present on the dynamic equation. Referring to (2.2), it is desired to develop a control law that transforms the feedback system into a linear model in the joint angles using u. In general, the computed torque strategy can be used if the following hypothesis hold:

1. The dynamic model is well-known;

2. High-performance drivers are available for controlling the actuator torques.

However, the geometric and dynamic parameters for a real system can be difficult to obtain, leading to imperfect cancellations of the non-linear terms in (2.2). In practice, this will cause a non-zero offset error in the feedback system.

For tackling the problem of imperfect cancellation of the non-linear terms, one must implement the computed torque plus PID control scheme. This can be done with the control law:

$$u(t) = D_n(x_1)\tau + C_n(x_1, x_2)x_2 + G_n(x_1)\,, \tag{3.3}$$

$$\tau = \ddot{q}_d + K_p(q_d - x_1) + K_d(\dot{q}_d - x_2) + K_i \int_0^t e\, dt\,. \tag{3.4}$$

The matrices K_p, K_d, and K_i contain the proportional, derivative, and integral gains, respectively. The corresponding feedback error equation is now given by

$$\dddot{e} + K_d \ddot{e} + K_p \dot{e} + K_i e = \varepsilon \tag{3.5}$$

Supposing that all gain matrices are diagonal (so that the equations are uncoupled), the *Routh-Hurwitz* criterion gives us a sufficient condition for guaranteeing stability of the closed-loop system:

$$\begin{aligned} K_d K_p, \text{ and } K_i \text{ are positive} \\ K_d K_p > K_i \,, \end{aligned} \tag{3.6}$$

where the terms above denote the diagonal elements of K_d, K_p and K_i. In the present case, this gains are represented by $K_i := k_i(I_{4\times4})$, $K_p := k_p(I_{4\times4})$ and $K_d := k_d(I_{4\times4})$.

The inclusion of an integrator in the control law can help to reject the offset error due to imperfect cancellation of the non-linear terms. On the hypothesis that the closed-loop system's response will be similar to the response of a third-order linear system given by:

$$(s^2 + 2\xi\omega_n + \omega_n^2)(s+p) = 0\,. \tag{3.7}$$

where ω_n, ξ and p are design constants.

We make use of the analytical approach to choose the system's closed-loop poles. For each of the n uncoupled equations in (3.5), proceed as follows.

1. First, choose a pole p in the left-half plane, sufficiently distant from the origin (obviously, here the expression *sufficiently distant* is relative, dependent on the desired settling time);

2. With the distant stable pole p, divide the close-loop system characteristic equation given by (3.5) in the form of $(s+p)$, where s is the Laplace variable, and obtain the corresponding second-order characteristic equation, whose coefficients are functions of the gains K_p, K_d and K_i;

3. Compute the gains K_p, K_d and K_i by comparing the coefficients of the resulting second order equation with the reference model (2.8), with ξ as the damping factor and ω_n as the natural frequency of a general second order linear system.

The controller gains k_i, k_p, and k_d are thus calculated as:

$$\begin{aligned} k_i &:= \omega_n^2 p \\ k_p &:= \omega_n^2 + 2\xi\omega_n p \\ k_d &:= p + 2\xi\omega_n, \end{aligned} \tag{3.8}$$

It is important to notice that this kind of strategy for adjusting the gains can lead to high amplitudes of the control signal. Therefore, the presence of saturation on the

actuators must be taken into account.

3.2 Simulation Results

This section shows simulation results from a state-feedback closed-loop system using PID and computed torque controller (3.3 and 3.4), and assuming that all plant states (x_1 and x_2) are measured.

The state-feedback simulation aims to find a set of control gains which assures an acceptable tracking performance with control effort that could be implemented in a real application, since we have evaluated the simulation under parametric uncertainties and noise disturbance. In other words, a good trade-off between the magnitude of the control signal and tracking accuracy. A desirable performance achievement requires root-mean-square tracking errors lower than 1.8, 1.9, and 1,5 degree for hip, knee, and ankle joints respectively [5]. A settling time lower than 0.2 seconds while also having feasible control signals. No value has been found in the literature for the hip vertical displacement.

Initially, the simulation is conducted in an ideal scenario. Later, parametric uncertainties and measurement noise reduce the tracking performance.

Plant	
$x_1(0) =$	$\begin{bmatrix} 0 & 24.99 & 0 & 0 \end{bmatrix}^T$
$x_2(0) =$	$\begin{bmatrix} 0 & 0 & 0 & 0 \end{bmatrix}^T$
Reference Signal	
$x_1(0) =$	$\begin{bmatrix} 0.0216 & 30.51 & -1.46 & -2.76 \end{bmatrix}^T$
$x_2(0) =$	$\begin{bmatrix} 0.3342 & 16.83 & -161.82 & -38.92 \end{bmatrix}^T$

Table 3.1: Initial conditions from Prosthesis Plant and the Reference Model

Gain	Value
k_p	2337
k_d	82.93
k_i	23813

Table 3.2: PID control parameters

It is important to notice in Table 3.1 that the plant initial conditions differ little from the reference signal, which jeopardizes a transitory analysis from the closed loop system. The author uses these values in order to evaluate only the steady state behavior.

Figure 3.1 shows the simulation block diagram, comprised by a Model Reference block, responsible for reference signal generation, the prosthesis plant in orange, and the PID with computed torque controller in green. The plant's initial conditions are shown

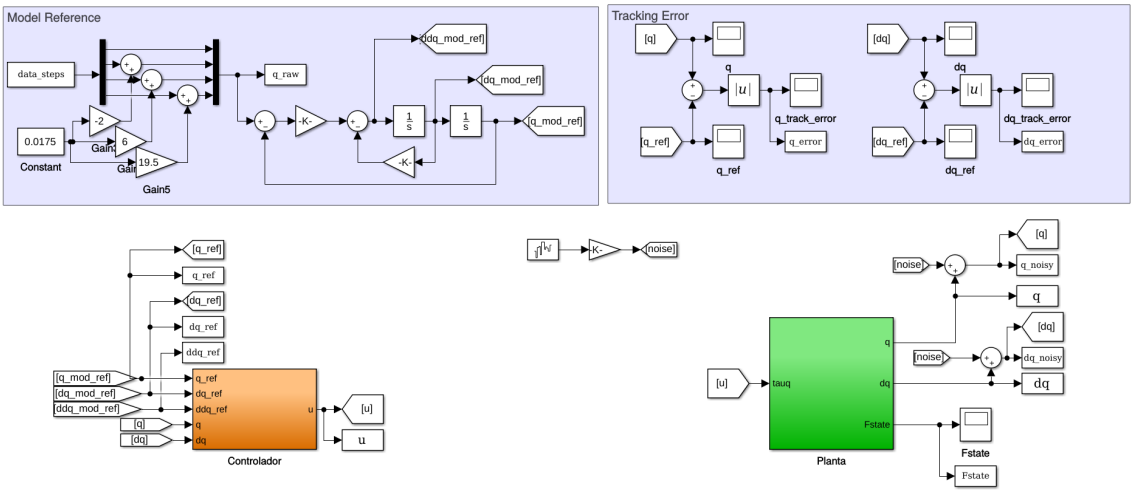

Figure 3.1: State feedback block diagram.

in Tables 3.1. The controller gains are shown in Table 3.2, and were obtained using the parameters $\omega_n = 4\pi$, $\xi = 0.9$, and $p = 1.5\omega_n$ in (3.8).

According to Tables 3.1 and 3.2, an initial error of $[0.0216, 5.5, 1.46, 2.75]$ in x_1 and $[0.33, 16.83, -161.83, -38.92]$ in x_2 is expected. One must be aware of the high initial error in the knee joint when comparing the simulation results.

In Figure 3.2 (a) and (b), one may see the overall tracking accuracy for a gait cycle of 1s. Figure 3.2 (d) shows that the transient tracking error reaches values lower than 3mm after 200 ms, and a steady state tracking error lower than 1mm. For that performance, the required control signal has magnitude ranging from -800 to 200 N, with a peak of 1200 N in the transient period, according to Figure 3.2 (c).

In Figure 3.3 (a) and (b), one may see the overall tracking accuracy. Figure 3.3 (d) shows that the transient tracking error reaches values lower than 0.6 degree after 200 ms, and a steady state tracking error lower than 0.2 degree. For that performance, the required control signal has magnitude ranging from -140 to 100 N, with a peak of 500 N during transient, according to Figure 3.3 (c).

In Figure 3.4 (a) and (b), one may see the overall tracking accuracy. Figure 3.4 (d) shows that the transient tracking error reaches values lower than 0.4 degree after 200 ms, and a steady state tracking error lower than 0.3 degree. For that performance, the required control signal has magnitude ranging from -40 to 30 N, with a peak of 120 N during transient, according to Figure 3.4 (c)

In Figure 3.5 (a) and (b), one may see the overall tracking accuracy. Figure 3.5 (d) shows that the transient tracking error reaches values lower than 0.4 degree after 200 ms, and a steady state tracking error lower than 0.3 degree. For that performance, the required control signal has magnitude ranging from -3 to 4 N, with a peak of 6 N during transient, according to Figure 3.5 (c). The ankle torques required for a scenario with ground contact forces demand more torque than the simulation results obtained. This deviation occurs

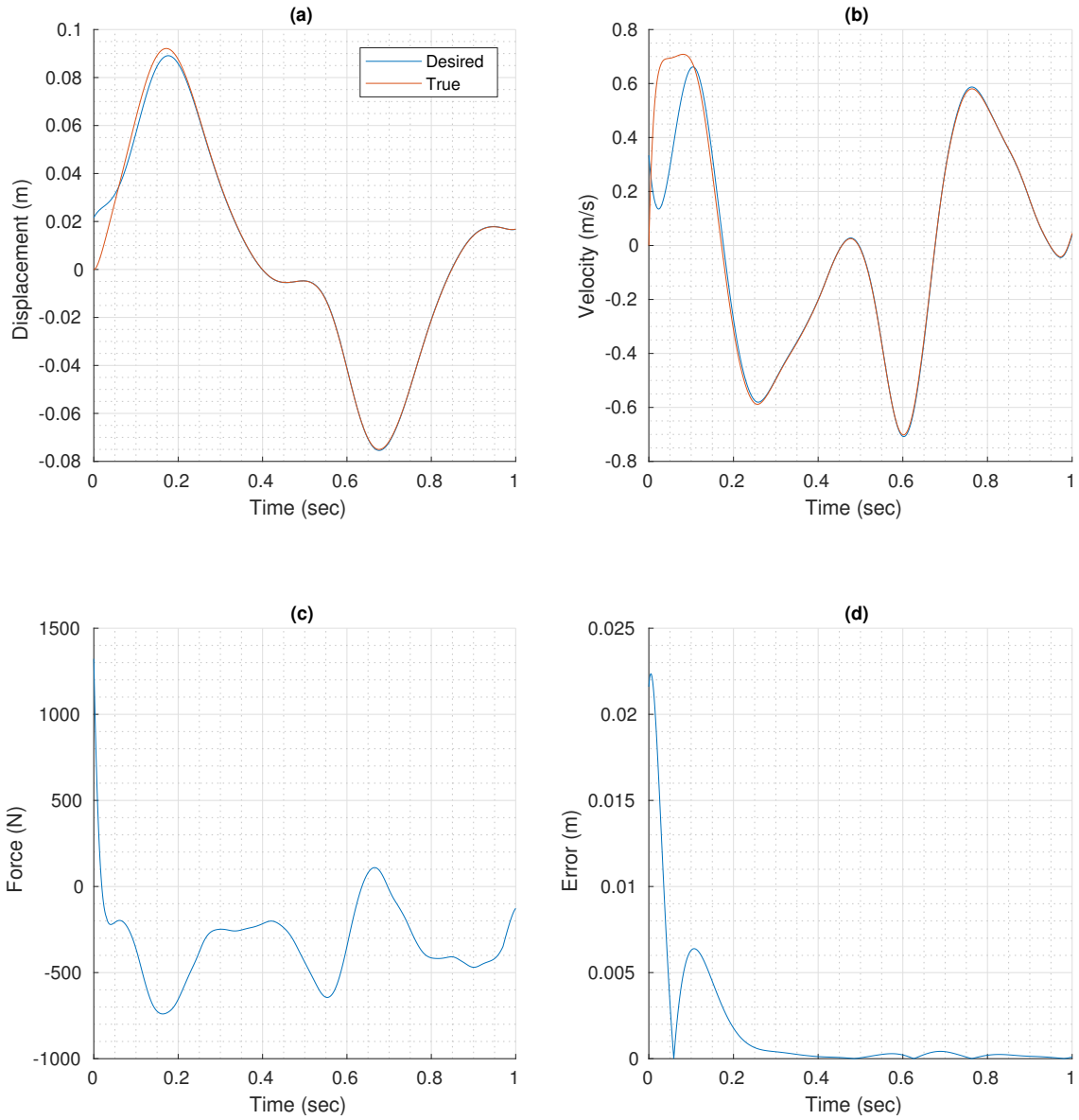

Figure 3.2: Comparison between hip linear displacement reference signal provided by filter and the signal obtained from the plant. (a): tracking result, (b): real $\times$ desired joint velocity, (c) effort signal, (d) tracking error.

because of the ankle impulse necessary in the pre-swing phase.

Figures 3.2, 3.3, 3.4, and 3.5 show the results obtained for each joint in an ideal scenario. A high error occurs due to initial conditions difference between the reference signal and the plant's outputs, as stated in Table 3.1.

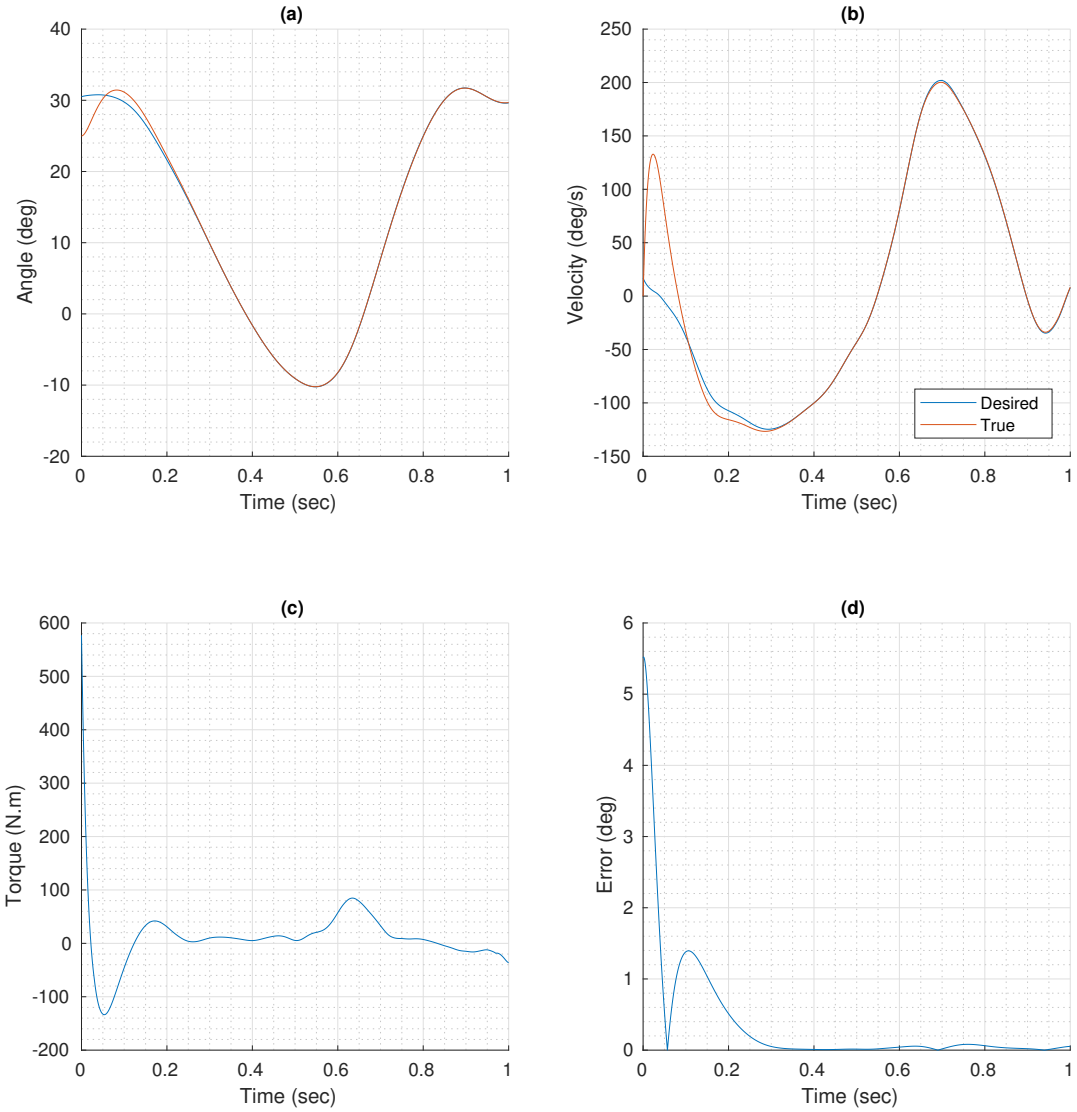

Figure 3.3: Comparison between hip extension/flexion reference signal provided by filter and the signal obtained from the plant. (a): tracking result, (b): real $\times$ desired joint velocity, (c) effort signal, (d) tracking error.

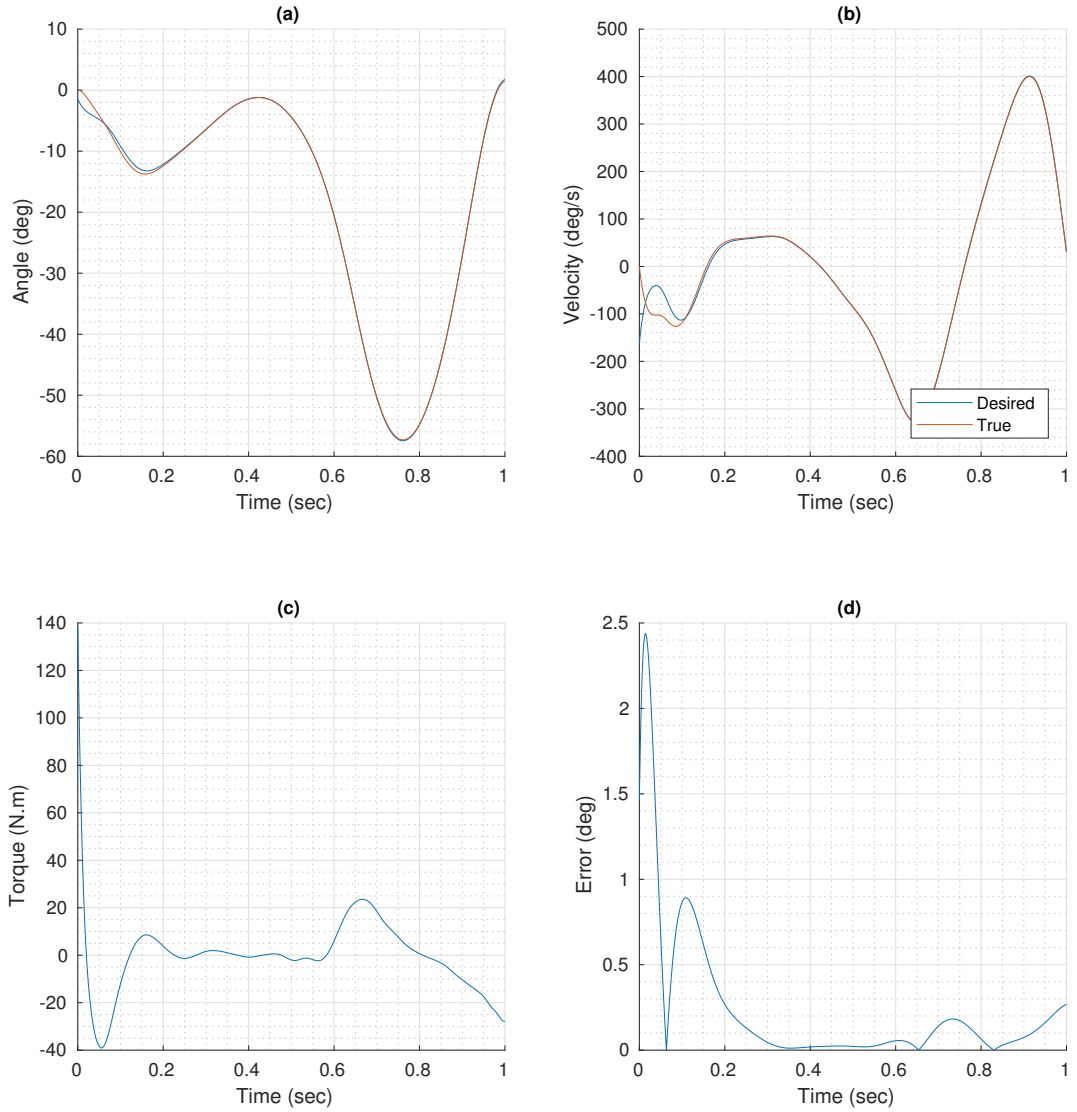

Figure 3.4: Comparison between knee extension/flexion reference signal provided by filter and the signal obtained from the plant. (a): tracking result, (b): real $\times$ desired joint velocity, (c) effort signal, (d) tracking error.

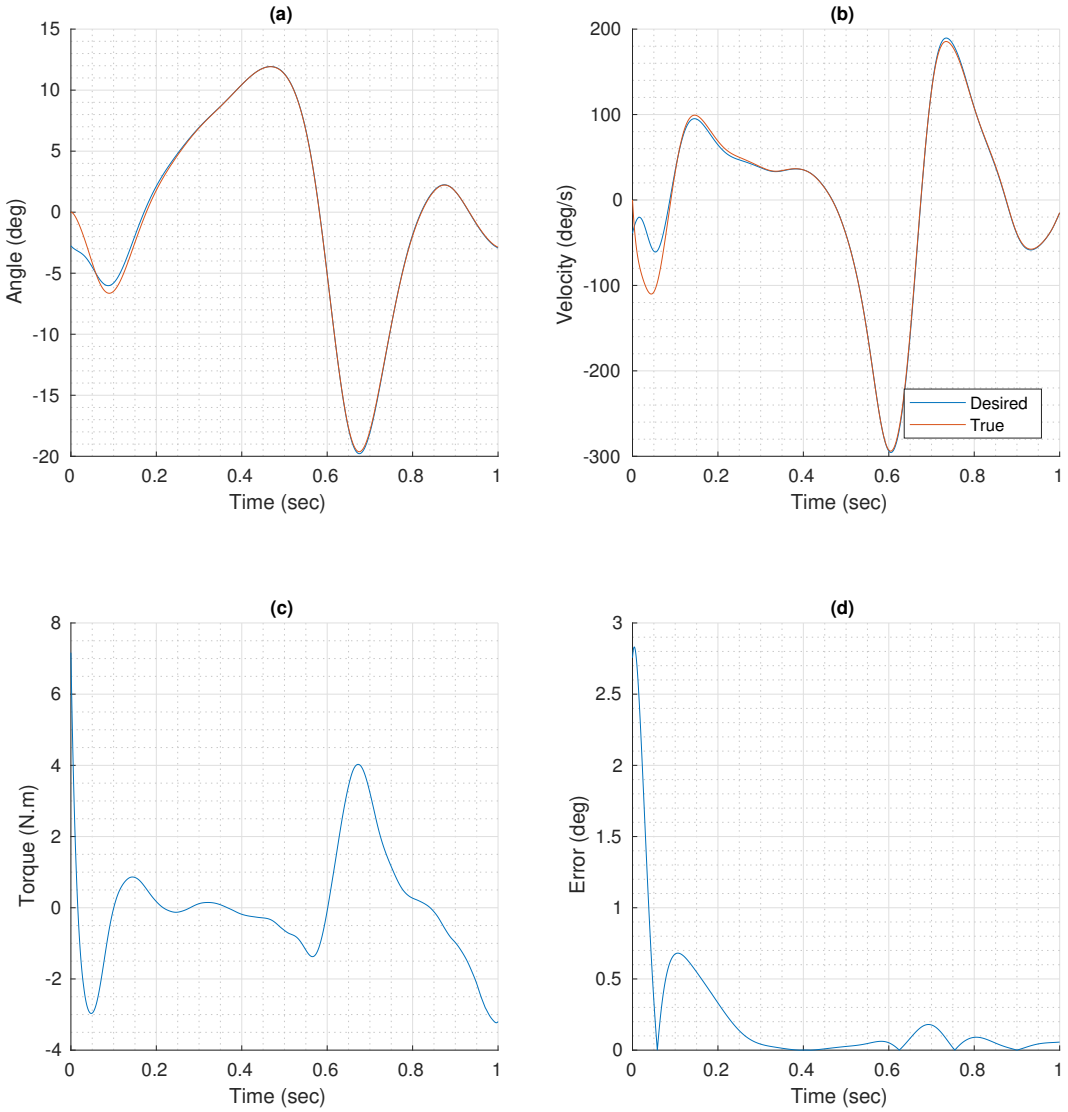

Figure 3.5: Comparison between ankle dorsiflexion/plantarflexion reference signal provided by filter and the signal obtained from the plant. (a): tracking result, (b): real $\times$ desired joint velocity, (c) effort signal, (d) tracking error.

3.2.1 Noise Effect and Parametric Uncertainties

In this subsection, the simulation scenario is different. There are disturbances caused by the presence of noise, possibly due to quantization error on sensors, and parametric uncertainties. Their effect in the system is evident when comparing the control signal and the overall tracking error.

In the presence of model uncertainties and numerical errors, the prosthetic system can be described as

$$\begin{aligned} \dot{x}_1 &= x_2\,, && (3.9)\\ \dot{x}_2 &= f(x_1,x_2,u,t)+\delta_f(x_1,x_2,u,t)\,, \quad u:=F_a\,, && (3.10)\\ y &= \begin{bmatrix} x_1 \\ x_2 \end{bmatrix} \in \mathbb{R}^{8\times 1}\,, && (3.11) \end{aligned}$$

where the nominal part of the system dynamics is represented by

$$f(x_1,x_2,u,t) := D^{-1}(x_1)u - D^{-1}(x_1)\left[C(x_1,x_2)x_2 + G(x_1)\right]\,, \tag{3.12}$$

while the uncertainties are concentrated in the term

$$\begin{aligned} \delta_f(x_1,x_2,u,t) := & \left[D^{-1}D - D^{-1}D_n(x_1)\right]u + \\ & D^{-1}(x_1)\left[C(x_1,x_2) - C_n(x_1,x_2)\right]x_2 + \\ & D^{-1}(x_1)\left[G(x_1) - G_n(x_1)\right]\,. \end{aligned} \tag{3.13}$$

The term $\delta_f(\cdot)$ can be uniformly bounded (converging or not to a residual set) or can be unbounded. Thus, stability/convergence analysis must be conducted, carefully.

Using the same error formulation from (3.5), now we obtain:

$$\dddot{e} + K_d\ddot{e} + K_p\dot{e} + K_i e = \delta_f(x_1,x_2,u,t)\,. \tag{3.14}$$

For these simulations, a band-limited white noise is used to simulate noises disturbances caused by sensors, signal interference, and quantization error. The block implements normally distributed random numbers that are suitable for use in continuous or hybrid systems with a desired (1×10^{-6} W/Hz) noise power. A parametric error of 4% has also been added as a perturbation.

In Figure 3.6 (a) and (b), one may see the overall tracking accuracy for a gait cycle of 1s. Figure 3.6 (d) shows that the transient tracking error reaches values lower than 3mm after 200 ms, and a steady state tracking error lower than 1mm. For that performance, the required control signal has magnitude ranging from -800 to 200 N, with a peak of 1500 N

Tracking Error			
e_1 (m)	e_2 (deg)	e_3 (deg)	e_4 (deg)
0.0004	0.0653	0.2064	0.1096

Table 3.3: State feedback RMS steady-state tracking error in the presence of noise and parametric model uncertainty.

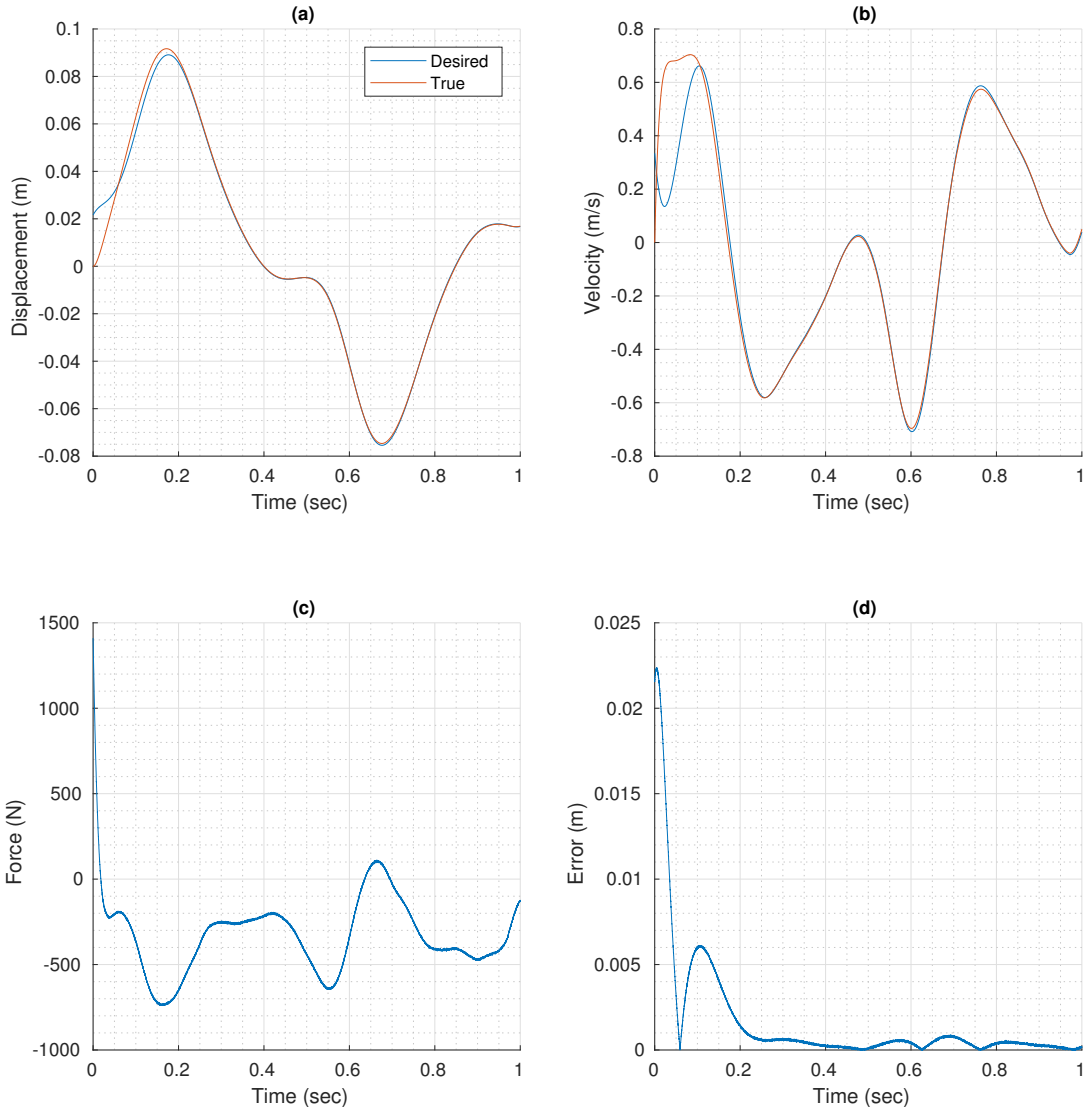

Figure 3.6: Hip linear displacement reference signal provided by filter and the real signal in the presence of noise with 1×10^{-6} W/Hz and model uncertainties. (a): tracking result, (b): real $\times$ desired joint velocity, (c) effort signal, (d) tracking error.

in the transient period, according to Figure 3.6 (c). Table 3.3 shows a joint RMS tracking error of 3.9mm.

In Figure 3.7 (a) and (b), one may see the overall tracking accuracy. Figure 3.7 (d) shows that the transient tracking error reaches values lower than 0.6 degree after 200 ms, and a steady state tracking error lower than 0.2 degree. For that performance, the required control signal has magnitude ranging from -140 to 100 N, with a peak of 700 N during

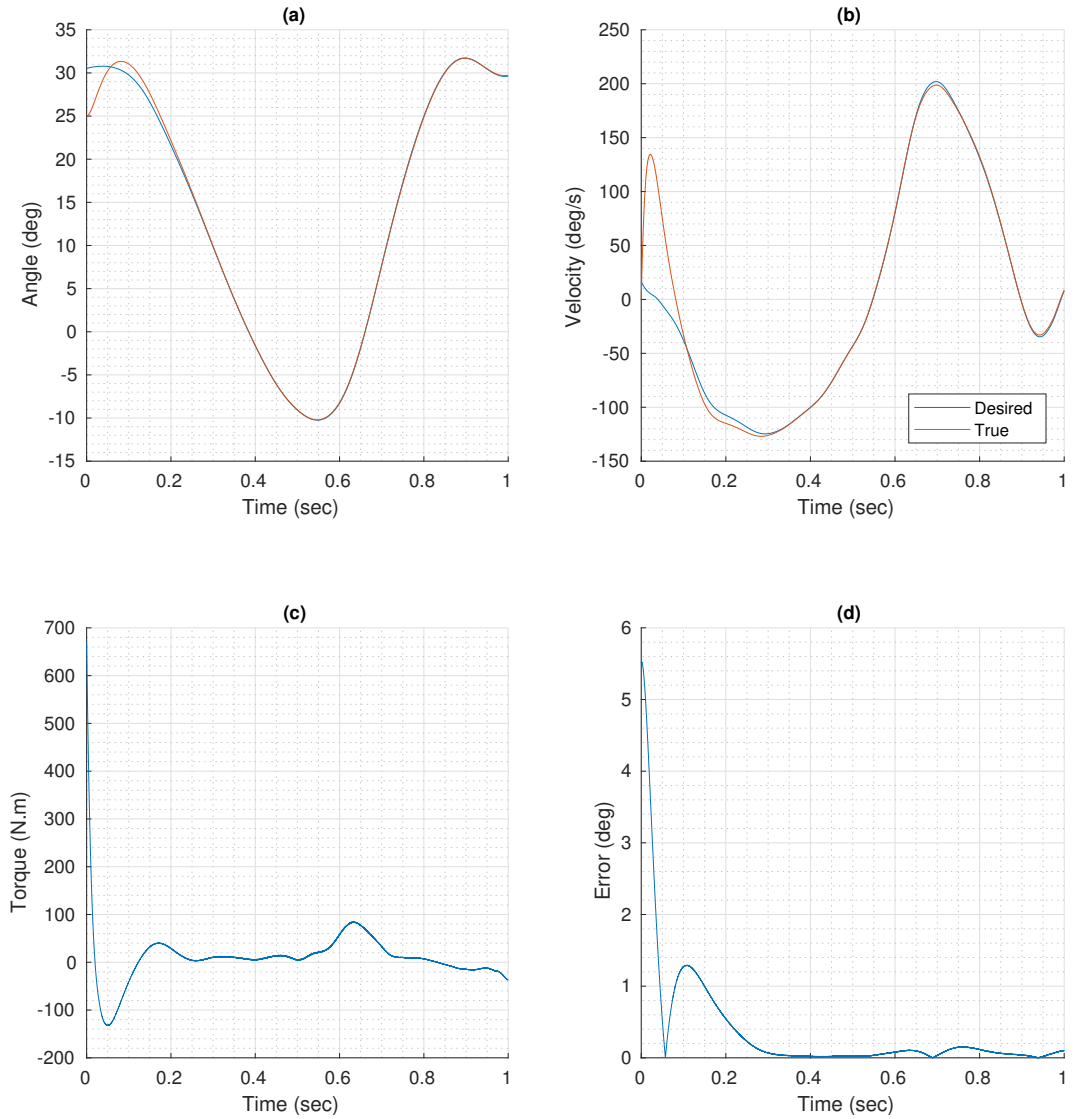

Figure 3.7: Hip angular displacement reference signal provided by filter and the real signal in the presence of noise with 1×10^{-6} W/Hz and model uncertainties. (a): tracking result, (b): real $\times$ desired joint velocity, (c) effort signal, (d) tracking error.

transient, according to Figure 3.7 (c). Table 3.3 shows a joint RMS tracking error of 0.89 degree.

In Figure 3.8 (a) and (b), one may see the overall tracking accuracy. Figure 3.8 (d) shows that the transient tracking error reaches values lower than 0.3 degree after 200 ms, and a steady state tracking error lower than 0.5 degree.For that performance, the required control signal has magnitude ranging from -40 to 30 N, with a peak of 160 N during transient, according to Figure 3.8 (c). Table 3.3 shows a joint RMS tracking error of 0.5 degree.

It is possible to see the influence of parametric error in this joint, as the tracking error in steady state is higher than in Figure 3.4 (d). The RMS tracking error is also higher.

In Figure 3.9 (a) and (b), one may see the overall tracking accuracy. Figure 3.9 (d) shows that the transient tracking error reaches values lower than 0.4 degree after 200 ms,

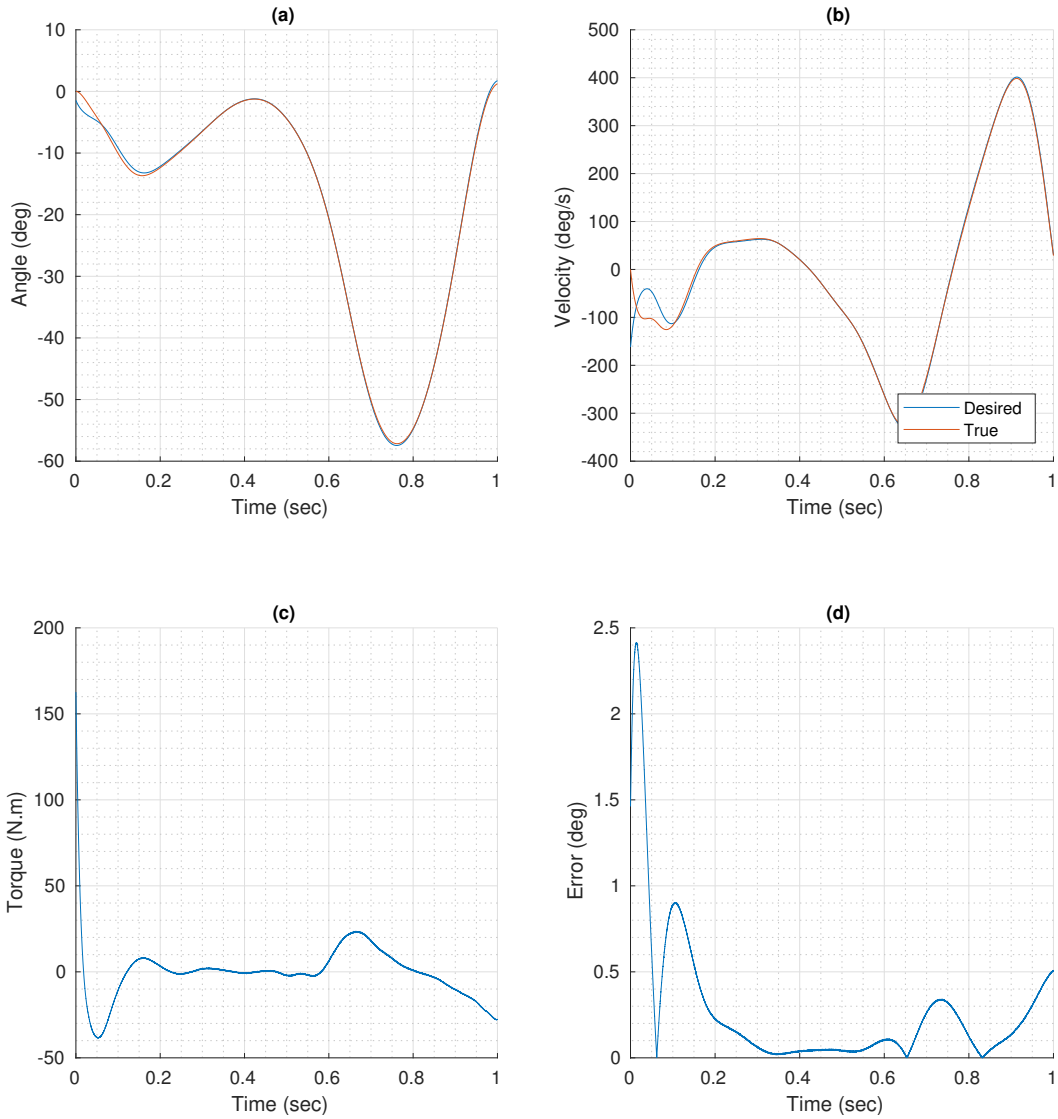

Figure 3.8: Knee reference signal provided by filter and the real signal in the presence of noise with 1×10^{-6} W/Hz and model uncertainties. (a): tracking result, (b): real $\times$ desired joint velocity, (c) effort signal, (d) tracking error.

and a steady state tracking error lower than 0.3 degree. For that performance, the required control signal has magnitude ranging from -3 to 4 N, with a peak of 9 N during transient, according to Figure 3.9 (c). Table 3.3 shows a joint RMS tracking error of 0.48 degree.

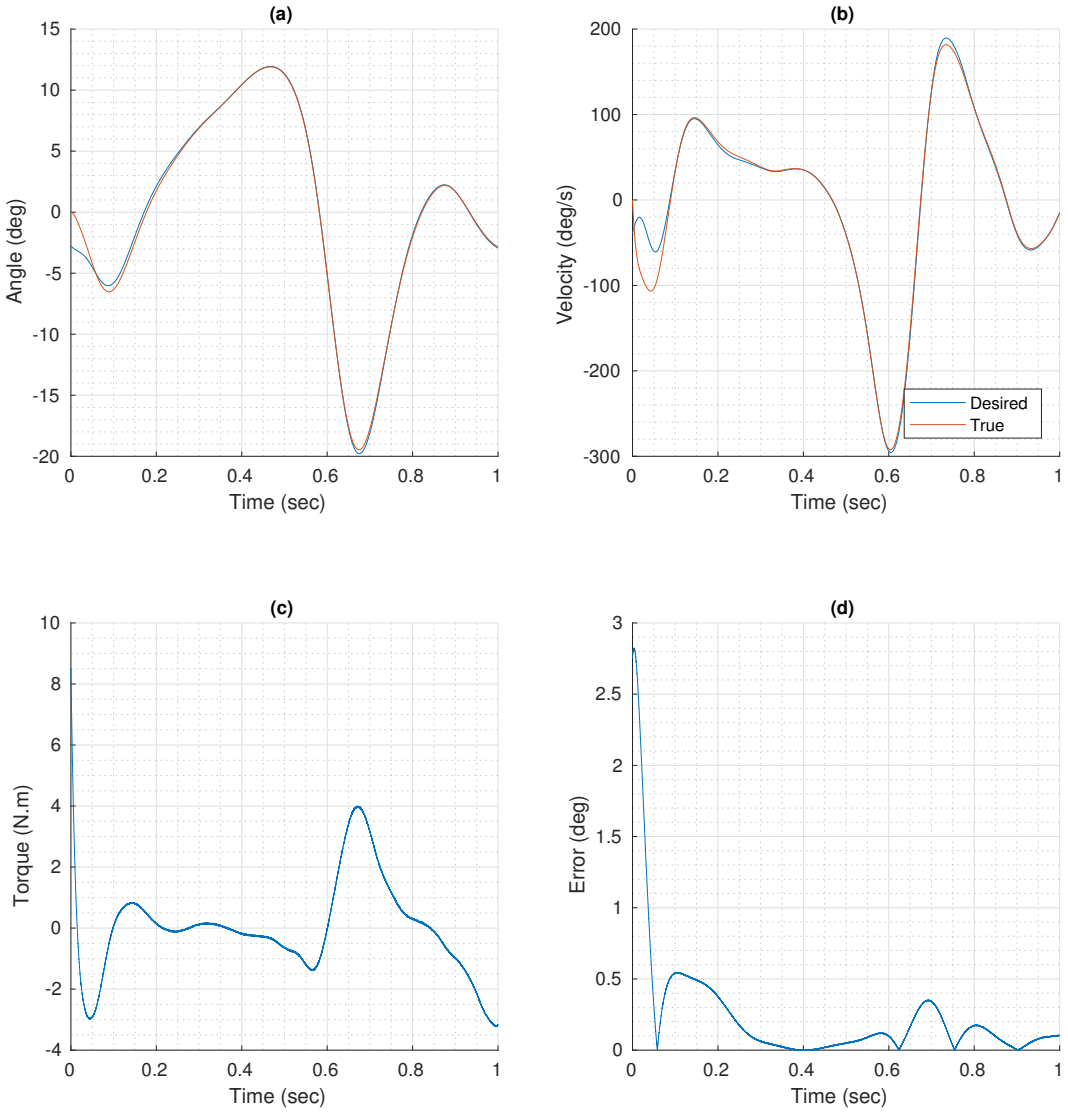

Figure 3.9: Ankle reference signal provided by filter and the real signal in the presence of noise with 1×10^{-6} W/Hz and model uncertainties. (a): tracking result, (b): real $\times$ desired joint velocity, (c) effort signal, (d) tracking error.

3.3 Remarks

Most of the control signal's magnitude are due to computed torque. More specifically, because of the term $D_n(q)\ddot{q}$. As the gait cycle has 1Hz frequency in this simulation, one could decrease the joint acceleration by decreasing the gait cycle frequency. That would decrease the required torque signal controlling the plant.

The results shown previously suggest a viability to implement this control in a real, whether with 4 link joints or less. The lack of ground contact caused some joints to require less torque then found in literature, however the values are close within the magnitude found in other works [7].

The real prosthesis may, however, only have position measurement, and for that case a full state-feedback control wouldn't be a possible approach. It is necessary to estimate the states previously obtained via tachometers. The next chapter focus on this case, explaining one possible approach and the implementation.

Chapter 4

Output Feedback Control

This chapter introduces an observer technique to estimate an unmeasurable state x_2. Later, the controller uses it in a control law that also implements CTPID control. Simulations are then conducted to test the system's robustness.

The observation approach chosen in this project is the High-Gain Observer. The simulations implements this technique with three fixed gains and then propose a variable gain, which is dependent on control signal noise and tracking error.

4.1 High Gain Observer

In some cases, all states variables are measured, allowing a state feedback scheme, as simulated in Chapter 3. However, the state may not be observable. In this case, estimates $\hat{x}$ are required from these sates.

In this section, it is considered that only x_1 is available and an approach to estimate the system's state x_2 via High-Gain Observer (HGO) [70] is shown.

4.1.1 Fixed HGO

One could design an observer as

$$\dot{\hat{x}} = A_\rho \hat{x} + B_\rho k_p^n u + H_\mu L_o (y - C_\rho \hat{x}), \tag{4.1}$$

where k_p^n is a nominal value of the plant high frequency gain (HFG) k_p. The matrices L_o and H_μ compose the observer gain and are given by:

$$L_o = \begin{bmatrix} l_1 I_{4\times 4} & l_2 I_{4\times 4} \end{bmatrix}^T \in \mathbb{R}^{8\times 4} \tag{4.2a}$$

$$H_\mu := \mathrm{diag}(\mu^{-1} I_{4\times 4},\ \mu^{-2} I_{4\times 4}) \in \mathbb{R}^{8\times 8}, \tag{4.2b}$$

where μ is a design parameter, and l_1 and l_2 are such that $s^2 + l_1 s + l_2$ is Hurwitz.

4.1.2 Variable HGO

In this work, instead of using a constant μ, we use a *variable* parameter $\mu = \mu(t) \neq 0, \forall t \in [0, t_M)$ according to what has been proposed in [44]. In this dissertation, we use the theoretical tools developed in [44] and, in contrast to [44], the **proposed time-varying** μ depend on the signal-to-noise ratio of the effort signal and the tracking error. The $\mu(t)$ is of the form

$$\mu(t) := \frac{\bar{\mu}}{1 + \psi_\mu(\omega(t), t)}, \tag{4.3}$$

where ψ_μ, named **adapting function**, is a non-negative function continuous in its arguments and $\omega(t)$ is an available signal [44], both to be designed later on. This structure will be used so that $\mu \approx \bar{\mu} \pm \delta$ adapts to a certain criteria.

The parameter $\bar{\mu} > 0$ is a design constant. For each system trajectory, μ is absolutely continuous and $\mu \leq \bar{\mu}$. Note that μ is bounded for t in any finite sub-interval of $[0, t_M)$. Therefore,

$$\mu(t) \in [\underline{\mu}, \bar{\mu}], \quad \forall t \in [t_*, t_M), \tag{4.4}$$

for some $t_* \in [0, t_M)$ and $\underline{\mu} \in (0, \bar{\mu})$.

The transformation [44]

$$\zeta := T_\mu \tilde{x}, \quad T_\mu := [\mu^2 H_\mu]^{-1} \in \mathbb{R}^{8\times 8}, \quad \tilde{x} := x - \hat{x}, \tag{4.5}$$

is fundamental to represent the $\tilde{x}$-dynamics in convenient coordinates allowing us to show that $\tilde{x}$ is arbitrarily small, *modulo* exponentially decaying term (one could also implement another transformation [71]). First, note that:

$$(i)\ T_\mu (A_\rho - H_\mu L_o C_\rho) T_\mu^{-1} = \frac{1}{\mu} A_o, \quad (ii)\ T_\mu B_\rho = B_\rho,$$

$$\text{and} \quad (iii)\ \dot{T}_\mu T_\mu^{-1} = \frac{\dot{\mu}}{\mu} \Delta,$$

where $A_o := A_\rho - L_o C_\rho$ and $\Delta := \text{diag}(-I_{4\times 4},\ 0_{4\times 4}) \in \mathbb{R}^{8\times 8}$. Then, subtracting (4.1) from (2.4) and applying the above relationships (i), (ii) and (iii), the dynamics of $\tilde{x}$ in the new coordinates $\hat{x}_1$ (4.5) is given by:

$$\mu \dot{\zeta} = [A_o + \dot{\mu}(t)\Delta]\zeta + B_\rho [\mu \nu], \tag{4.6}$$

where

$$\nu := (k_p - k_p^n) u + k_p d, \tag{4.7}$$

and

$$\dot{\mu}(t) = -\frac{\mu^2}{\bar{\mu}} \left[\frac{\partial \psi_\mu}{\partial \omega} \dot{\omega} + \frac{\partial \psi_\mu}{\partial t} \right]. \tag{4.8}$$

The HGO gain ($H_\mu L_o$) is inversely proportional to the small parameter μ, allowed to be time-varying.

The Adapting Function ψ_μ

The adapting function $\psi_\mu(\omega(t),t)$ used in the time-varying parameter $\mu(t)$ defined in (4.3), can assume different forms depending on the choice of the signal $\omega(t)$ and the available information about the plant.

As an example, consider the following cases:

From a practical point of view : the adapting function ψ_μ can be chosen in order to allow local stability (or only convergence) properties for the closed-loop control system. Moreover, one can select a time-varying adapting function ψ_μ to assure an acceptable level of noise in the control signal while keeping a good transient for the output tracking error.

1. **The system states can be assumed bounded**: The plant state, in particular the unavailable state x_2, is uniformly bounded. Such assumption of the state boundedness is true, for example, when (2.4) is BIBS stable, and the control input is bounded. Moreover, by considering that the acceleration ($\dot{x}_2$) in the mechanical system is bounded by a known constant, then a constant upper bound for the velocity x_2 can be found by using the "dirty derivative":

$$\eta := \frac{\tau}{\tau s + 1} y \,. \tag{4.9}$$

   Indeed, by noting that

$$x_2 = \eta + \frac{\tau}{\tau s + 1} \dot{x}_2 \,, \tag{4.10}$$

   one can obtain the following norm bound

$$|x_2| \leq |\eta| + \mathscr{O}(\tau)\,|\dot{x}_2| \,. \tag{4.11}$$

   In this case, we can use this rough estimate for $\dot{x}_2$ and less conservative estimates for the terms depending on y, so that $\omega(t)$ can be implemented.

2. **Signal-to-Noise Ratio in $|u|$ $\times$ Tracking Error Norm**: By using some measurement of the amount of noise in the control signal, for example, the Signal-to-Noise Ratio (SNR), the adapting function can be implemented as a function of the SNR and the tracking error, so that μ increases when the SNR in the control effort increases and μ decreases when the tracking error norm increases. This can be accomplished, for example, by defining a cost function depending on the control signal-to-noise ratio and the output tracking error, so that the time-varying μ reaches an optimum value.

From a theoretical point of view: the adapting function ψ_μ can be chosen in order to allow global/semi-global stability (or only convergence) properties for the closed-loop control system.

1. **Norm Observability**: The plant (2.4)–(2.4) admits a norm observer which provides an upper bound for the plant state norm by using only available signals: plant input (u) and plant output (y). In this case, global or semi-global results could be obtained when, for example, a sliding mode based control is employed, as in [50].

   More precisely, a norm observer for system (2.4)–(2.4) is a m-order dynamic system of the form:

   $$\tau_1 \dot{\omega}_1 = -\omega_1 + u\,, \tag{4.12}$$
   $$\tau_2 \dot{\omega}_2 = \gamma_o(\omega_2) + \tau_2 \varphi_o(\omega_1, y, t)\,, \tag{4.13}$$

   with states $\omega_1 \in \mathbb{R}$, $\omega_2 \in \mathbb{R}^{m-1}$ and positive constants τ_1, τ_2 such that for $t \in [0, t_M)$: (i) if $|\varphi_o|$ is uniformly bounded by a constant $c_o > 0$, then $|\omega_2|$ can escape at most exponentially and there exists $\tau_2^*(c_o)$ such that the ω_2-dynamics is BIBS (Bounded-Input-Bounded-State) stable w.r.t. φ_o for $\tau_2 \leq \tau_2^*$; (ii) for each $x(0), \omega_1(0), \omega_2(0)$, there exists $\bar{\varphi}_o$ such that

   $$|x(t)| \leq \bar{\varphi}_o(\omega(t), t) + \pi_o(t)\,, \quad \omega := [\omega_1 \ \omega_2^T \ y]^T\,, \tag{4.14}$$

   where $\pi_o := \beta_o(|\omega_1(0)| + |\omega_2(0)| + |x(0)|)e^{-\lambda_o t}$ with some $\beta_o \in \mathscr{K}_\infty$ and positive constant λ_o.

2. **Global Stability Properties**: when the class of plants are such that a norm observer can be implemented, then **global** results can be achieved via Output Feedback Sliding Mode (OFSM) control, as in [50]. This is the case when, for example, the Coriolis term can be neglected ($C(x_1, x_2)x_2 \equiv 0$).

3. **Semi-Global Stability Properties**: it is not a restrictive assumption consider the existence of a class $\mathscr{K}_\infty$ function $\Psi(\cdot)$ and a positive constant k_ψ such that

   $$\|d(x,t)\| \leq \Psi(\|x\|) + k_\psi\,,$$

   $\forall x$ and $\forall t$. In other words, the disturbance can always be norm bounded afinelly in the state norm, when it is norm bounded in the second argument. Thus, given $R > 0$ and $0 < R_0 < R$, then for some $t^* \in (0, t_M)$ and $\|x(0)\| < R_0$ one has $\|x(t)\| < R$ for $t \in [0, t^*)$. Assume $t \in [0, t^*)$. Since the nonlinear terms in the robot dynamic equation are usually assumed sufficiently smooth and locally Lipschitz in its arguments, then $\Psi(\cdot)$ can be chosen locally Lipschitz in it argument. In addition, while

$t \in [0, t^*)$, the state x is bounded by the arbitrary constant R. Thus, one has that the following upper bound holds $\Psi(\|x\|) \leq \kappa(R)\|x\|$, where $\kappa(\cdot)$ being of class $\mathscr{K}$. For a given R, $\kappa(R)$ is a positive constant which increases as $R \to +\infty$, but is not necessarily unbounded. By noting that R depends on the initial condition (due to R_0), then only **semi-global** stability properties follows. In fact, this semi-global result can be obtained via a particular case of the OFSM control given in [50]. This is the case when, for example, the Coriolis term can not be neglected ($C(x_1, x_2)x_2 \neq 0$). Additionally, [72] and [73] also proved that global stability properties may be achieved in the presence of the Coriolis terms using a PD.

One Particular Design for ψ_μ

In this paper, we are focused in the following particular choice for time varying HGO parameter $\mu(t)$ where noise energy in the control signal and tracking error are taken into account:

$$\mu(t) := \frac{\alpha \mathscr{N}\{u\}}{1 + \beta|e|} = \frac{\bar{\mu}}{1 + \psi_\mu(\omega(t), t)}, \tag{4.15}$$

where α, β are positive design constants, $\mathscr{N}\{u\} > 0$ is the noise energy presented in the control effort $u(t)$ and e is the tracking error. Note that, this choice fits the general format (4.3) with

$$\psi_\mu(\omega(t), t) = [(1 + \beta|e|)\bar{\mu} - \alpha \mathscr{N}\{u\}]/(\alpha \mathscr{N}\{u\})$$

and $\bar{\mu}$ big enough to assure that $\psi_\mu(\omega(t), t) > 0$.

Noise Energy and Noise Measurement

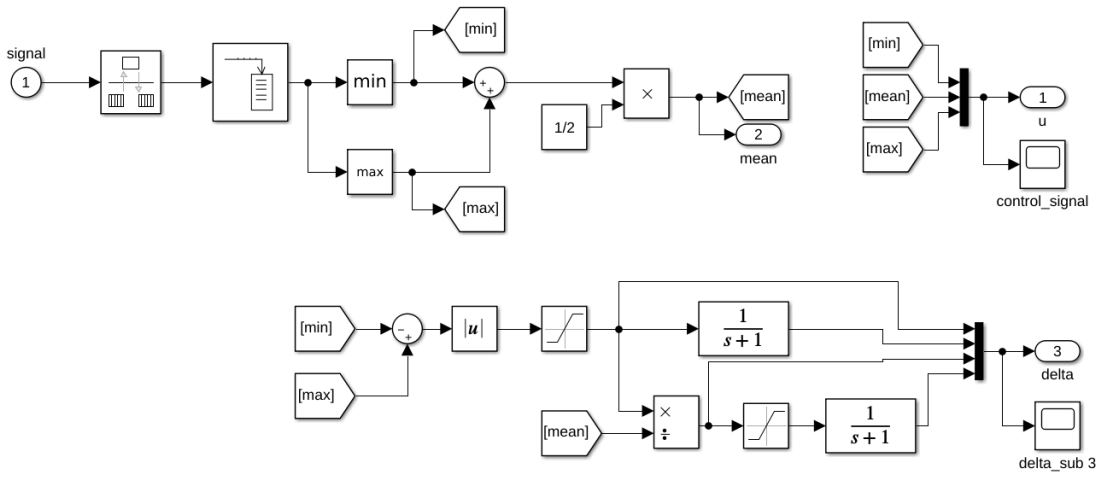

Figure 4.1: Noise estimator inner block. Calculates four possible values.

The noise energy is obtained by filtering the norm of the difference between the upper

U^+ and lower U^- envelopes of the control signal u, which is contaminated by noise. This scheme is depicted in Figure 4.1. Another approach divides this value by a mean U_{mean} from the difference between the envelopes.

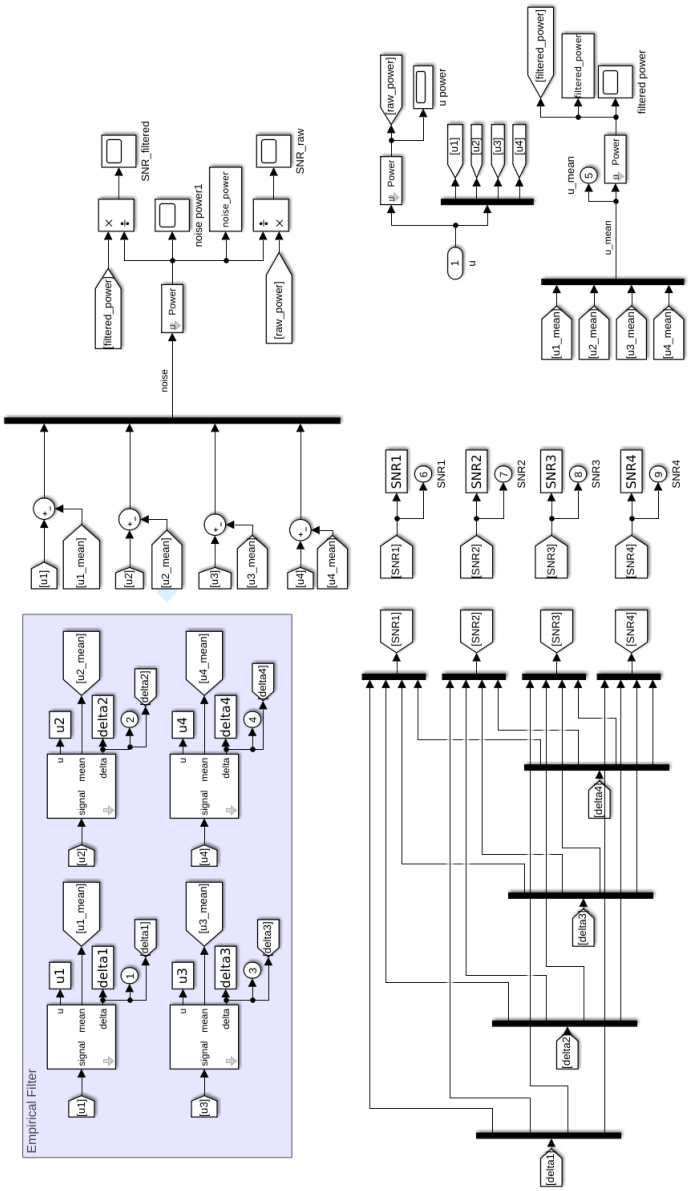

Figure 4.2: Noise estimator block diagram. The blocks inside the rectangular area implement the estimator approaches.

According to Figure 4.1, the noise energy $\mathscr{N}\{u\}$ could be defined as four distinct equations:

$$\mathscr{N}\{u(t)\} := \begin{cases} \left|U^+(t) - U^-(t)\right|, \\ \\ \frac{1}{\tau_n s+1}\left|U^+(t) - U^-(t)\right|, \\ \\ \frac{\left|U^+(t) - U^-(t)\right|}{U_{mean}}, \\ \\ \frac{1}{\tau_n s+1}\frac{\left|U^+(t) - U^-(t)\right|}{U_{mean}} \end{cases} \tag{4.16}$$

where $\tau_n > 0$ is a design constant and $|U^+(t) - U^-(t)|$ may be subject to saturation. Several on-line methodologies for estimation of noise energy in a available signal (Signal-to-Noise Ratio) can be found in the literature. A fair comparison is left for a future work.

Note that, in this case, the time derivative $\frac{d\mathscr{N}\{u(t)\}}{dt}$ can be norm bounded if the noise energy is norm bounded, which is reasonable to assume.

After testing the four possibilities presented in (4.16), the formulation

$$\mathscr{N}\{u(t)\} := \frac{1}{\tau_n s+1}\left|U^+(t) - U^-(t)\right|,$$

was empirically chosen due to its smoothness compared to the others.

4.2 Output Feedback CTPID Control

As the observer has already been introduced, this section focus on implementing it with different gains in a closed-loop system. The simulation using fixed gains serves as a way to compare their performances with the proposed variable gain in the presence of perturbations.

By recalling that matrices $D_n(q)$, $C_n(q,\dot{q})$, and $G_n(q)$ are known nominal values from $D(q)$, $C(q,\dot{q})$, and $G(q)$, the control signal required for this task is now designed as:

$$u(t) := D_n(\hat{x}_1)\tau + C_n(\hat{x}_1,\hat{x}_2)\hat{x}_2 + G_n(\hat{x}_1), \tag{4.17}$$

$$\tau := \ddot{q}_d + K_p e(t) + K_d(\dot{q}_d - \hat{x}_2) + K_i\int_0^t e\,dt, \tag{4.18}$$

where $\hat{x}_2$ is the estimate for x_2 obtained from the HGO. The gains are designed in order to match the equations used in (3.5), resulting in (3.8).

4.3 Simulation Results

This section shows simulation results from an output-feedback closed-loop with the same PID and computed torque controller parameters from Chapter 3. The tracking/observation performance is undermined by parametric uncertainties (4%) and noise injection (1×10^{-6} W/Hz). However, differently than Section 3.2, the feedback uses the estimates $\hat{x}_1$ and $\hat{x}_2$ provided by the HGO.

The closed-loop system simulation aims to compare tracking and observation accuracy when using different values for parameter μ (0.0004, 0.001, 0.0019, and variable gain). The controller performance criteria for tracking are the same as in Section 3.2.

A desirable observer performance requires an estimation error convergence to zero or a small residual according to values found in the literature [34][9].

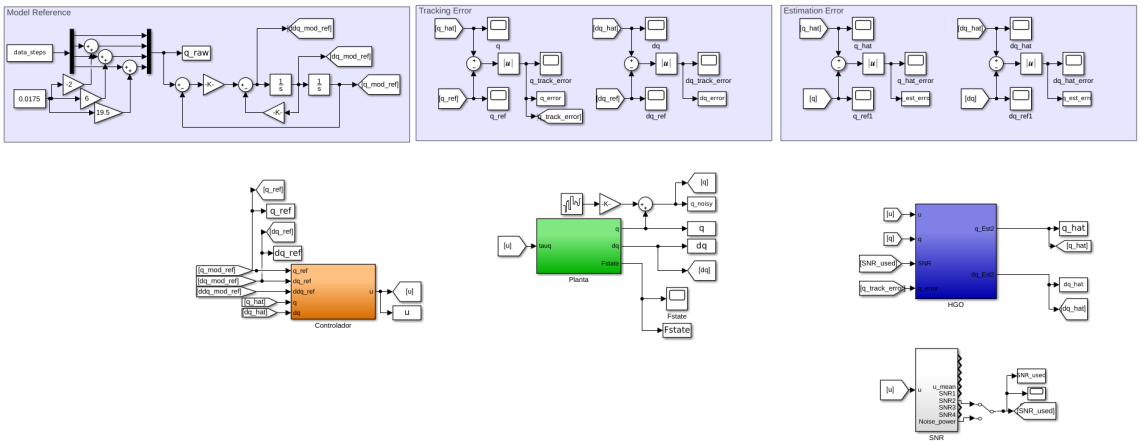

Figure 4.3: HGO simulation.

Plant	
$x_1(0) =$	$\begin{bmatrix} 0 & 24.99 & 0 & 0 \end{bmatrix}^T$
$x_2(0) =$	$\begin{bmatrix} 0 & 0 & 0 & 0 \end{bmatrix}^T$
Reference Signal	
$x_1(0) =$	$\begin{bmatrix} 0.0216 & 30.51 & -1.46 & -2.76 \end{bmatrix}^T$
$x_2(0) =$	$\begin{bmatrix} 0.3342 & 16.83 & -161.82 & -38.92 \end{bmatrix}^T$
Observer	
$x_1(0) =$	$\begin{bmatrix} 0 & 0 & 0 & 0 \end{bmatrix}^T$
$x_2(0) =$	$\begin{bmatrix} 0 & 0 & 0 & 0 \end{bmatrix}^T$

Table 4.1: Initial conditions from Prosthesis Plant, Reference Model and Observer

One of the simulations is conducted under fixed μ parameters. The next test shows the results when implementing the observer with a variable μ parameter, whose adaptation is described in Section 4.1.2.

Gain	Value
k_p	2337
k_d	82.9
k_i	23,813

Table 4.2: PID control parameters

Tracking Error				
μ	e_1 (m)	e_2 (deg)	e_3 (deg)	e_4 (deg)
0.0004	0.0007	0.0660	0.2156	0.1137
0.0010	0.0026	0.0683	0.2301	0.1294
0.0019	0.0065	0.0746	0.2521	0.1482

Joint Position Estimation Error				
μ	$\tilde{x}_1$ (m)	$\tilde{x}_2$ (deg)	$\tilde{x}_3$ (deg)	$\tilde{x}_4$ (deg)
0.0004	0.00002	0.0014	0.0014	0.0014
0.0010	0.0001	0.0009	0.0010	0.0010
0.0019	0.0003	0.0011	0.0014	0.0013

Joint Velocity Estimation Error				
μ	$\tilde{x}_5$ (m/s)	$\tilde{x}_6$ (deg/s)	$\tilde{x}_7$ (deg/s)	$\tilde{x}_8$ (deg/s)
0.0004	0.1006	6.2534	6.4175	6.4550
0.0010	0.1348	1.6847	1.8512	1.8582
0.0019	0.2681	1.1532	1.4586	1.3798

Table 4.3: Observer/Controller performance in steady-state with 4% parametric uncertainties over 1 step of walking using 3 HGO μ gains.

Figure 4.3 shows the block diagram from the simulation, comprised by Model Reference, generating the joint reference signal and its derivatives, the prosthesis plant block in orange, the PID with computed torque controller block in green, the HGO block in purple and a noise estimator block in white. The closed-loop system's initial conditions and required parameters are shown in 4.1 and 4.2, respectively.

The expected simulation result is that higher values of parameter μ means higher tracking and estimation errors, and noise rejection in the control signal. Therefore, lower μ means better estimation and tracking error, but noisier effort signal.

4.3.1 Fixed HGO

This subsection shows simulation results using three different fixed μ parameter values, which are used in an HGO according to Section 4.1.1.

Figure 4.4 (a) - (f) shows the overall tracking and estimation performance for the hip vertical displacement joint obtained using three different observer gains. According to Figures 4.4 (a), (c), and (e), the lowest value of parameter μ produces the best tracking result. The simulation with the highest HGO parameter shows the worst tracking perfor-

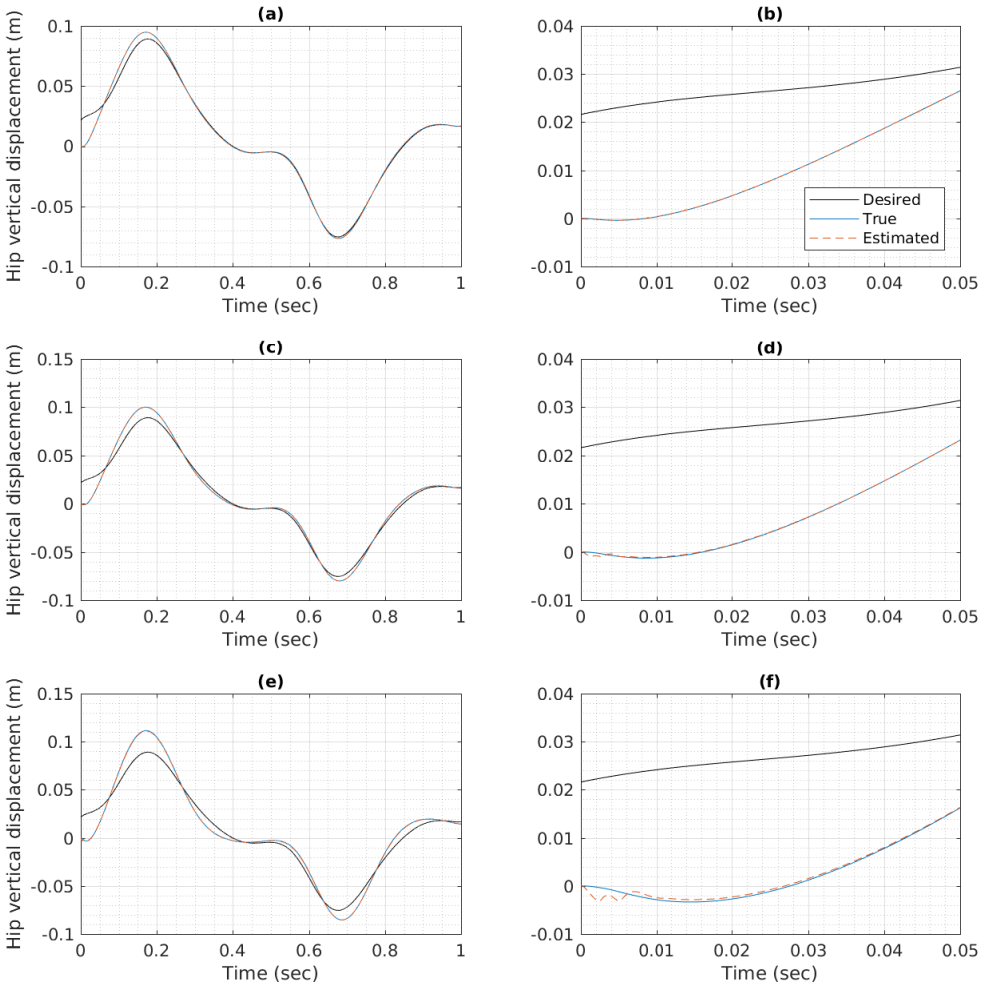

Figure 4.4: {Fixed μ} Simulation results from hip vertical displacement in one gait cycle. (a) performance with $\mu = 0.0004$, (b) performance in the first 50ms, (c) performance with $\mu = 0.001$, (d) performance in the first 50ms, (e) performance with $\mu = 0.0019$, (f) performance in the first 50ms.

mance. This result is also shown in Table 4.3. From visual inspection in Figure 4.4 (a) and (c), it is possible to infer that the transient state happens until 300ms approximately.

Figure 4.5 (a) - (d) shows the position and velocity estimation results. Figure 4.5 (a) and (c) depicts a peaking error of 0.003 mm and 4 m/s while in transient period of $\hat{x}_1$ and $\hat{x}_5$, respectively. It is possible to see in Figure 4.5 (b) that $\hat{x}_1$ reaches an estimation error of 0.5, 0.2, and lower than 0.1 mm in steady-state with μ equals to 0.0019, 0.001 and 0.0004, respectively. One may notice that the lower the μ parameter, the better the $\hat{x}_1$ estimation. In addition, $\hat{x}_5$ becomes more sensitive to noise. According to Table 4.3, the RMS observation errors for $\mu = [0.0004, 0.0010, 0.0019]$ is $[0.02, 0.1, 0.3]$ mm for $\hat{x}_1$ and $[0.1, 0.13, 0.27]$ m/s for $\hat{x}_5$.

The tracking error e_1 (in the first joint) is depicted in Figure 4.6. As expected, there

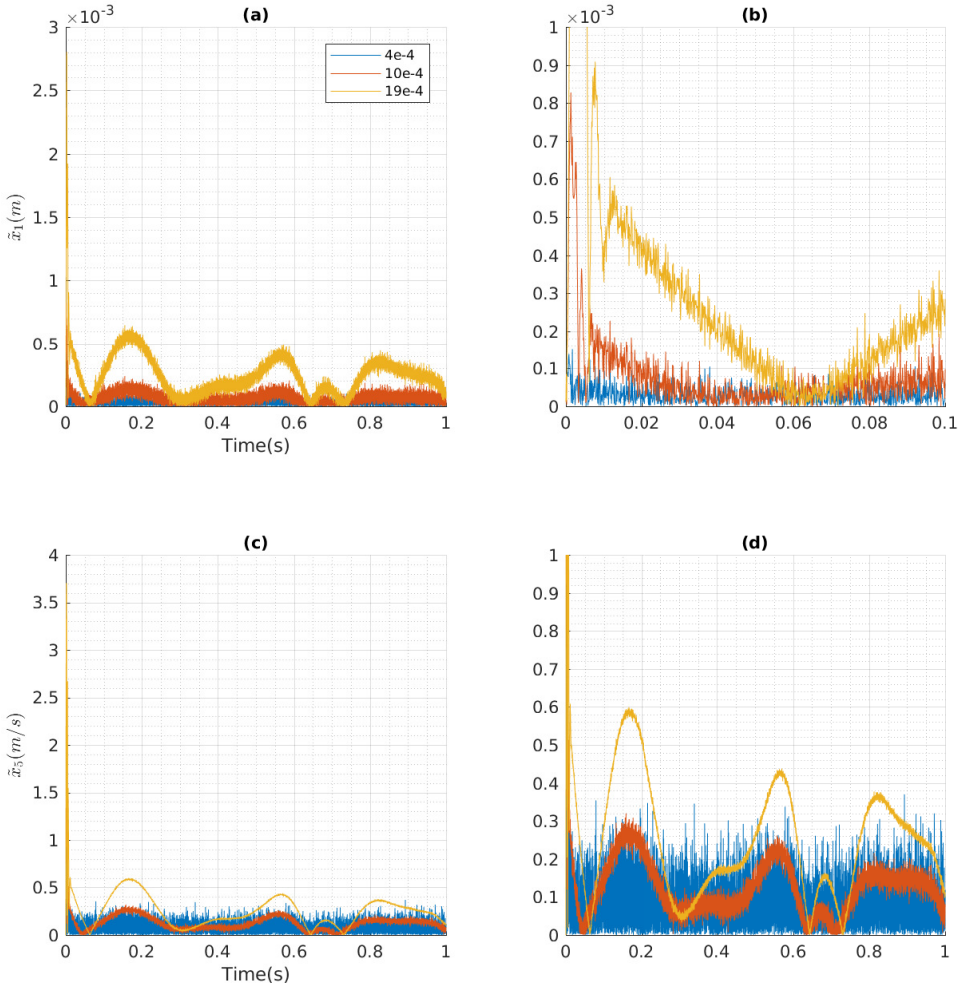

Figure 4.5: {Fixed μ} Simulation results from hip vertical displacement and velocity estimation errors. (a) estimation error from $\hat{x}_1$, (b) $\hat{x}_1$ with zoom in X and Y axis. (c) velocity estimation error from $\hat{x}_5$, (d) $\hat{x}_5$ with zoom in X and Y axis. Curves in blue, red, and yellow represent the result obtained using μ gain equals to 0.0004, 0.001, and 0.0019, respectively.

is a higher degradation in the closed-loop tracking accuracy when using higher observer parameter values. The system shows the worst performance when μ value is equal to 0.0019, presenting a steady-state tracking error lower than 12 mm. This results is almost twelve times worst than the maximum error value when μ equals to 0.0004.

Figures 4.7 (a) and (b) illustrates the effort signal to control joint q_1. The initial condition errors lead to high forces which reach the saturation levels of -4000 and 2000. The control signal stays between 1000 and -1500 N in a worst case scenario, or approximately -1000 and 300 with the highest observer gain. It is visible that higher μ parameter values are less sensitive to noise.

Additionally, one may notice that the lower the μ parameter, the closer state x_1 gets

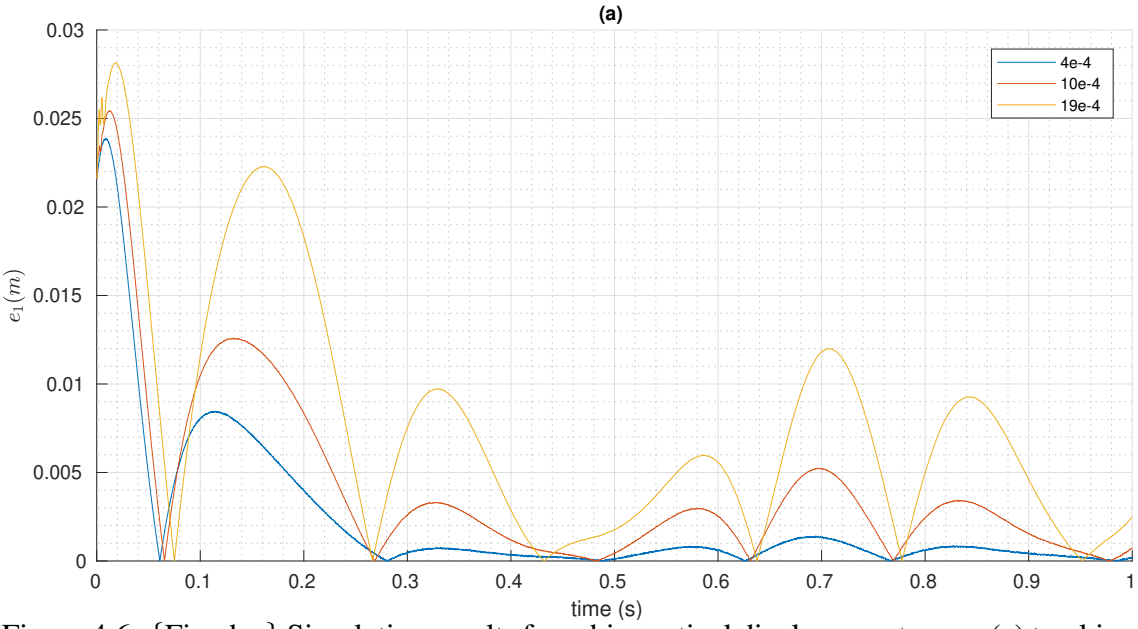

Figure 4.6: {Fixed μ} Simulation results from hip vertical displacement error. (a) tracking error e_1, (b) e_1 with zoom in X and Y axis. Curves in blue, red, and yellow represent the result obtained using μ gain equals to 0.0004, 0.001, and 0.0019, respectively.

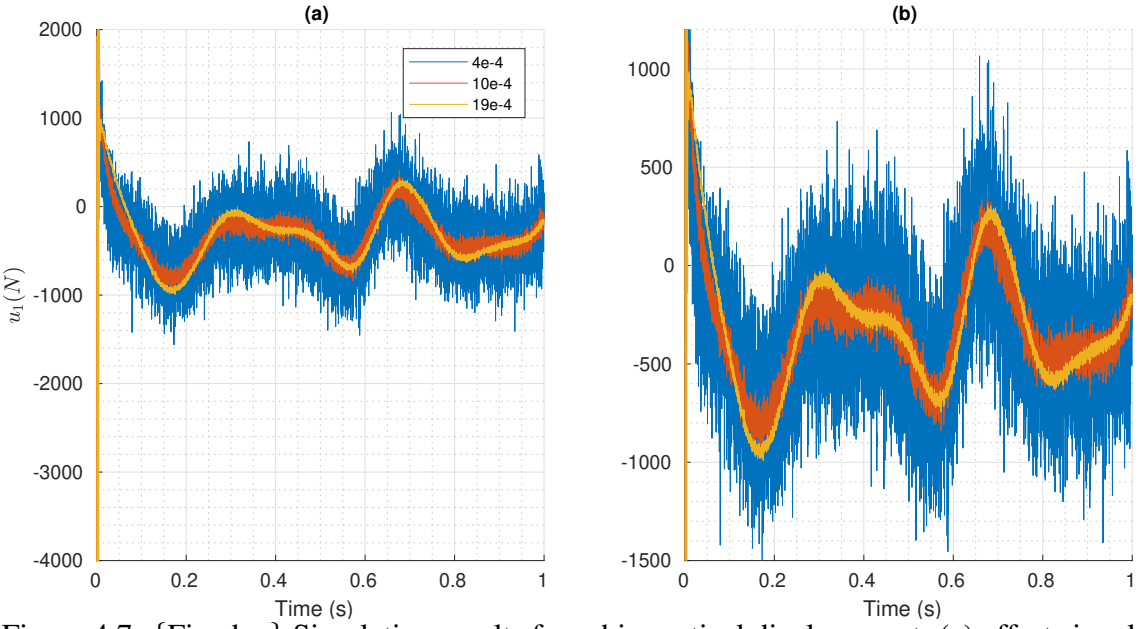

Figure 4.7: {Fixed μ} Simulation results from hip vertical displacement. (a) effort signal u_1, (b) effort signal with zoom in Y axis. Curves in blue, red, and yellow represent the result obtained using μ gain equals to 0.0004, 0.001, and 0.0019, respectively.

to q_d. This improvement in performance happens because the estimation error converges faster to zero and, therefore, x adrift less from q_d. In counterpart, the control signal becomes noisier.

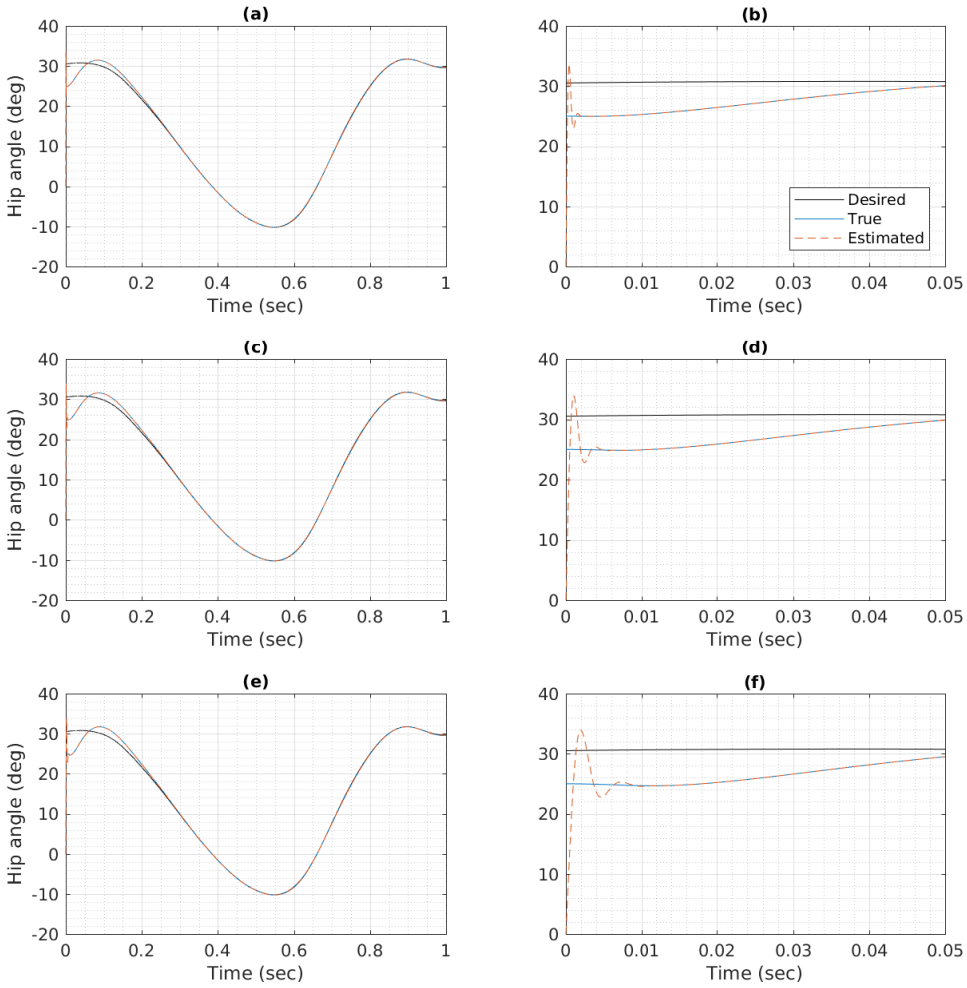

Figure 4.8: {Fixed μ} Simulation results from hip angular displacement in one gait cycle. (a) performance with $\mu = 0.0004$, (b) performance in the first 50ms, (c) performance with $\mu = 0.001$, (d) performance in the first 50ms, (e) performance with $\mu = 0.0019$, (f) performance in the first 50ms.

Figure 4.8 (a)-(f) shows the overall tracking and estimation performance for the hip extension and flexion joint. The peaking phenomenon is depicted in Figures 4.8(b), (d), and (f), due to higher initial condition errors than illustrated in Figure 4.4. Additionally, the joint position estimate converges faster to the desired value with the lowest parameter μ. The peaking phenomenon takes 2, 5 or 10 ms to settle depending on the gains.

Estimation errors $\tilde{x}_2$ and $\tilde{x}_6$ are shown in Figure 4.9. Despite presenting the peaking phenomenon, the estimation error is lower than 0.1 degree by 10 ms. This occurs due to the addition of a saturation on the input signal, otherwise the performance would be way worst. These saturation dependency is better explained later. According to Table 4.3 the best estimation accuracy of x_2 occurs when the μ is equal to 0.001, probably a further analysis would show that this noise power set a lower bound for the parameter μ above

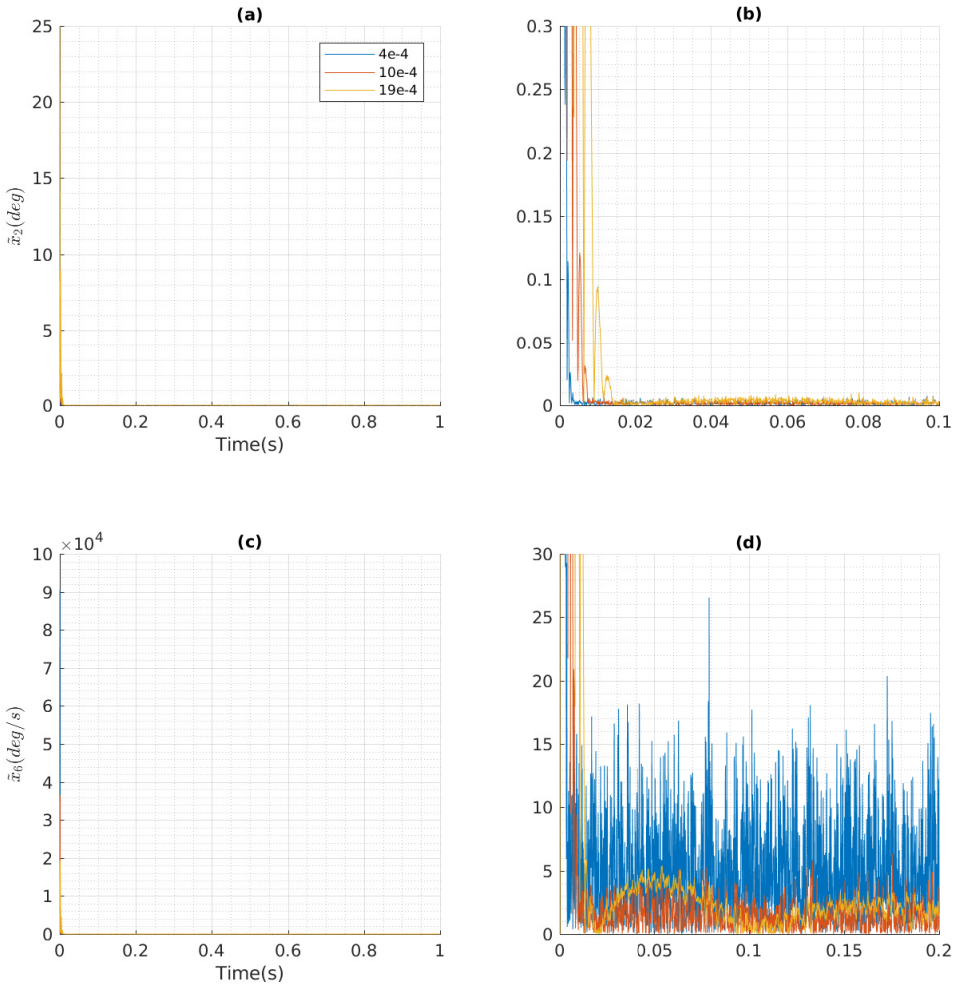

Figure 4.9: {Fixed μ} Simulation results from hip angular displacement estimation errors. (a) estimation error from $\hat{x}_2$, (b) $\hat{x}_2$ with zoom in X and Y axis. (c) estimation error from $\hat{x}_6$, (d) $\hat{x}_6$ with zoom in X and Y axis. Curves in blue, red, and yellow represent the result obtained using μ gain equals to 0.0004, 0.001, and 0.0019, respectively.

0.0004. Figure 4.9 (d) illustrates the noise measurement affecting the estimation accuracy. The lowest μ value should have the worst performance, but as shown in Table 4.3, $\tilde{x}_6$ is more accurate when μ is equal to 0.0019.

Figure 4.10 shows the tracking error results. It is possible to see in Figure 4.10(b) that e_2 in approximately 300 ms reaches the steady-state with tracking errors of lower than 0.2 deg.

Figure 4.11 illustrates the difference between μ values regarding the control signal. A saturation of 250 and -300 is applied to the system, and after this peak the joint requires effort signal ranging from -200 to 200. The lowest parameter value depicts the lowest noise sensibility, however presents the worst tracking accuracy (0.074 degrees RMS) according to Table 4.3.

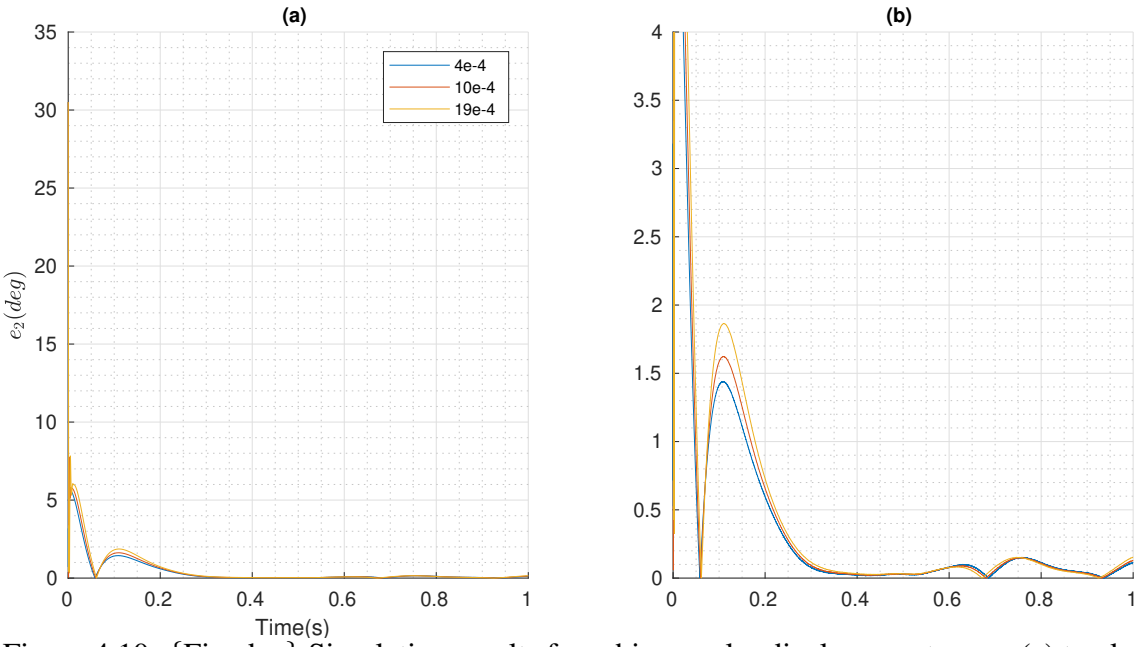

Figure 4.10: {Fixed μ} Simulation results from hip angular displacement error. (a) tracking error e_2, (b) e_2 with zoom in X and Y axis. Curves in blue, red, and yellow represent the result obtained using μ gain equals to 0.0004, 0.001, and 0.0019, respectively.

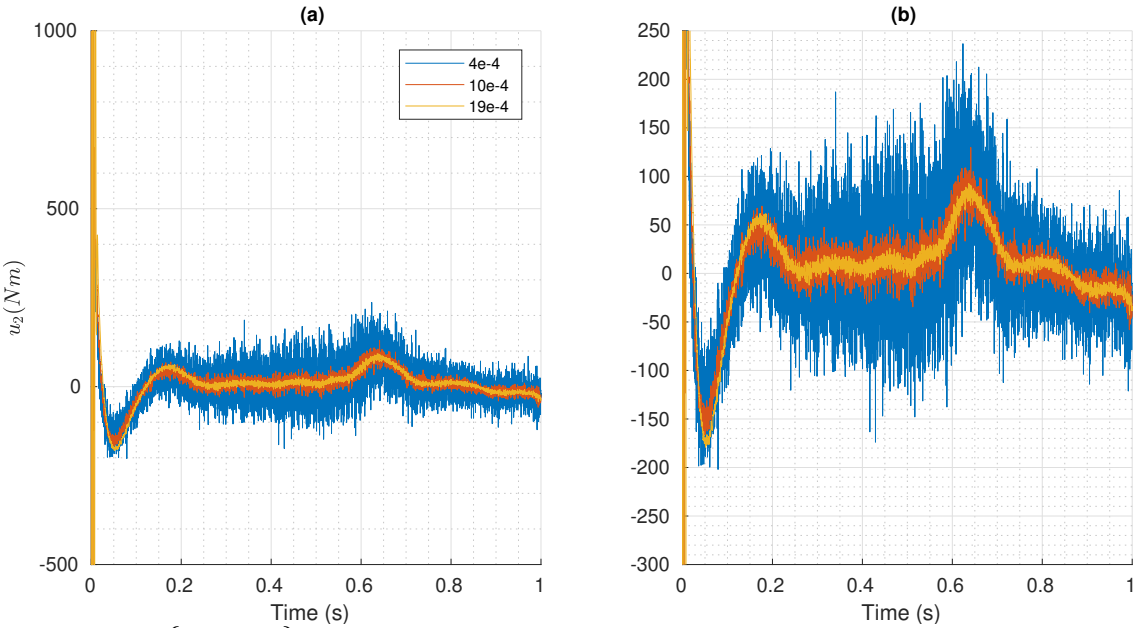

Figure 4.11: {Fixed μ} Simulation results from hip vertical displacement. (a) effort signal u_2, (b) effort signal with zoom in Y axis. Curves in blue, red, and yellow represent the result obtained using μ gain equals to 0.0004, 0.001, and 0.0019, respectively.

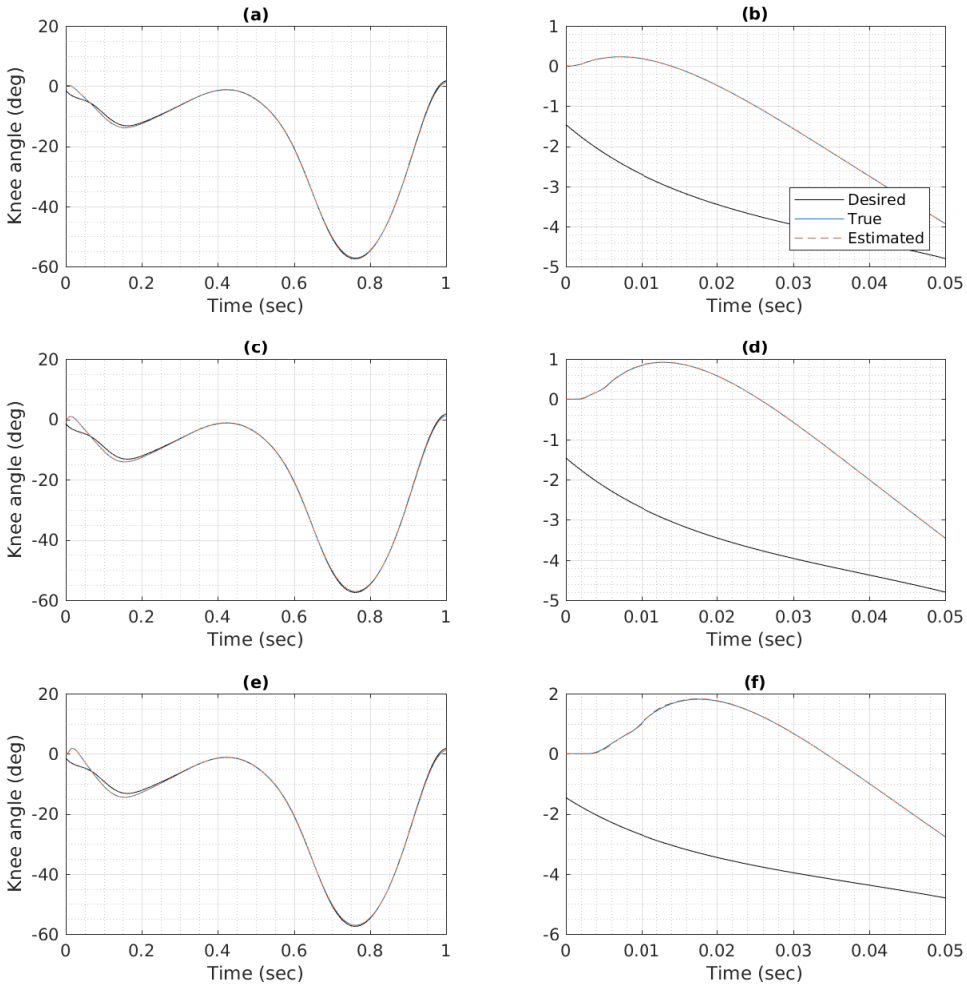

Figure 4.12: {Fixed μ} Simulation results from knee joint in one gait cycle. (a) performance with $\mu = 0.0004$, (b) performance in the first 50ms, (c) performance with $\mu = 0.001$, (d) performance in the first 50ms, (e) performance with $\mu = 0.0019$, (f) performance in the first 50ms.

Figure 4.12 shows the overall tracking and estimation performance for the knee extension and flexion joint obtained using as μ parameter values $[0.0004, 0.0010, 0.0019]$. This joint seems to show the same transient state duration than the previous ones, by visual inspection.

Figure 4.13 (a)-(d) shows the estimation errors $\tilde{x}_3$ and $\tilde{x}_7$. The measurement seems to affect equally the observer independently of μ value. According to Table 4.3, the lowest position estimation error is achieved when μ is equal to 0.001, and $\tilde{x}_7$ shows better results when the estimation is less sensitive to noise.

Figure 4.14 shows the tracking error performance of e_3 . It is possible to see in Figure 4.14(b) that e_3 reaches a tracking error lower than 0.75 in steady-state with oscillations from model uncertainties. The same observations apply here, that the higher parameter

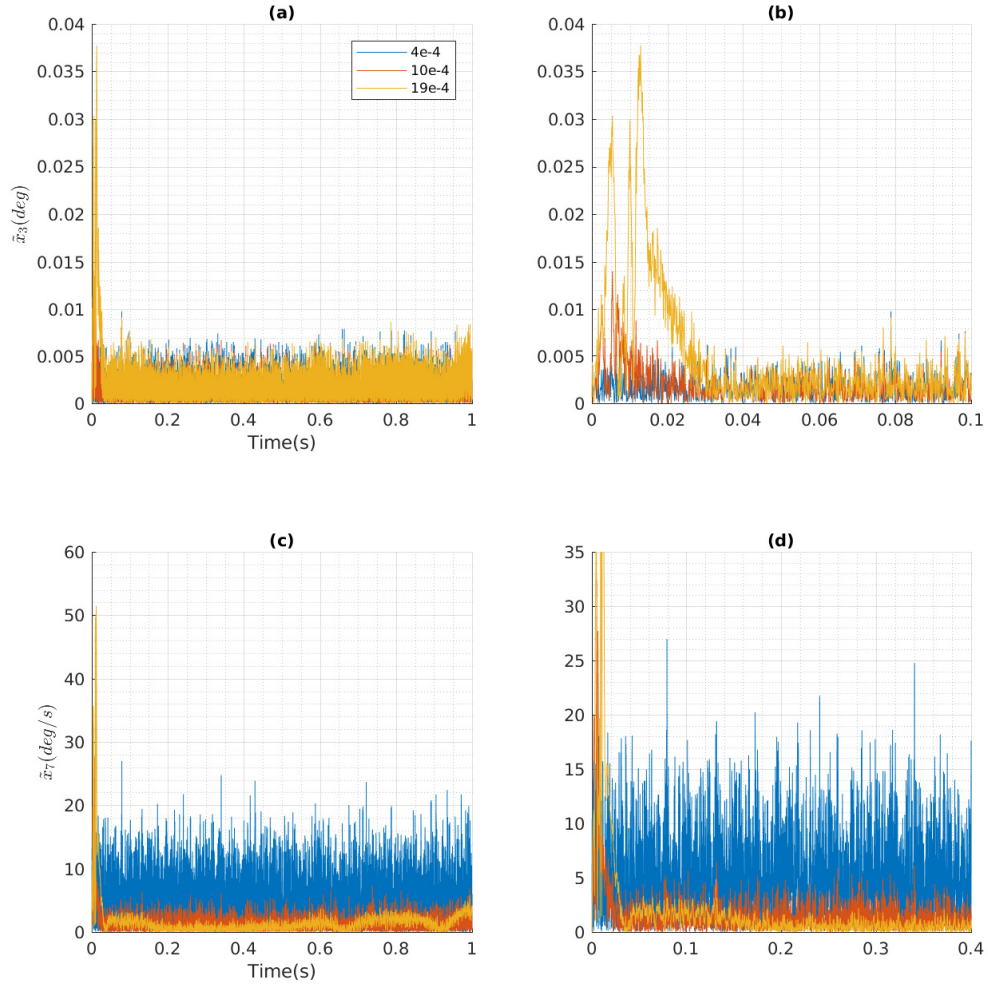

Figure 4.13: {Fixed μ} Simulation results from knee joint estimation errors. (a) estimation error from $\hat{x}_3$, (b) $\hat{x}_3$ with zoom in X and Y axis. (c) estimation error from $\hat{x}_7$, (d) $\hat{x}_7$ with zoom in X and Y axis. Curves in blue, red, and yellow represent the result obtained using μ gain equals to 0.0004, 0.001, and 0.0019, respectively.

μ values reject more noise, however shows worst tracking performance, while the lower noise shows better tracking performance, but is more sensitive to noise.

Interestingly, when considering tracking error, the results are as expected, lower μ values perform better than higher. This behavior was shown for linear systems by [55], were tracking error don't suffer from the same trade-off constraints as estimate error. The Table 4.3 shows RMS tracking error ranging from 0.21 to 0.25 degrees.

Figure 4.15 illustrates the difference between μ gains regarding the control signal. A saturation of -200 and 500 is applied to the system, and after this peak the joint requires effort signal ranging from -80 to 80 or from -40 to 20, if using the highest μ gain.

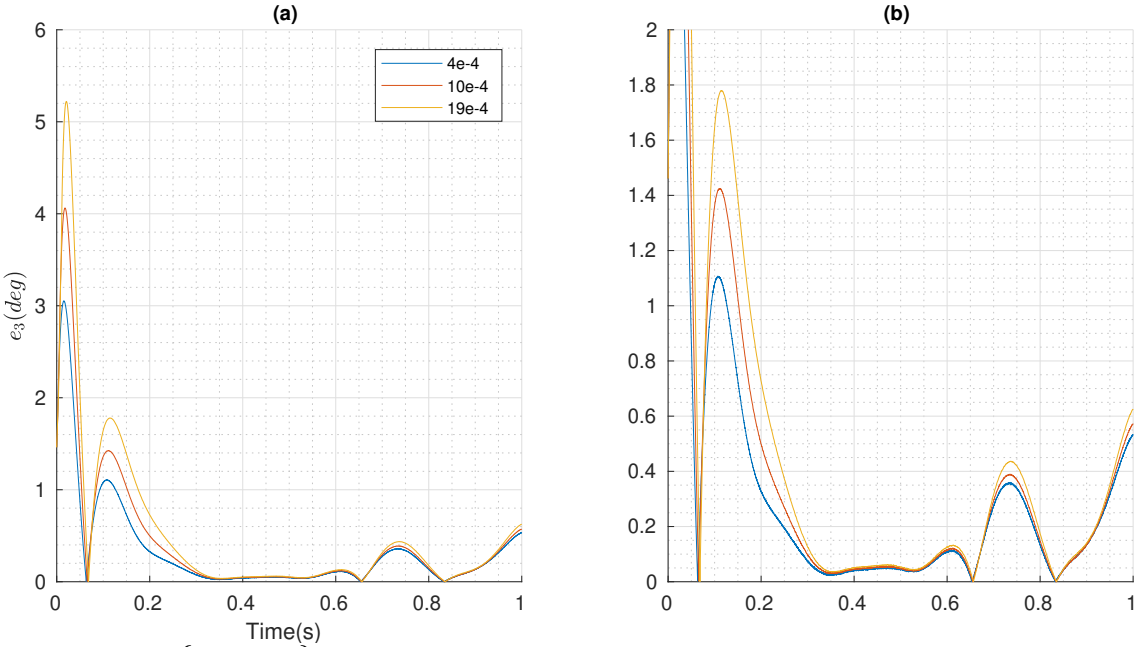

Figure 4.14: {Fixed μ} Simulation results from knee joint tracking error. (a) tracking error e_3, (b) e_3 with zoom in X and Y axis. Curves in blue, red, and yellow represent the result obtained using μ gain equals to 0.0004, 0.001, and 0.0019, respectively.

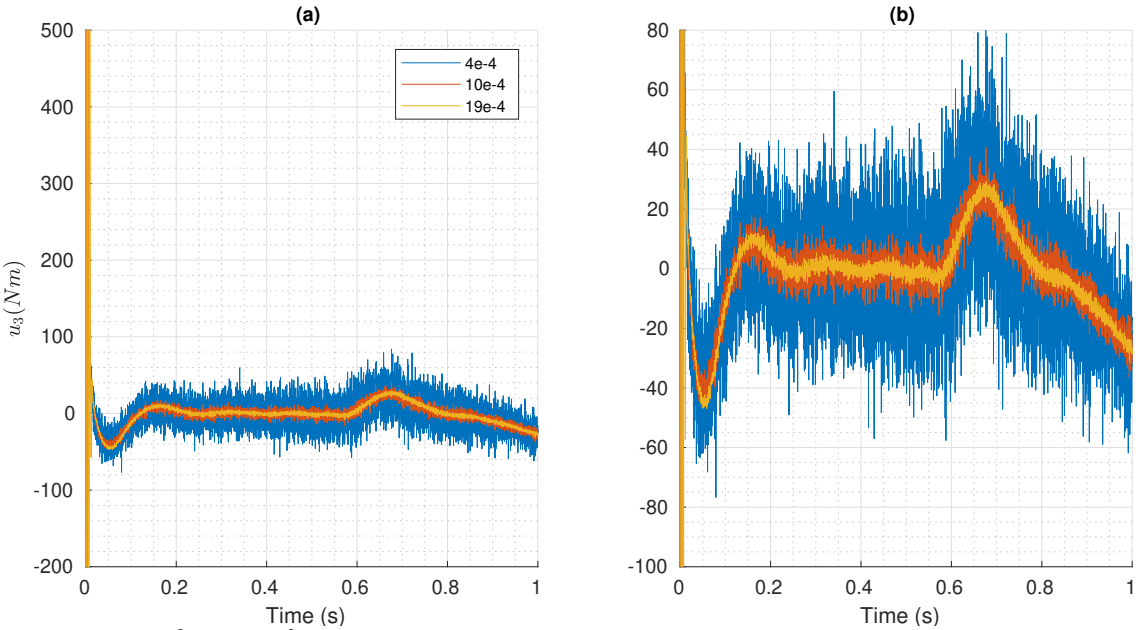

Figure 4.15: {Fixed μ} Simulation results from knee joint. (a) effort signal u_3, (b) effort signal with zoom in Y axis. Curves in blue, red, and yellow represent the result obtained using μ gain equals to 0.0004, 0.001, and 0.0019, respectively.

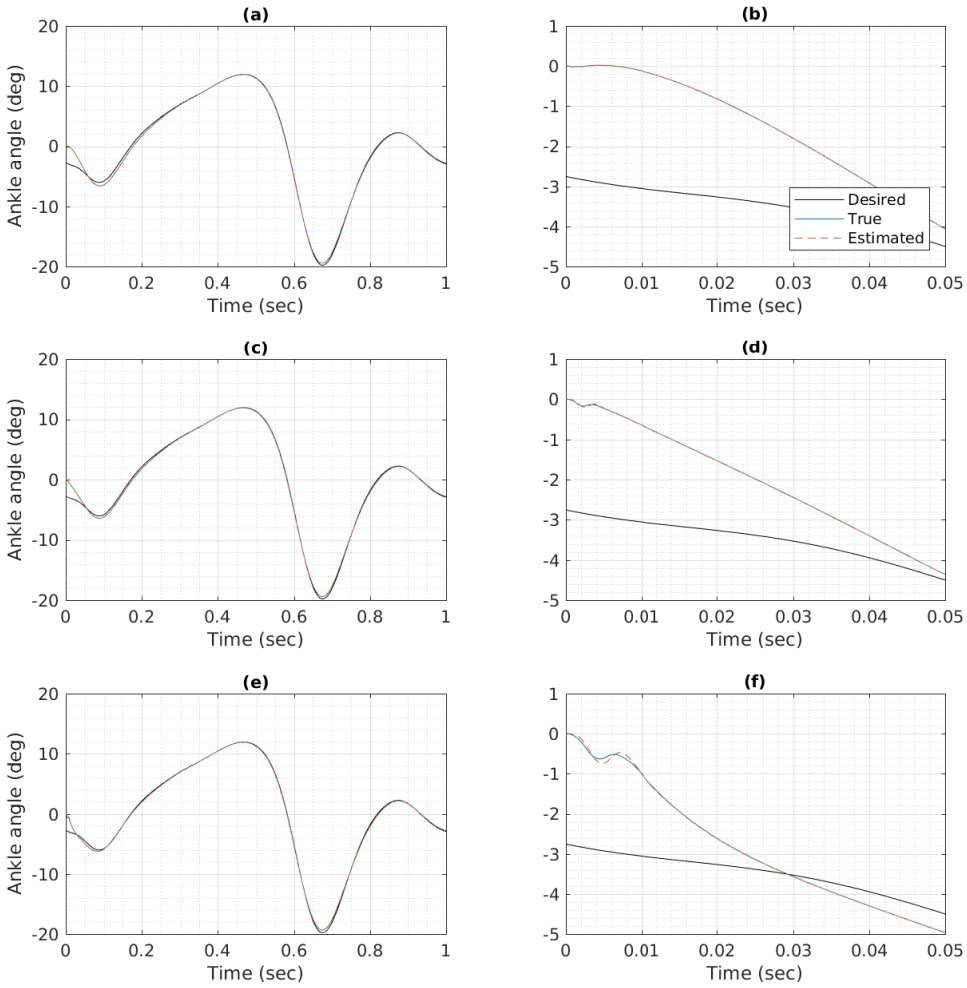

Figure 4.16: {Fixed μ} Simulation results from ankle joint in one gait cycle. (a) performance with $\mu = 0.0004$, (b) performance in the first 50ms, (c) performance with $\mu = 0.001$, (d) performance in the first 50ms, (e) performance with $\mu = 0.0019$, (f) performance in the first 50ms.

Figure 4.16 shows the overall tracking and estimation performance for the ankle plantarflexion and dorsiflexion joint. By visual inspection, the estimation transient state takes approximately 15 ms, while the tracking takes 300ms.

This joint shows similar results when compared to previous 2 ones. The best position estimation performance happens when μ is equal to 0.001 according to Table 4.3. While velocity estimation is better when μ value is the highest one. This result is also visible in Figure 4.17 (d), where the velocity estimation with this parameter is less sensitive to noise.

Figure 4.18 shows the tracking error results. It is possible to see in plot (b) that e_4 after 300 ms reaches a tracking errors lower than 0.5 deg. The RMS tracking error e_4 shows the expected results obtained in the previous joints.

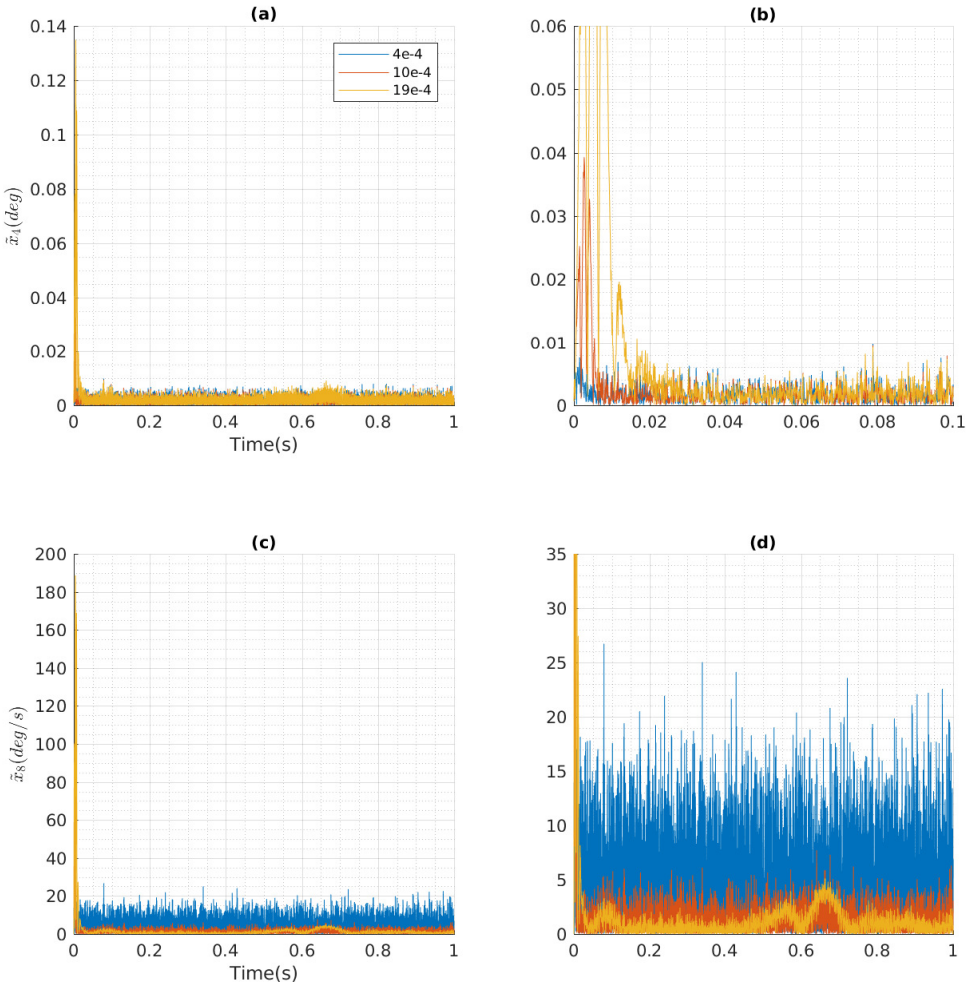

Figure 4.17: {Fixed μ} Simulation results from ankle joint estimation errors. (a) estimation error from $\hat{x}_4$, (b) $\hat{x}_4$ with zoom in X and Y axis. (c) estimation error from $\hat{x}_8$, (d) $\hat{x}_8$ with zoom in X and Y axis. Curves in blue, red, and yellow represent the result obtained using μ gain equals to 0.0004, 0.001, and 0.0019, respectively.

Figure 4.19 illustrates the difference between μ gains regarding the control signal. A saturation of 100 and -50 Nm is applied to the system, and after this peak the joint requires effort signal ranging from -6 to 8 Nm with the lowest observer gain and from -4 to 5 Nm using the highest one.

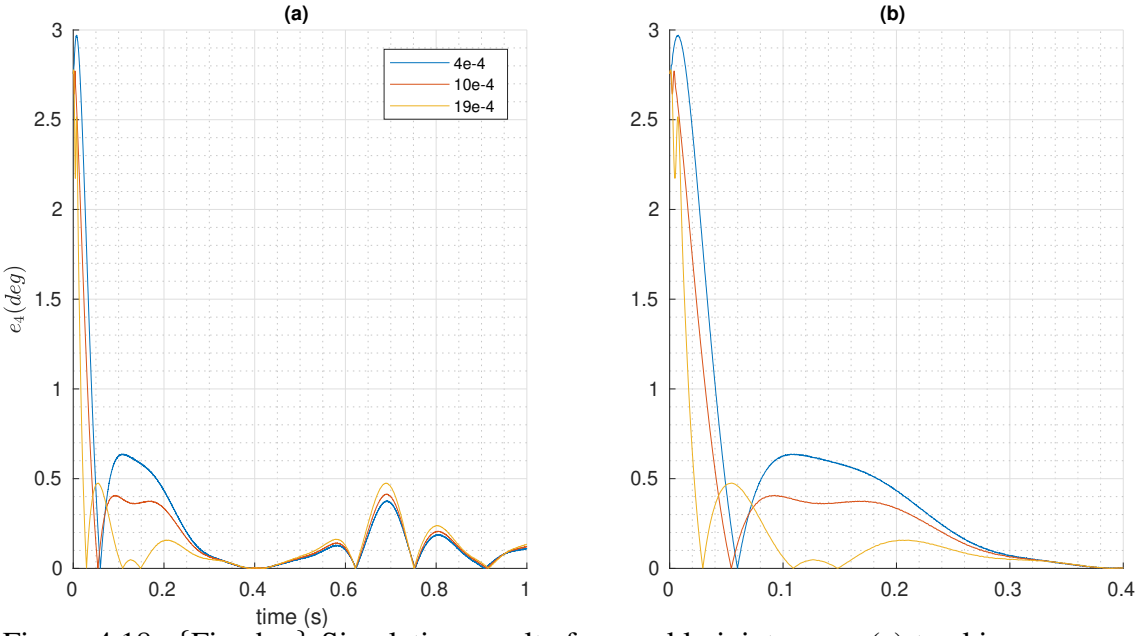

Figure 4.18: {Fixed μ} Simulation results from ankle joint error. (a) tracking error e_4, (b) e_4 with zoom in X and Y axis. Curves in blue, red, and yellow represent the result obtained using μ gain equals to 0.0004, 0.001, and 0.0019, respectively.

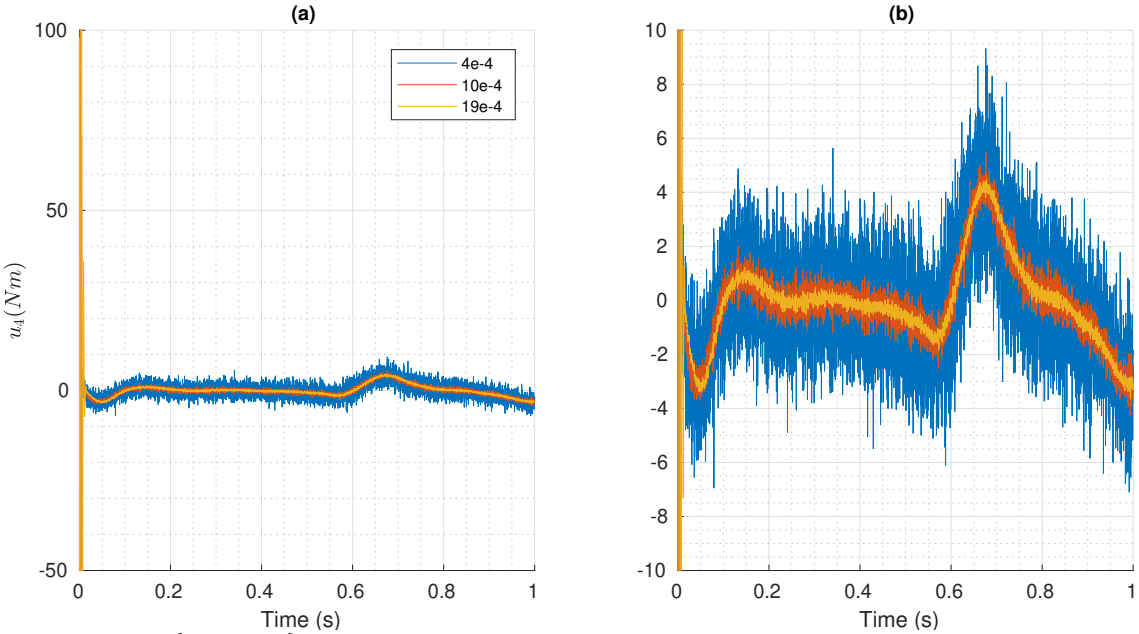

Figure 4.19: {Fixed μ} Simulation results from ankle joint. (a) effort signal u_4, (b) effort signal with zoom in Y axis. Curves in blue, red, and yellow represent the result obtained using μ gain equals to 0.0004, 0.001, and 0.0019, respectively.

Peaking Phenomenon

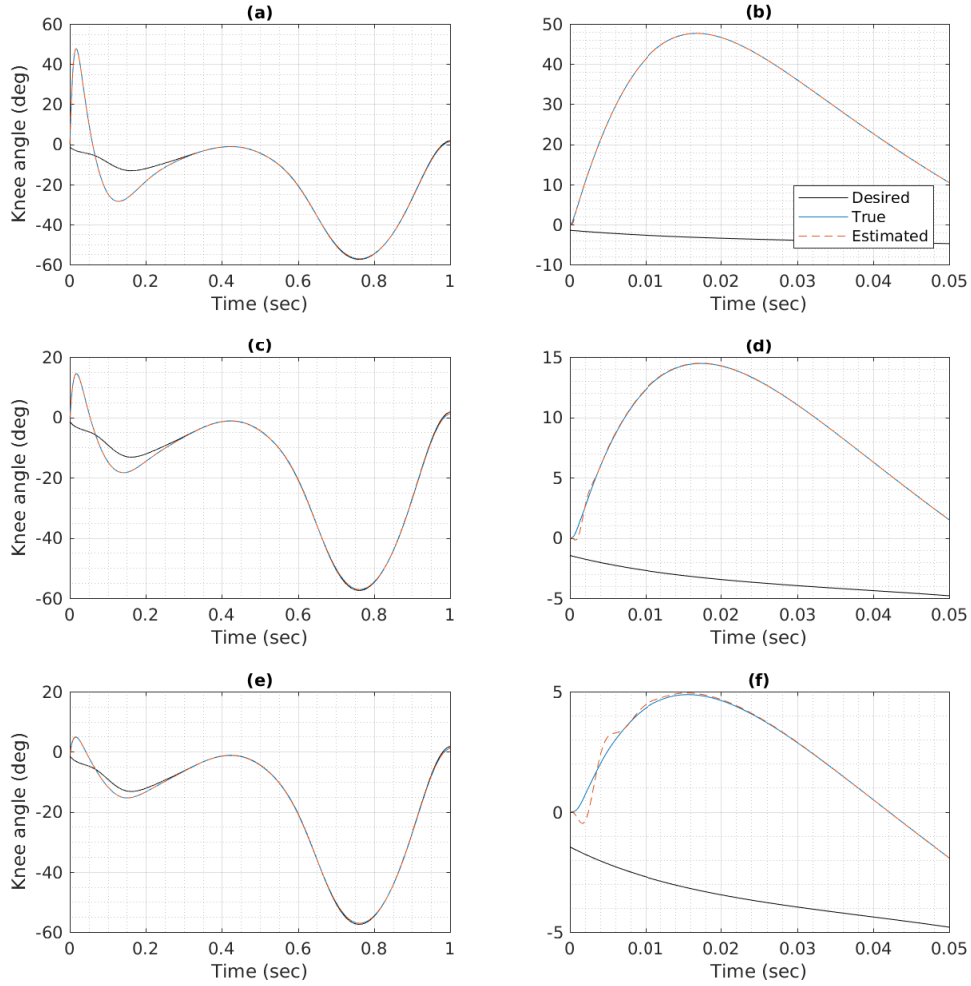

Figure 4.20: {Fixed μ} Simulation results from knee joint in the lack of saturation in the control signal in one gait cycle. (a) performance with $\mu = 0.0004$, (b) performance in the first 50ms, (c) performance with $\mu = 0.001$, (d) performance in the first 50ms, (e) performance with $\mu = 0.0019$, (f) performance in the first 50ms.

All the simulations so far used saturation on effort signal to prevent the propagation of initial condition error to F_a. The Figures 4.20- 4.23 show results for the knee joint in the absence of saturation. The tracking transient state is the same as obtained in with effort saturation, however the estimation transient state takes almost 20 ms when parameter μ is equal to 0.0019.

Figure 4.21 shows initial estimation errors 30 times higher for $\hat{x}_1$, and 80 times higher for $\hat{x}_2$ than in the presence of saturation, after 0.06 seconds the errors reach values similar to the ones found in Figure 4.13.

Figure 4.22 shows initial estimation errors 10 times higher for e than in the presence of saturation, after 0.3 seconds the errors reach values similar to the ones found in Fig-

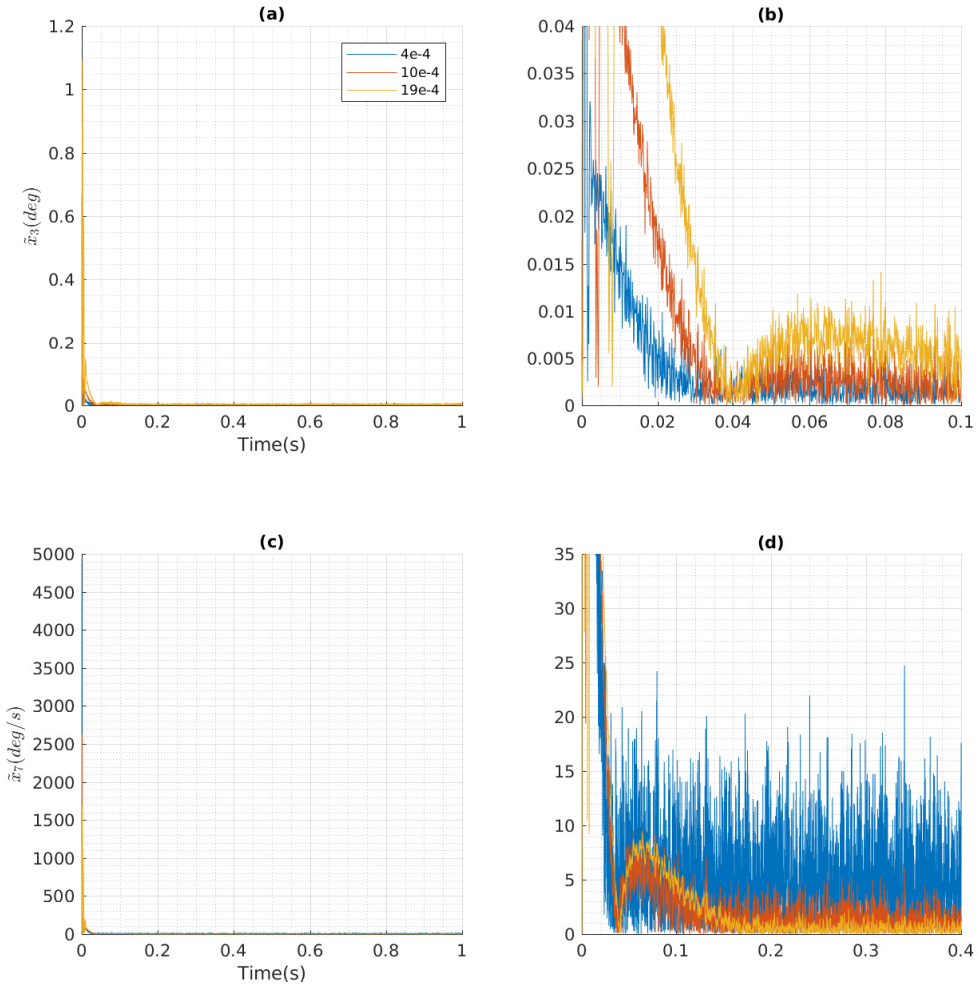

Figure 4.21: {Fixed μ} Simulation results from knee joint estimation estimation errors in the lack of saturation in the control signal. (a) estimation error from $\hat{x}_3$, (b) $\hat{x}_3$ with zoom in X and Y axis. (c) estimation error from $\hat{x}_7$, (d) $\hat{x}_7$ with zoom in X and Y axis. Curves in blue, red, and yellow represent the result obtained using μ gain equals to 0.0004, 0.001, and 0.0019, respectively.

ure 4.14. It is important to notice that usually the highest initial error occurs with the highest observer gain, but in the lack of saturation, the lowest gain is more sensitive to this error. After 0.4 seconds it is possible to see that the lowest gain also shows the lowest tracking error.

Figure 4.23 illustrates the effort signal without saturation, reaching for an instant the values of 50,000 and -18,000 Nm. But showing after that peak the same profile from Figure 4.15.

The lack of saturation undermine the system's transient performance, while requiring effort signals of unfeasible magnitudes. This problem lead to a finite escape time.

One way to mitigate this phenomenon is by adding saturation in the control signal,

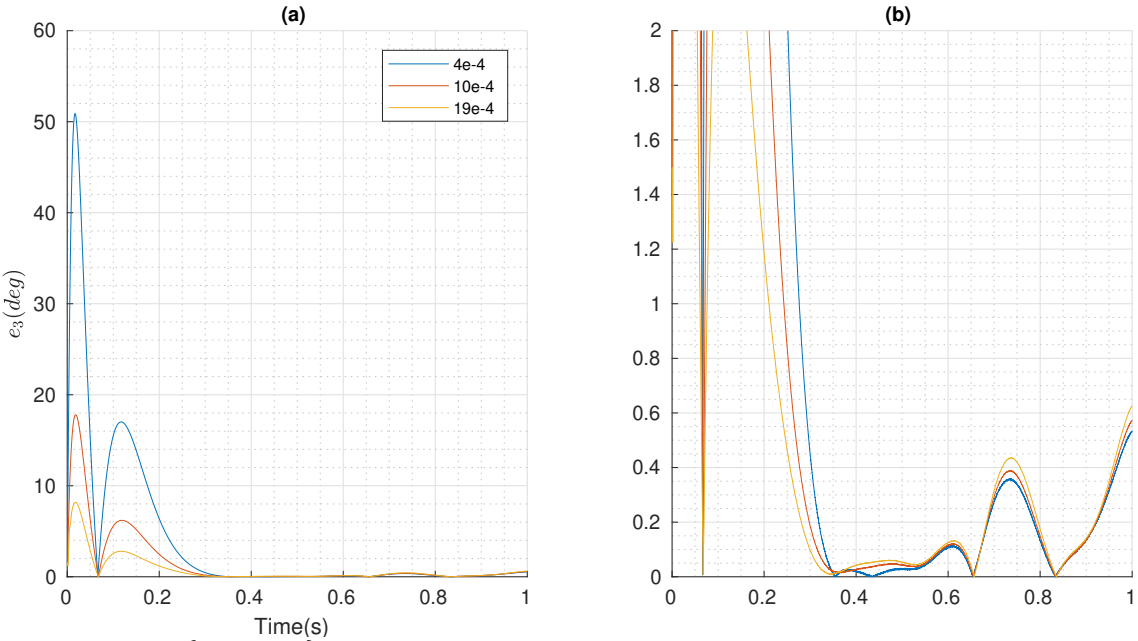

Figure 4.22: {Fixed μ} Simulation results from knee joint tracking error in the lack of saturation in the control signal. (a) tracking error e_3, (b) e_3 with zoom in X and Y axis. Curves in blue, red, and yellow represent the result obtained using μ gain equals to 0.0004, 0.001, and 0.0019, respectively.

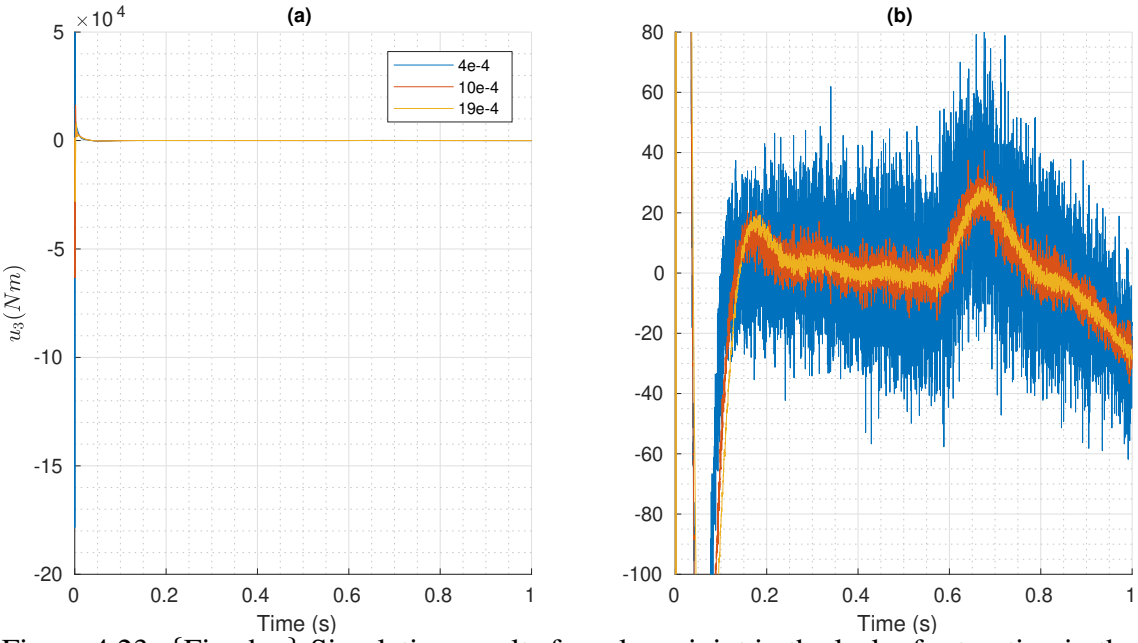

Figure 4.23: {Fixed μ} Simulation results from knee joint in the lack of saturation in the control signal. (a) effort signal u_3, (b) effort signal with zoom in Y axis. Curves in blue, red, and yellow represent the result obtained using μ gain equals to 0.0004, 0.001, and 0.0019, respectively.

which reduces the peaking phenomenon influence, as suggested in [74]. The saturation values are proportional to the maximum and minimum values obtained in state-feedback simulation.

4.3.2 Variable HGO

After the results obtained in the previous subsection, it is possible to conclude that a trade-off between tracking error and effort signal noise exists. The variable observer gain μ_{var} is the proposed approach to reach the required conditions while also reducing the noise sensibility.

The μ_{var}'s initial value is 0.0019 and it adapts towards a value that increases performance between tracking error and noise in control signal. The simulation obtains the same μ_{var} for all joints, and its implementation in simulation environment is as follows:

Listing 4.1: μ_{var}*implementation*

```
function [Hmu, Mu, Mu_calc] = fcn(SNR, q_error, clock)

% Empirical gain for variable gain results
K_num = 1e-5;
K_den = 1e+0;

% Start variable gain after 20e-3 seconds
if (clock > 20e-3)
    Mu = K_num*norm(SNR)/(1+norm(q_error)*K_den);
    Mu_calc = Mu;
    % Saturation
    if Mu > 1.9e-3
        Mu = 1.9e-3;
    elseif Mu < 4e-4
        Mu = 4e-4;
    end

% Starting fixed gain value
else
    Mu = 1.9e-3;
    Mu_calc = 1.9e-3;
end

% H_mu matrix
Hmu = [eye(4)/Mu zeros(4); zeros(4) eye(4)/Mu^2
```

The adapting function has a saturation implemented and adapts depending on the SNR and the joint tracking error e 4.16.

Figure 4.25(a) illustrates the μ_{var} adaption. According to the code 4.3.2, it start as 0.0019 and after 20ms the adaptation begins. Between 20ms and 1 second, μ_{var} is equal to

Tracking Error				
μ	e_1 (m)	e_2 (deg)	e_3 (deg)	e_4 (deg)
0.0004	0.0007	0.0660	0.2156	0.1137
variable	0.0042	0.0706	0.2400	0.1381
0.0019	0.0065	0.0746	0.2521	0.1482

Joint Position Estimation Error				
μ	$\tilde{x}_1$ (m)	$\tilde{x}_2$ (deg)	$\tilde{x}_3$ (deg)	$\tilde{x}_4$ (deg)
0.0004	0.00002	0.0014	0.0014	0.0014
variable	0.0001	0.0009	0.0010	0.0010
0.0019	0.0003	0.0011	0.0014	0.0013

Joint Velocity Estimation Error				
μ	$\tilde{x}_5$ (m/s)	$\tilde{x}_6$ (deg/s)	$\tilde{x}_7$ (deg/s)	$\tilde{x}_8$ (deg/s)
0.0004	0.1006	6.2534	6.4175	6.4550
variable	0.1936	1.1936	1.4276	1.3955
0.0019	0.2681	1.1532	1.4586	1.3798

Table 4.4: Observer/Controller performance with 4% parametric uncertainties over 1 step of walking using variable HGO μ gain, 0.0019, and 0.0004.

0.0004. After that, its value increases until reaching a value close to 0.013. Figure 4.25(b) shows the noise estimation $\mathscr{N}$ increasing for each joint, which makes μ_{var} increase. The noise energy $\mathscr{N}$ measured in the effort signal of each joint is depicted in Figure 4.24. By visual inspection one may notice that the $\mathscr{N}$ in the variable parameter μ shows results better than the fixed 0.0004, but worst than 0.0019, as expected.

The expected result throughout these simulations is to obtain initially a noisy u signal due to the low μ_{var} value and low tracking error. After 100ms, as the value of parameter μ increases, the observer bandwidth reduces, along with tracking error performance. The tracking/observation steady-state errors should be closer to the ones achieved when μ was equal to 0.001 than the other values.

As seen in the previous Section 4.3.1, the estimation error $\tilde{x}$ in steady-state for joints 2, 3 and 4 achieved a better performance when the parameter μ was lower than 0.0019 and bigger than 0.0004. The same result is expected when implementing the variable HGO.

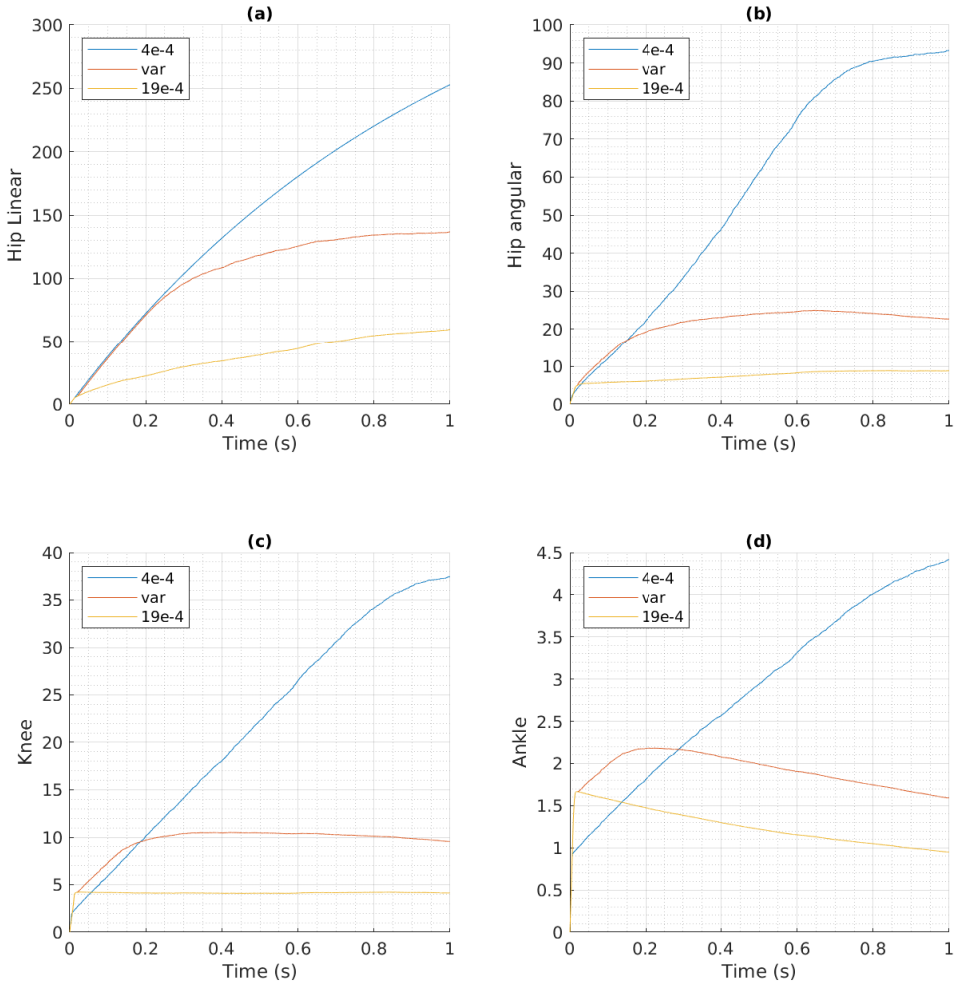

Figure 4.24: $\{\mu_{var}\}$ Noise energy $\mathcal{N}$ results in effort signal for different values of μ : (a) in Hip linear joint (b) Hip angular, (c) Knee, and (d) Ankle.

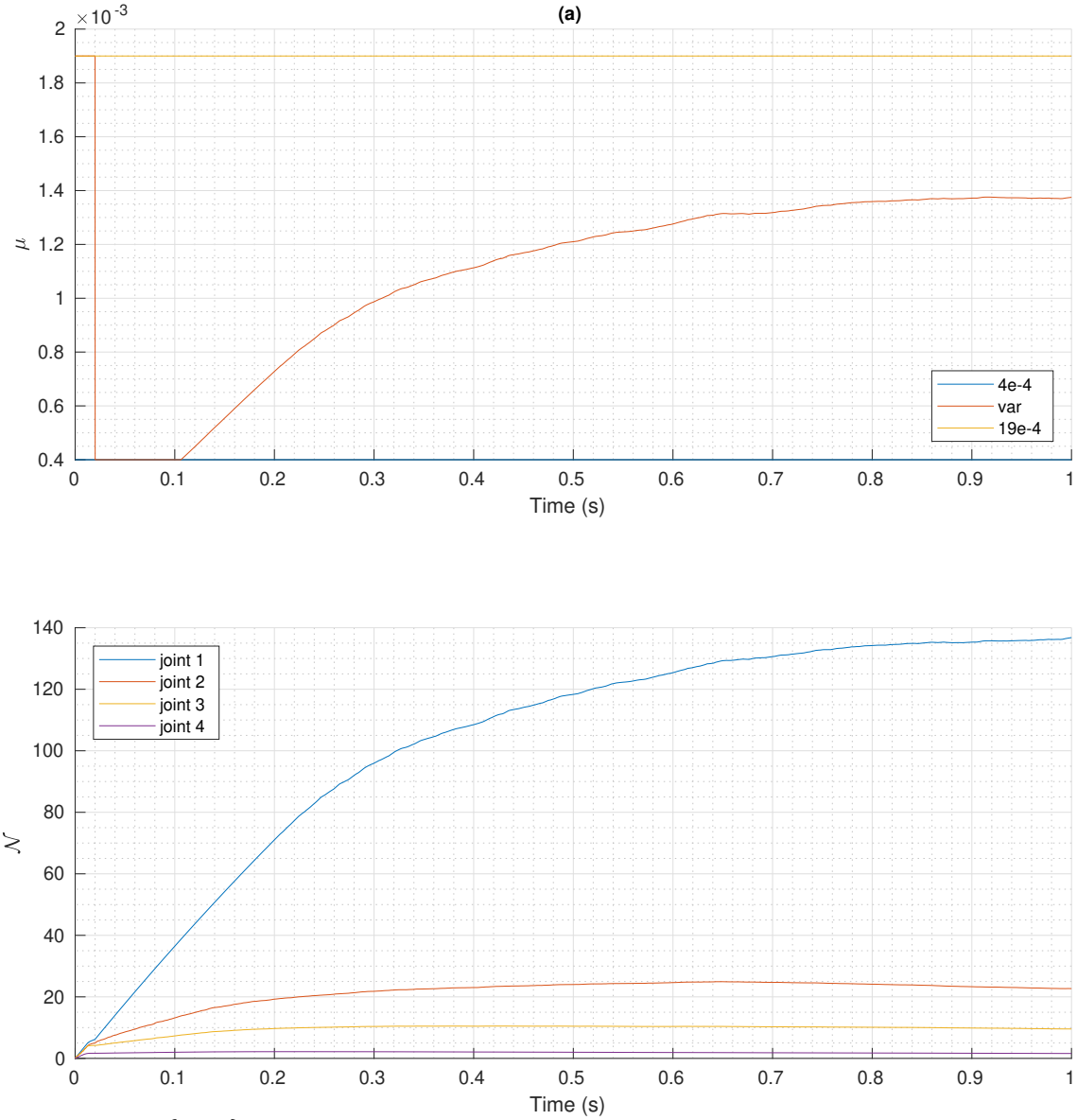

Figure 4.25: $\{\mu_{var}\}$ Simulation results: (a) μ_{var}, (b) noise energy $\mathscr{N}$ in the presence of noise with power 1×10^{-6} W/Hz.

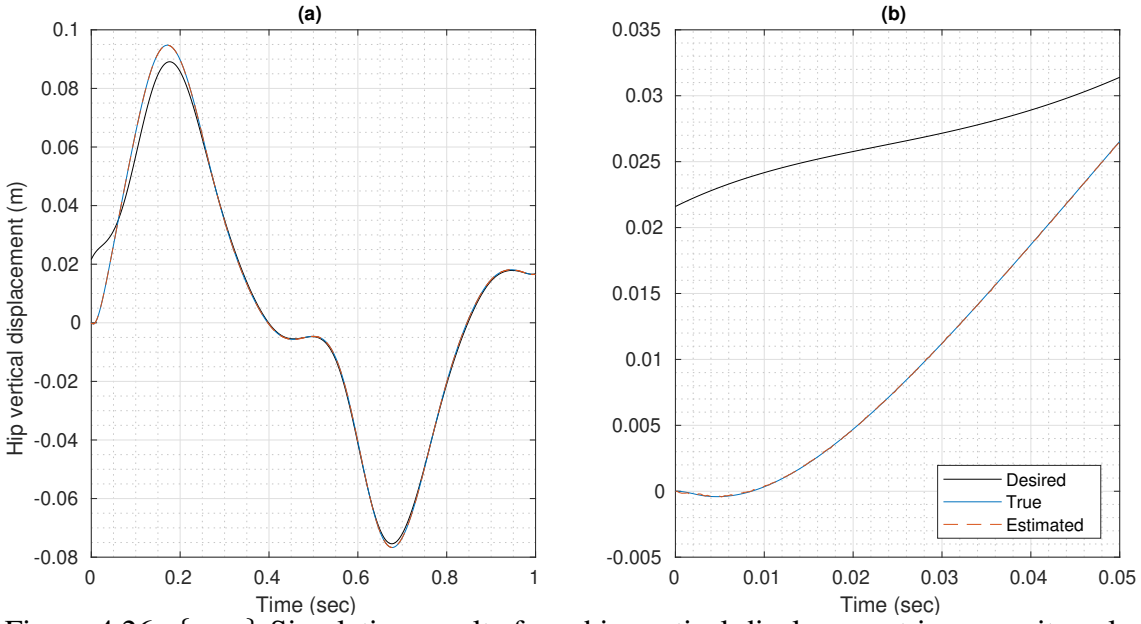

Figure 4.26: $\{\mu_{var}\}$ Simulation results from hip vertical displacement in one gait cycle. (a) performance with μ_{var}, (b) performance before 50ms.

Figure 4.26 depicts the system performance when tracking the desired trajectory. By visual inspection one may see that transient state takes approximately 300 ms. In Figures 4.27(a) and (b), it is possible to see an abrupt change in $\tilde{x}_1$ during 100ms in the form of a straight line going from 0.5 mm to a value closer to 0.1 mm. The same behavior happens on the other joints, however not visible as in the first joint. Figures 4.27(c) and (d) illustrates the variation in noise sensitivity for estimation $\hat{x}_5$, while also showing less estimation error than $\mu = 0.0019$ and 0.0004.

The tracking error is depicted in Figure 4.28, and, as expected, the steady-state tracking error performance of the variable approach is in between the other gains. This result is also present in Table 4.4.

Figure 4.29 depicts the μ_{var} until 100ms showing a noisy profile, similar to the one from $\mu = 0.0004$, and before 200ms it visibly starts reducing the noise sensibility.

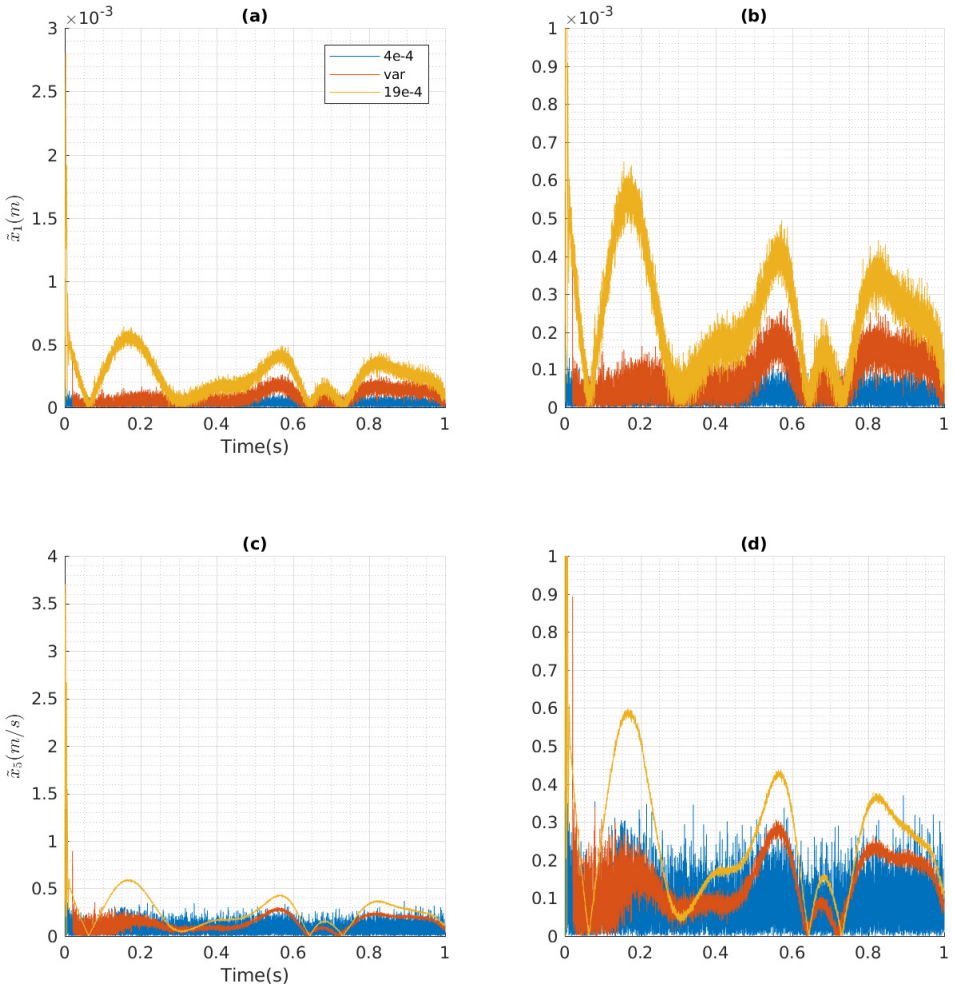

Figure 4.27: $\{\mu_{var}\}$ Simulation results from hip joint estimations. (a) estimation error from $\hat{x}_1$, (b) $\hat{x}_1$ with zoom in X and Y axis. (c) estimation error from $\hat{x}_5$, (d) $\hat{x}_5$ with zoom in X and Y axis. Curves in blue, red, and yellow represent the result obtained using μ gain equals to 0.0004, μ_{var}, and 0.0019, respectively.

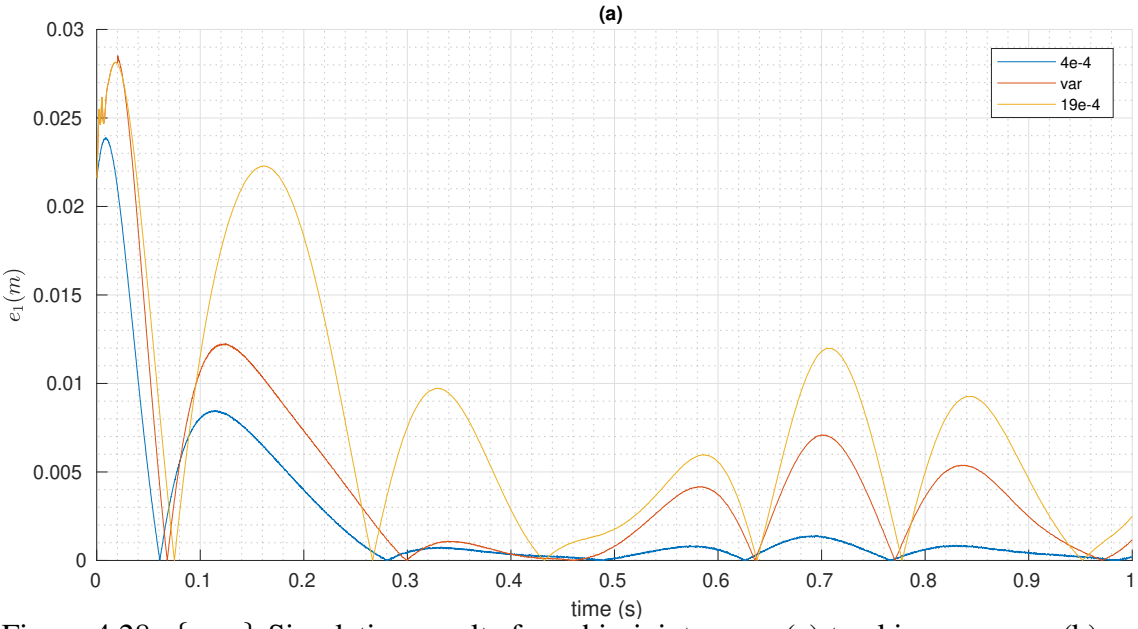

Figure 4.28: $\{\mu_{var}\}$ Simulation results from hip joint error. (a) tracking error e_1, (b) e_1 with zoom in X and Y axis. Curves in blue, red, and yellow represent the result obtained using μ gain equals to 0.0004, μ_{var}, and 0.0019, respectively.

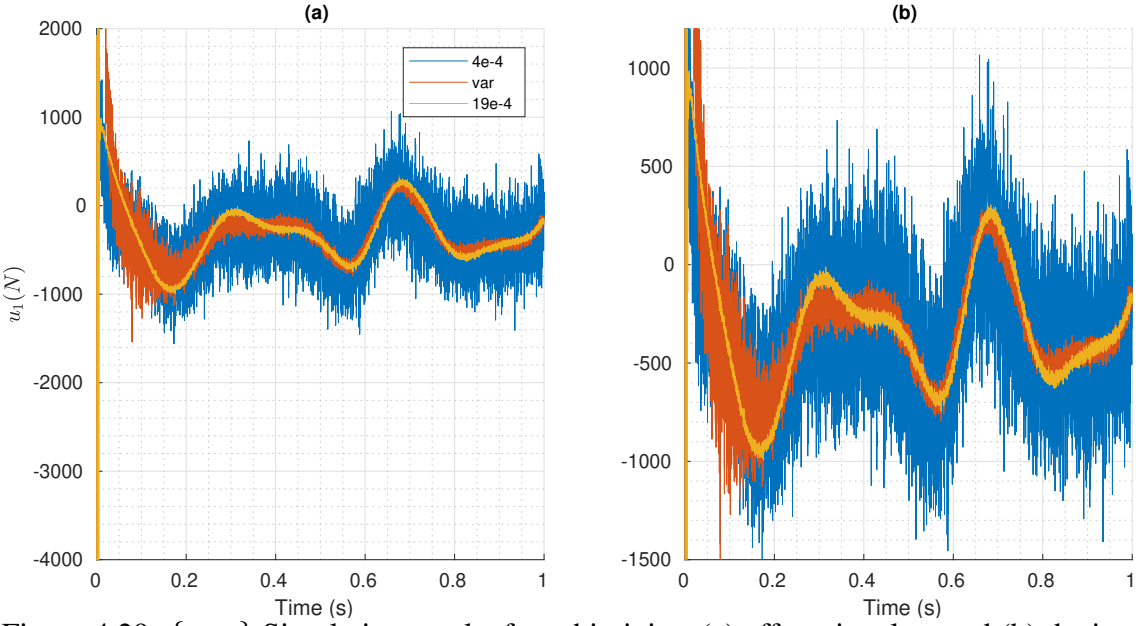

Figure 4.29: $\{\mu_{var}\}$ Simulation results from hip joint. (a) effort signal u_1 and (b) depicts a zoomed version of plot (a). Curves in blue, red, and yellow represent the result obtained using μ gain equals to 0.0004, μ_{var}, and 0.0019, respectively.

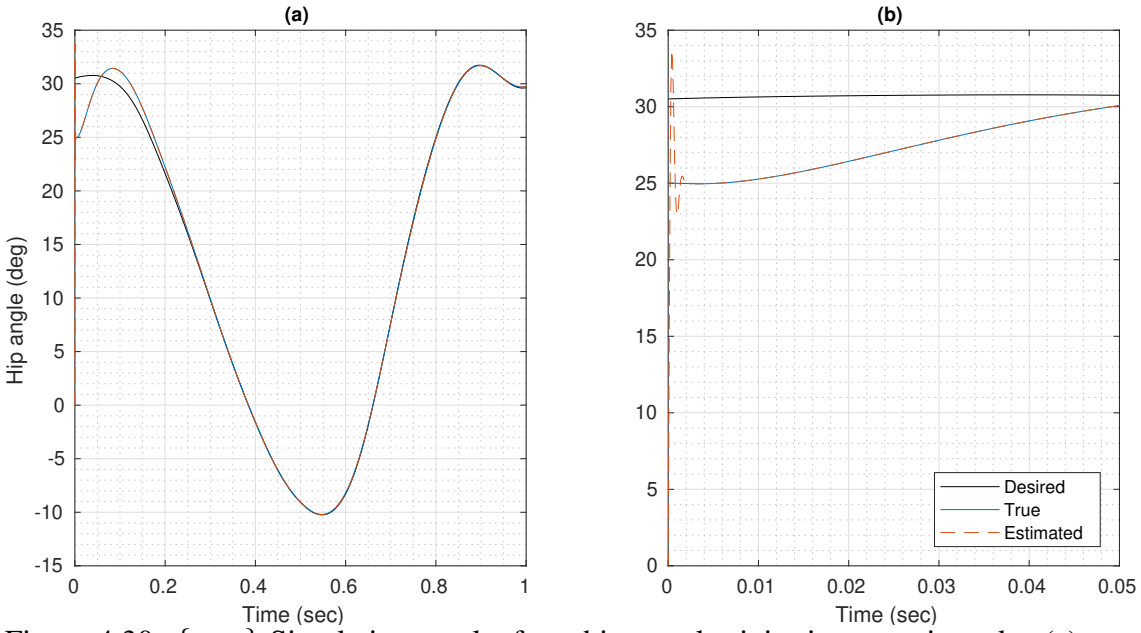

Figure 4.30: $\{\mu_{var}\}$ Simulation results from hip angular joint in one gait cycle. (a) performance with μ_{var}, (b) performance in the first 50ms.

The tracking performance for joint 2 is illustrated in Figure 4.30. With a peaking response equal to the obtained when μ was equal to 0.0019. Figures 4.31(a) and (b), show the estimation error $\tilde{x}_2$ in steady-state before 100 ms with noisy values making it hard to analyze the results. According to Table 4.4, the observer using variable μ performs better than the others, which is the same conclusion obtained with μ equals to 0.001 in Section 4.3.1. The observations regarding $\tilde{x}_6$ are also the same as in Section 4.3.1.

The tracking error is depicted in Figure 4.32, and, as expected, the steady-state tracking error performance of the variable approach is in between accuracy obtained when using the other parameter values. This result is also present in Table 4.4.

Figure 4.33 depicts the μ_{var} until 100ms showing a noisy profile, similar to the one from $\mu = 0.0004$, and before 200ms it visibly starts reducing the noise sensibility. The noise energy $\mathcal{N}$ when using the different parameter values is depicted in Figure 4.24.

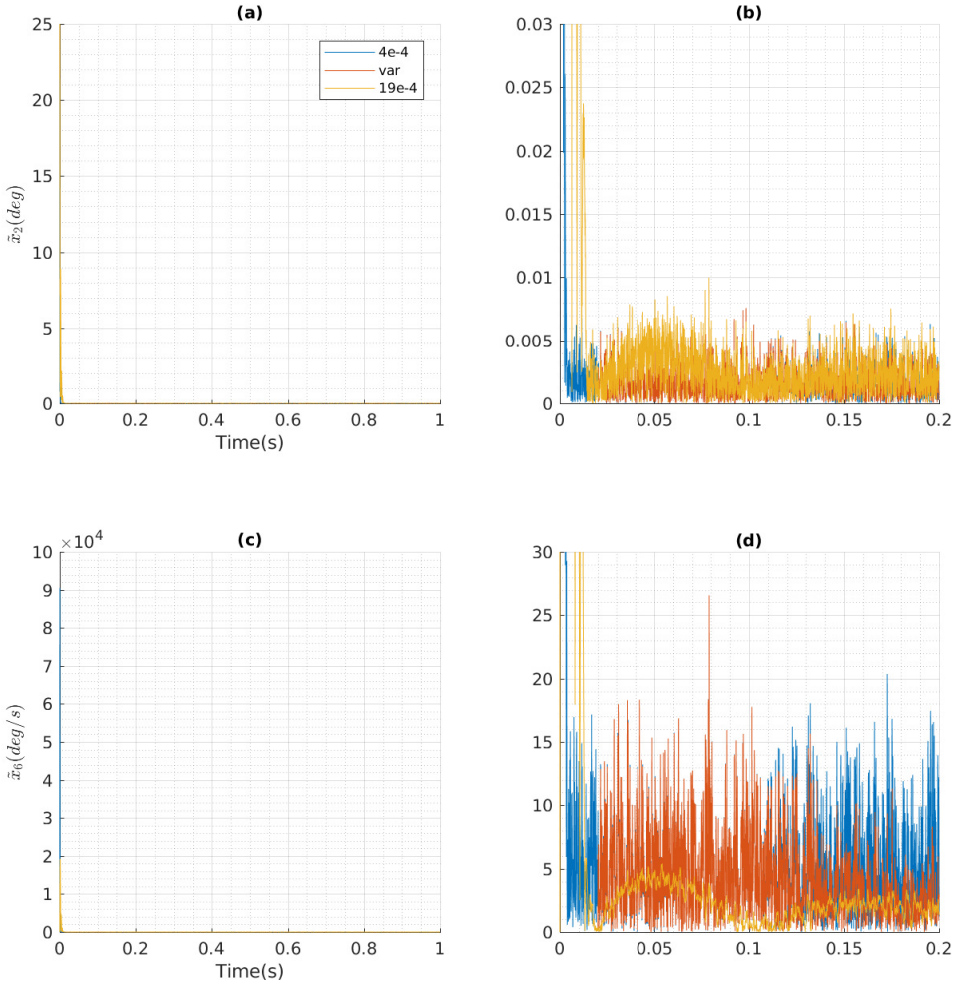

Figure 4.31: $\{\mu_{var}\}$ Simulation results from hip angular joint estimations. (a) estimation error from $\hat{x}_2$, (b) $\hat{x}_2$ with zoom in X and Y axis. (c) estimation error from $\hat{x}_6$, (d) $\hat{x}_6$ with zoom in X and Y axis. Curves in blue, red, and yellow represent the result obtained using μ gain equals to 0.0004, μ_{var}, and 0.0019, respectively.

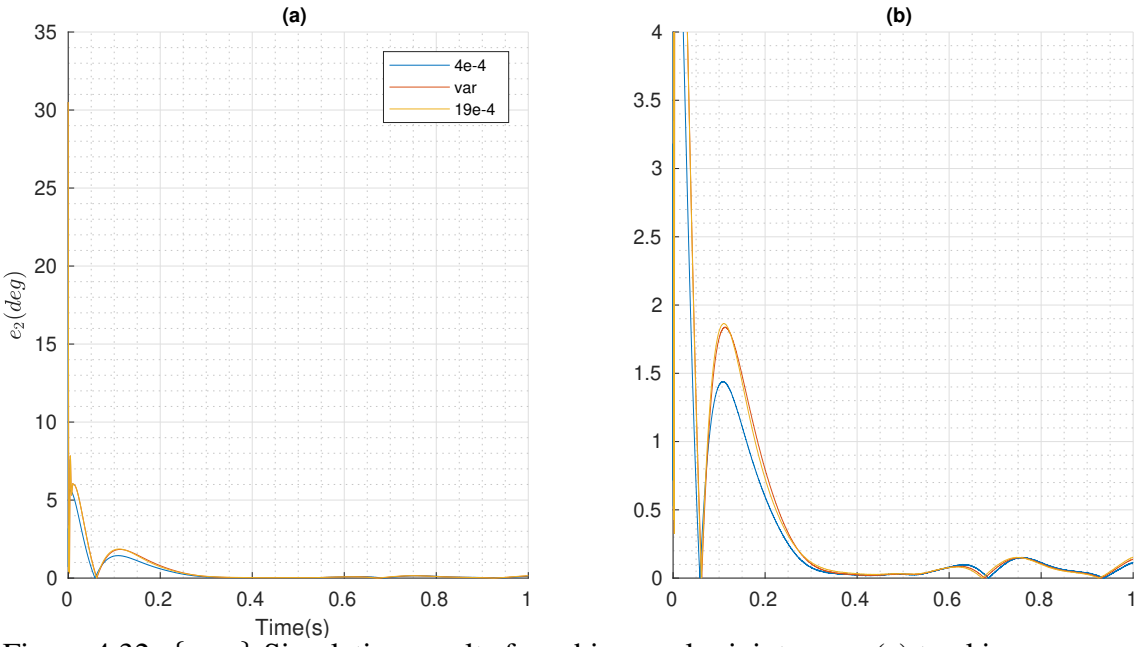

Figure 4.32: $\{\mu_{var}\}$ Simulation results from hip angular joint error. (a) tracking error e_2, (b) e_2 with zoom in X and Y axis. Curves in blue, red, and yellow represent the result obtained using μ gain equals to 0.0004, μ_{var}, and 0.0019, respectively.

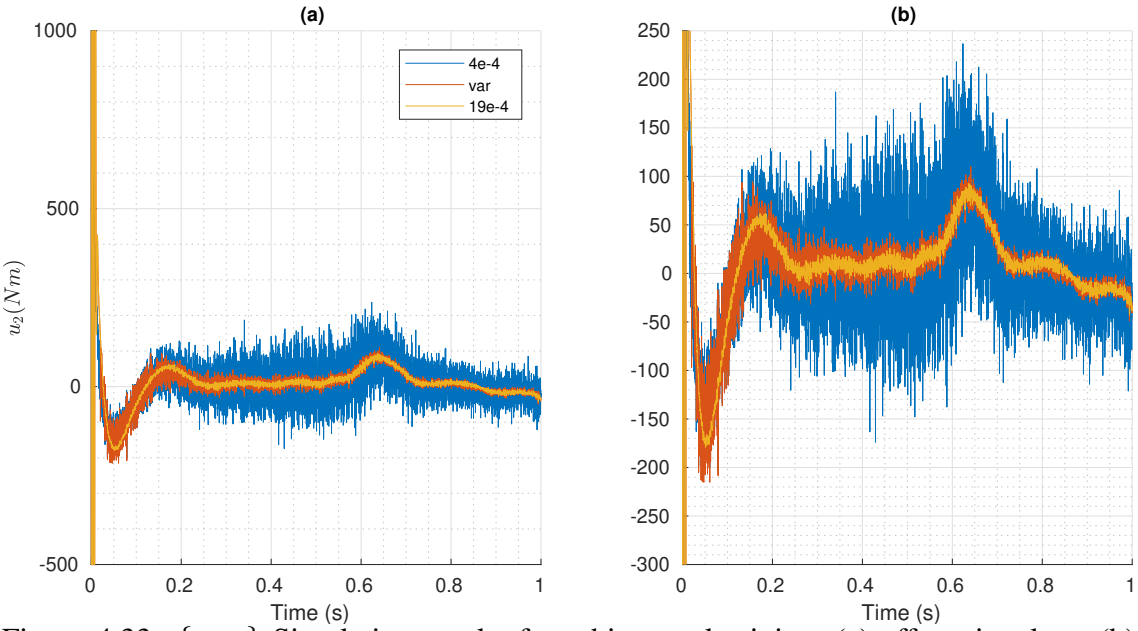

Figure 4.33: $\{\mu_{var}\}$ Simulation results from hip angular joint. (a) effort signal u_2, (b) effort signal with zoom in Y axis. Curves in blue, red, and yellow represent the result obtained using μ gain equals to 0.0004, μ_{var}, and 0.0019, respectively.

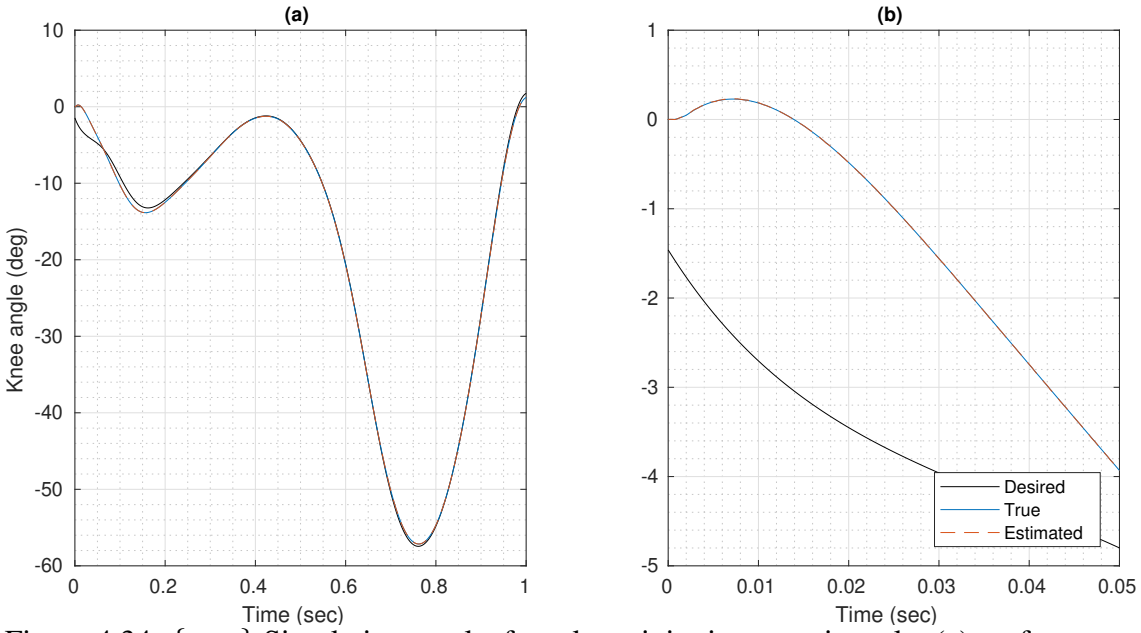

Figure 4.34: $\{\mu_{var}\}$ Simulation results from knee joint in one gait cycle. (a) performance with μ_{var}, (b) performance in the first 50ms.

Figures 4.34 4.37 show results obtained for joint 3. All the considerations for this joint tracking/observation performance is similar to the ones from the previous joint. The Figures present the expected behavior described in the beginning of this Section and RMS tracking and observation errors are depicted in Table 4.4.

It is interesting to notice that despite parameter μ value shifts from 0.0019 to 0.0004, according to Figure 4.25 (a), only the estimations present the same "shifting" behavior, while the tracking error remains with a lower dynamic.

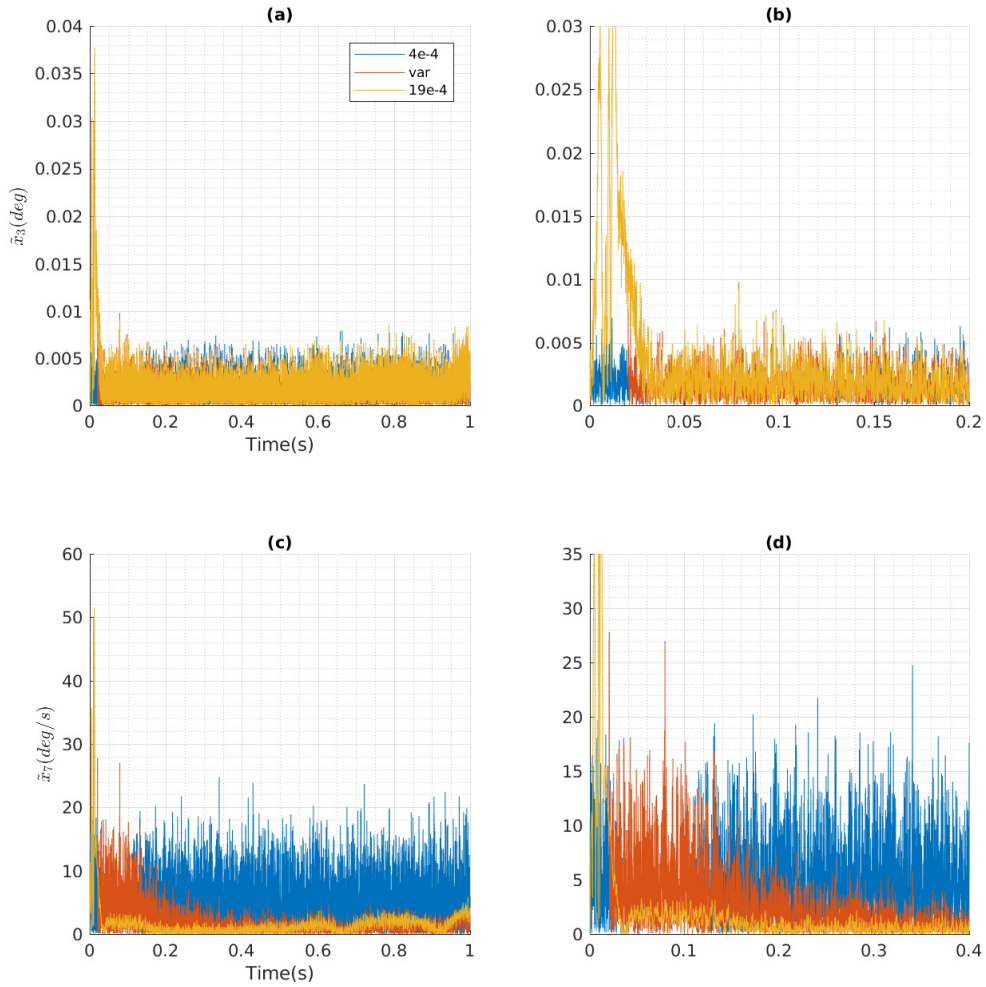

Figure 4.35: $\{\mu_{var}\}$ Simulation results from knee joint estimations. (a) estimation error from $\hat{x}_3$, (b) $\hat{x}_3$ with zoom in X and Y axis. (c) estimation error from $\hat{x}_7$, (d) $\hat{x}_7$ with zoom in X and Y axis. Curves in blue, red, and yellow represent the result obtained using μ gain equals to 0.0004, μ_{var}, and 0.0019, respectively.

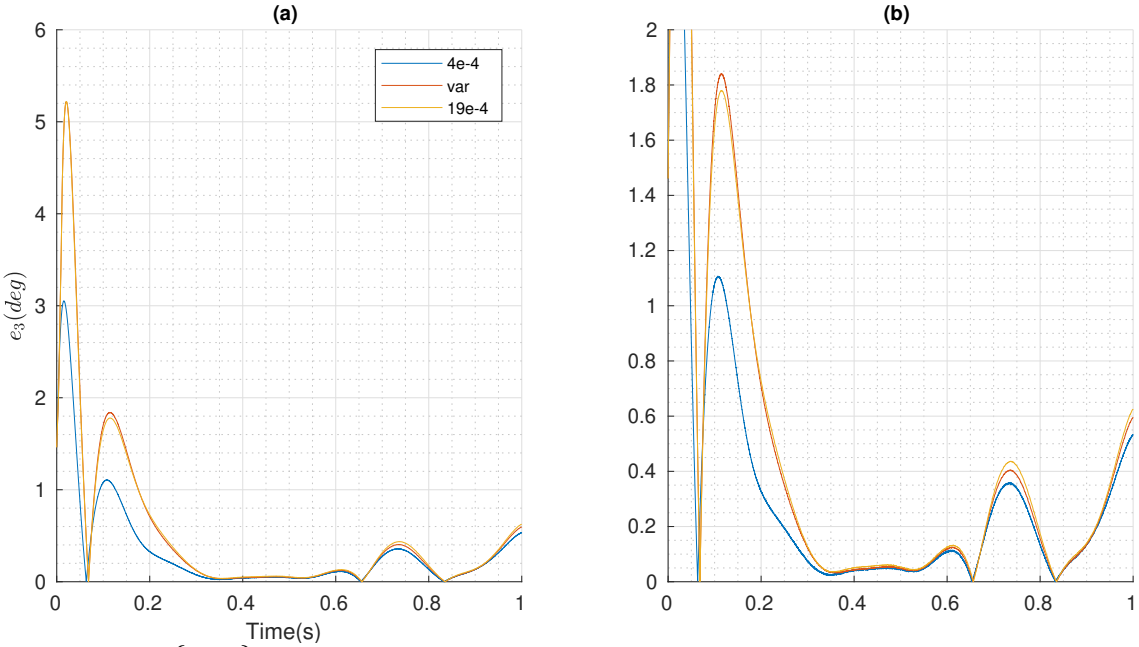

Figure 4.36: $\{\mu_{var}\}$ Simulation results from knee joint error. (a) tracking error e_3, (b) e_3 with zoom in X and Y axis. Curves in blue, red, and yellow represent the result obtained using μ gain equals to 0.0004, μ_{var}, and 0.0019, respectively.

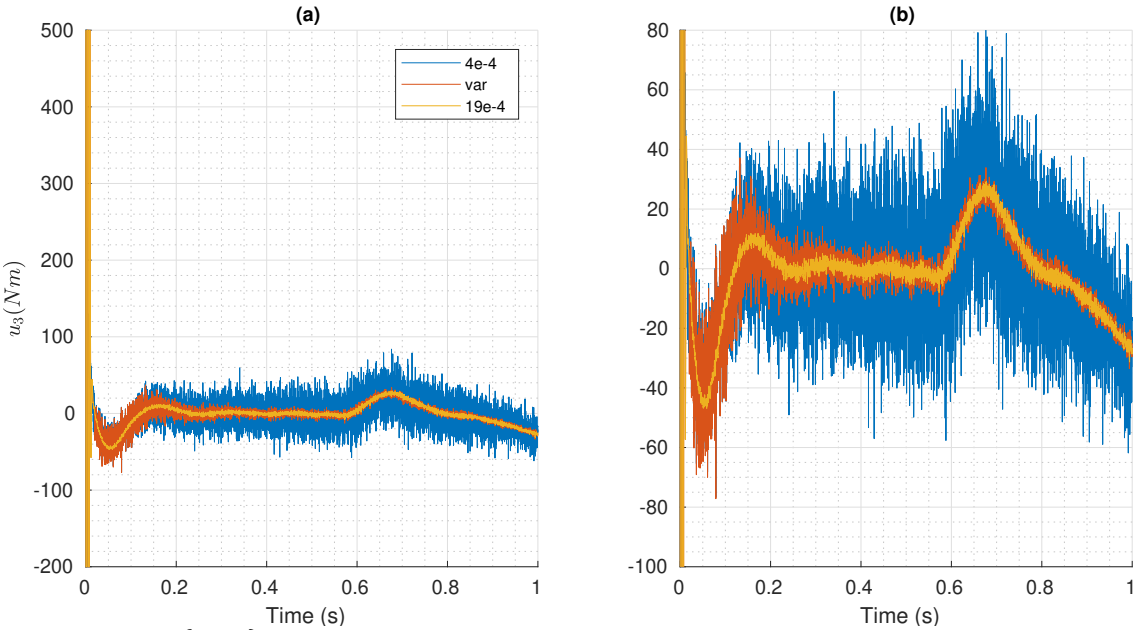

Figure 4.37: $\{\mu_{var}\}$ Simulation results from knee joint. (a) effort signal u_3, (b) effort signal with zoom in Y axis. Curves in blue, red, and yellow represent the result obtained using μ gain equals to 0.0004, μ_{var}, and 0.0019, respectively.

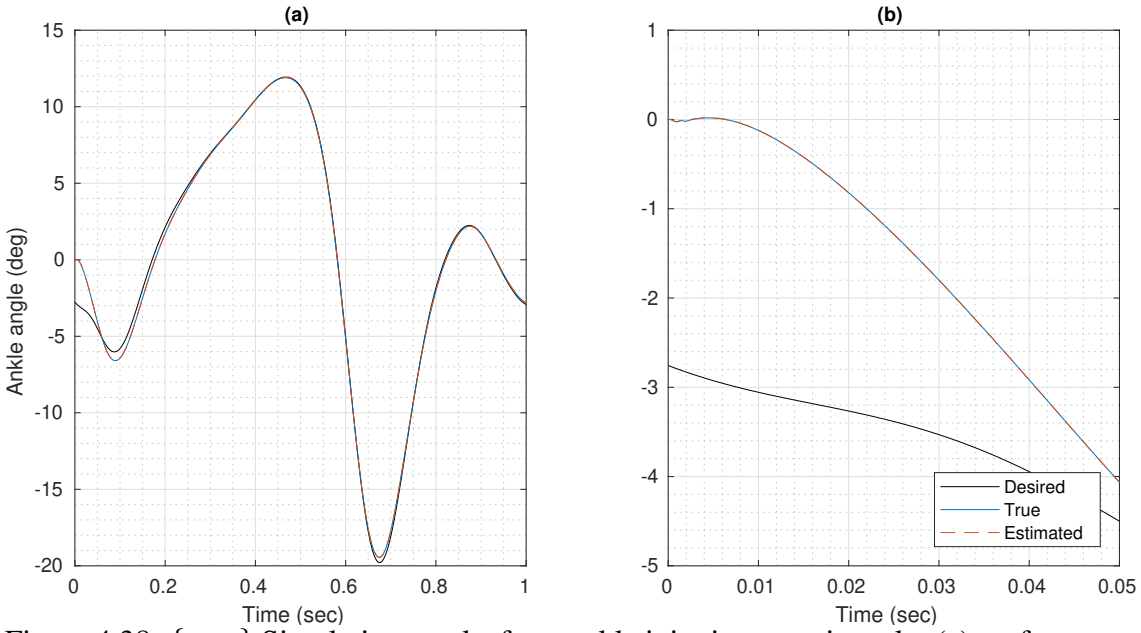

Figure 4.38: $\{\mu_{var}\}$ Simulation results from ankle joint in one gait cycle. (a) performance with μ_{var}, (b) performance in the first 50ms.

Figures 4.38 4.41 show results obtained for the ankle joint. All the considerations for this joint tracking/observation performance is similar to the ones from the previous joint. The Figures present the expected behavior described in the beginning of this Section.

The steady-state tracking error is lower than 0.5 degree, according to Figure 4.40 (a), and with RMS value equal to 1.381 degree.

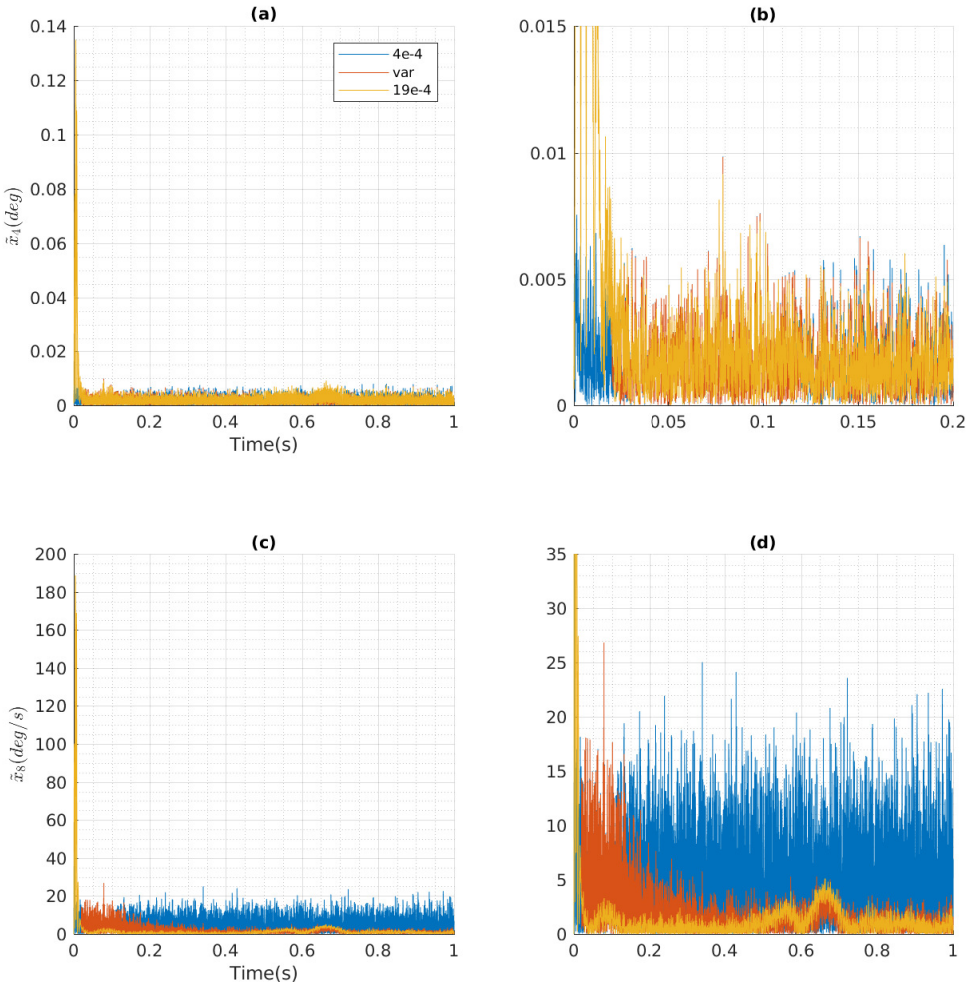

Figure 4.39: $\{\mu_{var}\}$ Simulation results from ankle joint estimations. (a) estimation error from $\hat{x}_4$, (b) $\hat{x}_4$ with zoom in X and Y axis. (c) estimation error from $\hat{x}_8$, (d) $\hat{x}_8$ with zoom in X and Y axis. Curves in blue, red, and yellow represent the result obtained using μ gain equals to 0.0004, μ_{var}, and 0.0019, respectively.

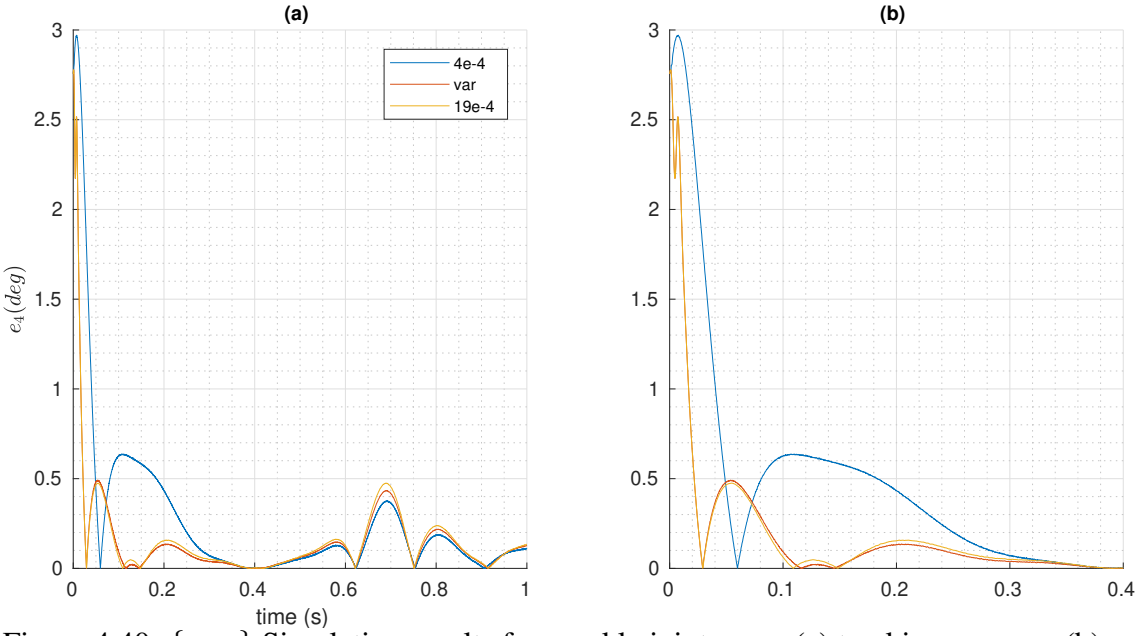

Figure 4.40: $\{\mu_{var}\}$ Simulation results from ankle joint error. (a) tracking error e_4, (b) e_4 with zoom in X and Y axis. Curves in blue, red, and yellow represent the result obtained using μ gain equals to 0.0004, μ_{var}, and 0.0019, respectively.

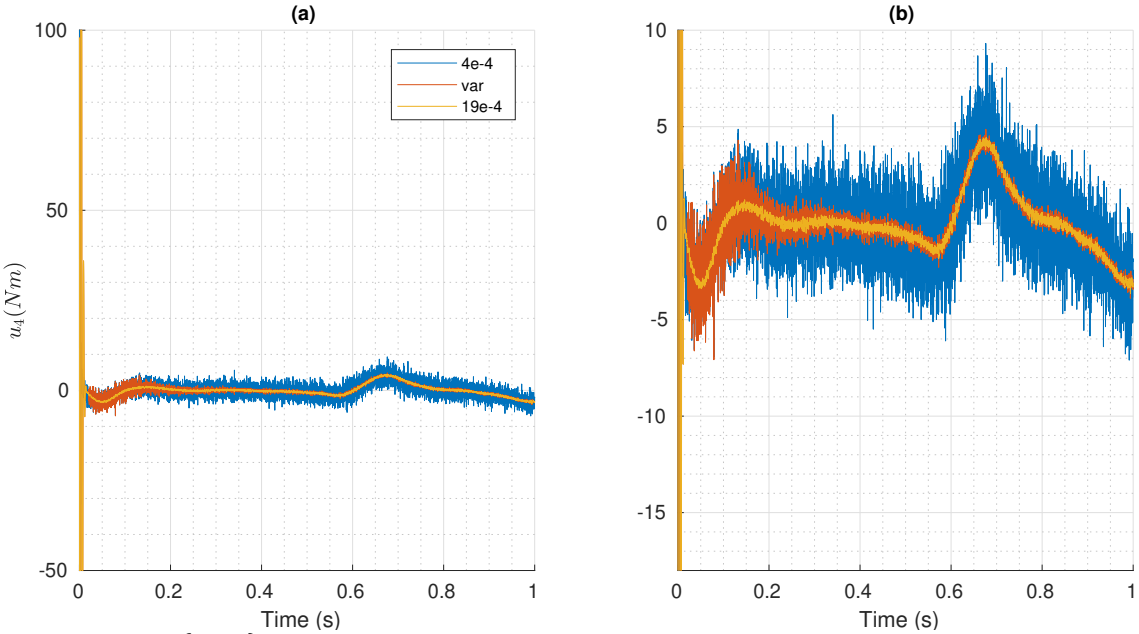

Figure 4.41: $\{\mu_{var}\}$ Simulation results from ankle joint. (a) effort signal u_4, (b) effort signal with zoom in Y axis. Curves in blue, red, and yellow represent the result obtained using μ gain equals to 0.0004, μ_{var}, and 0.0019, respectively.

4.4 Remarks

The results obtained with these simulations show that the variable parameter μ reaches a steady sate value of 0.0014. The hip vertical joint presented results standard results, where more of the measurement noise is attenuated when increasing the value of parameter μ. However, it shows a worst tracking performance.

The revolute hip, knee, and ankle joints show a different behavior, explained in [70]. According to this work, there is a tradeoff between estimation steady-state error due to model uncertainties and the measurement noise. It is left as future work, the proof that the parameter μ was lower than the ultimate bound, imposed by this constraint [70]. With this phenomenon, it is possible to notice in Table 4.4 that estimation of x_1 achieves better results for μ equal to 0.001 or variable is better than using 0.0004 or 0.0019.

The noise also affected the estimation of x_2, where it is possible to see, in Table 4.4, that the most accurate joint velocity estimation was with the highest parameter μ (0.0019).

The control effort required for trajectory tracking achieved feasible values. Additionally, it uses saturation to prevent state finite escape time.

Chapter 5

Conclusions

In this work, a variable HGO has been designed to estimate the states of a prosthesis test robot, reducing the amount of noise in the control effort while keeping an acceptable tracking error performance when compared to the literature.

A simplified plant model was proposed. This system is composed by a prismatic joint emulating vertical hip displacement, and three revolute joints representing hip (flexion/extension), knee (flexion/extension), and ankle (plantarflexion/dorsiflexion) motions. This robot dynamics were validated using Recursive Newton-Euler and Lagrangian approaches. A conditioned reference joint position trajectory has also been validated using the provided gait normative curves.

To simulate the prosthetic closed loop, a full state-feedback controller using computed torque with PID without noise and parametric uncertainties was designed. In sequel, noise and uncertainties were considered in the simulation and a tracking accuracy of 0.4 mm for hip vertical displacement, and $[0.065, 0.2, 0.11]$ degree for hip, knee, and ankle angular motions (RMS) was obtained. Since, the simulations were carried out by considering that no contact exists with the ground (no ground forces), it is expected that a better accuracy is obtained when compared to cases when the ground effect is taken into account, such as in [56] where the accuracy is four times greater (around 1.75mm for the first joint and 2.6 degrees for the others). Note that, despite of the different experiments, the results here are consistent with the literature. Additionally, the control magnitudes achieved for the first three joints were similar to abled-bodied averaged hip force (-800 to 200 N), thigh torque (-50 to 100 Nm) and knee torque (-50 to 50 Nm) obtained in [5][57][58]. The differences in the fourth joint control magnitude occurred mainly due to the absence of ground reaction forces.

The next step was to use state estimates in a velocity free closed-loop system instead of using the measured ones. Two approaches were implemented with a high gain observer: using fixed and variable gain. The former is important to show basic concepts of HGO properties such as peaking phenomenon and output feedback controller recovering performance from state feedback controller (as the observer dynamics become sufficiently

fast), and also for a benchmark with the proposed variable gain.

The estimation results with the fixed approach were conducted with parameter μ values equals to 0.0004, 0.0010, and 0.0019. The joint position and velocity estimates reached steady-state before 40ms and 50ms, respectively. In a worst scenario (under parametric uncertainties and measurement noise) and with nonzero initial condition for the estimation error, the RMS estimation errors in steady states obtained were acceptable: position error around 0.3 mm for the first joint and around 0.0014 degree for the other joints, while velocity errors of 0.27 m/s and 6.25 degree/s were obtained for the first joint and for the others joints, respectively.

For the time varying gain approach, the μ value is bounded between 0.0004 and 0.0019 due to results obtained with fixed parameter μ. The obtained steady-state tracking error is 0.7 mm for the first joint, 0.066 degree/s for the second joint, 0.216 degree/s for the third, and 0.117 degree/s for the fourth. The lower the μ parameter value, the closer the results are from state feedback. Which can be verified as the state feedback results are 0.4 mm, 0.065 degree/s, 0.206 degree/s, and 0.11 degree/s for hip vertical displacement joint, hip joint, knee, and ankle joint, respectively. The best μ parameter value for joint position estimation is 0.001, and 0.0019 for velocity in joints $\dot{q}_2$, $\dot{q}_3$, and $\dot{q}_4$. This result indicates that the state feedback performance recovery depends on the noise in effort signal as noticed in [74]. A lower noise perturbation would probably lead to the expected result of best estimation performance for the lowest parameter μ value.

As in the state feedback case, the results for the output feedback case propose here using an HGO with time varying gain are consistent with the literature. In fact, despite of the differences of the experiments, the estimation and tracking errors achieved are consistent with the main results found in the literature, even when a real prosthesis robot is considered and subject to noise with different energy. Indeed, in [6][9], the estimation root-mean-square errors using Kalman filters are 3 mm, 0.11 degree, 0.172 degree, and 0.287 degree for hip vertical displacement, then hip, knee, and ankle flexion/extension. In [56] the tracking root-mean-square error obtained was 1.75mm and 2.6 degrees in hip vertical displacement and hip flexion/extension. In [75] the knee tracking results were considered acceptable if the root-mean-square error was lower than 1.89 degree, and it obtained values ranging from 0.0458 to 2.59 degrees. Additionally, knee tracking error higher than 1.24 degrees (RMS) was obtained in [7], but real prosthetic system experiment was carried out.

The results obtained with variable gain HGO are promising in the sense that, when trying to tune the observer for a group of different prosthesis, one could switch the observer gain to the fixed value (which is not know *a priori*) obtained after the HGO gain reaches the steady-state. In the simulations, the parameter μ has converged to 0.0013 and has adapted according to the noise energy in the control effort signal and the magnitude of the tracking error. In steady- state, the variable gain approach for joint position estimation

performed better than using a fixed gain with μ equals to 0.0004 or 0.0019. Finally, from a practical point of view, the HGO can be implemented in a simple fashion by using only the plant output, being similar to a "dirty derivative" with a time constant varying with the tracking error and the control effort noise estimation.

5.1 Future Works

This work provides a framework for developing more features for a simulated prosthesis test robot. The simulation encompasses Recursive Newton-Euler for mechanics computation and computed torque controller. The stability analysis is left as future work.

So far, the literature showed that other observer techniques (via sliding mode or Kalman filters) estimate Ground Force Reactions accurately [34]. This estimate helps define gait phases when using finite state machines as a mid-level controller. To the best of the author's knowledge, there is no High-Gain Observer approach for this task, leaving as alternative future work. It would be possible to implement a finite-state-controller using ground force reactions and state estimates obtained from an augmented HGO.

One could also use an impedance-based tracking controller for some joints initially (ankle and knee) and position tracking control for the others. Additionally, a comparison between the proposed approach and a Kalman Filter approach should be realized under same noise levels and parametric uncertainties.

Bibliography

[1] PERRY, J., DAVIDS, J. R., OTHERS. "Gait analysis: normal and pathological function", *Journal of Pediatric Orthopaedics*, v. 12, n. 6, pp. 815, 1992.

[2] VERSLUYS, R., DESOMER, A., LENAERTS, G., et al. "From conventional prosthetic feet to bionic feet: A review study", *Proceedings of the 2nd Biennial IEEE/RAS-EMBS International Conference on Biomedical Robotics and Biomechatronics, BioRob 2008*, pp. 49–54, 2008.

[3] FUKUCHI, R. K., FUKUCHI, C. A., DUARTE, M. "A public dataset of running biomechanics and the effects of running speed on lower extremity kinematics and kinetics", *PeerJ*, v. 5, pp. e3298, 2017.

[4] CAPPOZZO, A., DELLA CROCE, U., LEARDINI, A., et al. "Human movement analysis using stereophotogrammetry: Part 1: theoretical background", *Gait & posture*, v. 21, n. 2, pp. 186–196, 2005.

[5] WINTER, D. A. "Kinematic and kinetic patterns in human gait: variability and compensating effects", *Human movement science*, v. 3, n. 1-2, pp. 51–76, 1984.

[6] FAKOORIAN, S. A., SIMON, D. "Ground Reaction Force Estimation in Prosthetic Legs with an Extended Kalman Filter", *Systems Conference (SysCon), 2016 Annual IEEE*, pp. 1–6, 2016.

[7] AZIMI, V., ABOLFAZL FAKOORIAN, S., TIEN NGUYEN, T., et al. "Robust adaptive impedance control with application to a transfemoral prosthesis and test robot", *Journal of Dynamic Systems, Measurement, and Control*, v. 140, n. 12, 2018.

[8] BONNET, V., RICHARD, V., CAMOMILLA, V., et al. "Joint kinematics estimation using a multi-body kinematics optimisation and an extended Kalman filter, and embedding a soft tissue artefact model", *Journal of biomechanics*, v. 62, pp. 148–155, 2017.

[9] FAKOORIAN, S., AZIMI, V., MOOSAVI, M., et al. "Ground reaction force estimation in prosthetic legs with nonlinear Kalman filtering methods", *Journal of Dynamic Systems, Measurement, and Control*, v. 139, n. 11, 2017.

[10] ZIEGLER-GRAHAM, K., MACKENZIE, E. J., EPHRAIM, P. L., et al. "Estimating the prevalence of limb loss in the United States: 2005 to 2050", *Archives of physical medicine and rehabilitation*, v. 89, n. 3, pp. 422–429, 2008.

[11] ALCAIDE-AGUIRRE, R. E., MORGENROTH, D. C., FERRIS, D. P. "Motor control and learning with lower-limb myoelectric control in amputees", *J. Rehabil. Res. Dev*, v. 50, n. 5, pp. 687–698, 2013.

[12] AWAD, M. I., ABOUHOSSEIN, A., DEHGHANI-SANIJ, A. A., et al. "Towards a Smart Semi-Active Prosthetic Leg: Preliminary Assessment and Testing", *IFAC-PapersOnLine*, v. 49, n. 21, pp. 170–176, 2016. Disponível em: <http://dx.doi.org/10.1016/j.ifacol.2016.10.539>.

[13] TUCKER, M. R., OLIVIER, J., PAGEL, A., et al. "Control strategies for active lower extremity prosthetics and orthotics: A review", *Journal of NeuroEngineering and Rehabilitation*, v. 12, n. 1, 2015.

[14] WATERS, R., PERRY, J., ANTONELLI, D., et al. "Energy cost of walking of amputees: the influence of level of amputation", *J Bone Joint Surg Am*, v. 58, n. 1, pp. 42–46, 1976.

[15] WINTER, D. A. *Biomechanics and motor control of human gait: normal, elderly and pathological*. 1991.

[16] WINDRICH, M., GRIMMER, M., CHRIST, O., et al. "Active lower limb prosthetics: A systematic review of design issues and solutions", *BioMedical Engineering Online*, v. 15, n. 3, pp. 5–19, 2016.

[17] JIMENEZ-FABIAN, R., VERLINDEN, O. "Review of control algorithms for robotic ankle systems in lower-limb orthoses, prostheses, and exoskeletons", *Medical engineering & physics*, v. 34, n. 4, pp. 397–408, 2012.

[18] NAITO, H., AKAZAWA, Y., TAGAYA, K., et al. "An ankle-foot orthosis with a variable-resistance ankle joint using a magnetorheological-fluid rotary damper", *Journal of Biomechanical Science and Engineering*, v. 4, n. 2, pp. 182–191, 2009.

[19] KIKUCHI, T., TANIDA, S., OTSUKI, K., et al. "Development of third-generation intelligently controllable ankle-foot orthosis with compact MR fluid brake".

In: *2010 IEEE International Conference on Robotics and Automation*, pp. 2209–2214. IEEE, 2010.

[20] MARTINEZ-VILLALPANDO, E. C., HERR, H. "Agonist-antagonist active knee prosthesis: a preliminary study in level-ground walking." *Journal of Rehabilitation Research & Development*, v. 46, n. 3, 2009.

[21] SUP F, BOHARA A, G. M. "Design and Control of a Powered Transfemoral Prosthesis", *The International journal of robotics research*, v. 27, n. 2, pp. 263–73, 2008.

[22] BÉDARD, S., ROY, P.-O. "Actuated leg prosthesis for above-knee amputees". jan. 1 2008. US Patent 7,314,490.

[23] MARTIN, J., POLLOCK, A., HETTINGER, J. "Microprocessor lower limb prosthetics: Review of current state of the art", *Journal of Prosthetics and Orthotics*, v. 22, n. 3, pp. 183–193, 2010.

[24] VAROL, H. A., SUP, F., GOLDFARB, M. "Real-time gait mode intent recognition of a powered knee and ankle prosthesis for standing and walking". In: *2008 2nd IEEE RAS & EMBS International Conference on Biomedical Robotics and Biomechatronics*, pp. 66–72. IEEE, 2008.

[25] SUP, F., VAROL, H. A., GOLDFARB, M. "Upslope walking with a powered knee and ankle prosthesis: Initial results with an amputee subject", *IEEE Transactions on Neural Systems and Rehabilitation Engineering*, v. 19, n. 1, pp. 71–78, 2011.

[26] GRIMES, D. L. *An active multi-mode above knee prosthesis controller*. Tese de Doutorado, Massachusetts Institute of Technology, 1979.

[27] GORŠIČ, M., KAMNIK, R., AMBROŽIČ, L., et al. "Online phase detection using wearable sensors for walking with a robotic prosthesis", *Sensors*, v. 14, n. 2, pp. 2776–2794, 2014.

[28] KAWAMOTO, H., KANBE, S., SANKAI, Y. "Power assist method for HAL-3 estimating operator's intention based on motion information". In: *The 12th IEEE International Workshop on Robot and Human Interactive Communication, 2003. Proceedings. ROMAN 2003.*, pp. 67–72. IEEE, 2003.

[29] SUP, F., VAROL, H. A., MITCHELL, J., et al. "Preliminary evaluations of a self-contained anthropomorphic transfemoral prosthesis", *IEEE/ASME Transactions on mechatronics*, v. 14, n. 6, pp. 667–676, 2009.

[30] AGHASADEGHI, N., ZHAO, H., HARGROVE, L. J., et al. "Learning impedance controller parameters for lower-limb prostheses". In: *2013 IEEE/RSJ International Conference on Intelligent Robots and Systems*, pp. 4268–4274. IEEE, 2013.

[31] RICHTER, H., SIMON, D., SMITH, W. A., et al. "Dynamic modeling, parameter estimation and control of a leg prosthesis test robot", *Applied Mathematical Modelling*, v. 39, n. 2, pp. 559–573, 2015.

[32] VALLERY, H., EKKELENKAMP, R., BUSS, M., et al. "Complementary limb motion estimation based on interjoint coordination: experimental evaluation". In: *2007 IEEE 10th International Conference on Rehabilitation Robotics*, pp. 798–803. IEEE, 2007.

[33] ARAGON, F. C., HUEGEL, J. C., VARGAS-MARTINEZ, A., et al. "Comparison between Classic Control Systems Techniques against Adaptive and Nonlinear Control Techniques in a Lower Limb Prostheses", *4th International Conference on Control and Robotics Engineering, ICCRE 2019*, pp. 75–78, 2019.

[34] AZIMI, V., NGUYEN, T. T., SHARIFI, M., et al. "Robust ground reaction force estimation and control of lower-limb prostheses: Theory and simulation", *IEEE Transactions on Systems, Man, and Cybernetics: Systems*, 2018.

[35] ESFANDIARI, F., KHALIL, H. K. "Output feedback stabilization of fully linearizable systems", *Int. J. Contr.*, v. 56, pp. 1007–1037, 1992.

[36] KHALIL, H., SABERI, A. "Adaptive stabilization of a class of nonlinear systems using high-gain feedback", *IEEE Transactions on Automatic Control*, v. 32, n. 11, pp. 1031–1035, 1987.

[37] TORNAMBÈ, A. "Use of asymptotic observers having-high-gains in the state and parameter estimation". In: *Proceedings of the 28th IEEE Conference on Decision and Control,*, pp. 1791–1794. IEEE, 1989.

[38] ESFANDIARI, F., KHALIL, H. K. "Observer-based design of uncertain systems: recovering state feedback robustness under matching conditions". In: *Proc. Allerton Conf*, pp. 97–106, 1987.

[39] GAUTHIER, J.-P., HAMMOURI, H., OTHMAN, S. "A simple observer for nonlinear systems applications to bioreactors", *IEEE Transactions on automatic control*, v. 37, n. 6, pp. 875–880, 1992.

[40] MITA, T. "On zeros and responses of linear regulators and linear observers", *IEEE Transactions on Automatic Control*, v. 22, n. 3, pp. 423–428, 1977.

[41] POLOTSKIY, V. “On maximal errors of an asymptotic state identifier”, *Avtomatika i Telemekhanika*, , n. 8, pp. 26–32, 1978.

[42] ESFANDIARI, F., KHALIL, H. K. “Output feedback stabilization of fully linearizable systems”, *International Journal of control*, v. 56, n. 5, pp. 1007–1037, 1992.

[43] LEE, K. W., KHALIL, H. K. “Adaptive output feedback control of robot manipulators using high-gain observer”, *International Journal of Control*, v. 67, n. 6, pp. 869–886, 1997.

[44] OH, S., KHALIL, H. K. “Nonlinear output-feedback tracking using high-gain observer and variable structure control”, *Automatica*, v. 33, n. 10, pp. 1845–1856, 1997.

[45] PRALY, L. “Asymptotic stabilization via output feedback for lower triangular systems with output dependent incremental rate”. In: *Proc. IEEE Conf. on Decision and Control*, pp. 3808–3813, Orlando, Florida USA, 2001.

[46] KRISHNAMURTHY, P., KHORRAMI, F., JIANG, Z. P. “Global output feedback tracking for nonlinear systems in generalized output-feedback canonical form”, *IEEE Trans. Aut. Contr.*, v. 47, n. 5, pp. 814–819, 2002.

[47] KRISHNAMURTHY, P., KHORRAMI, F., CHANDRA, R. S. “Global High-Gain-Based Observer and Backstepping Controller for Generalized Output-Feedback Canonical Form”, *IEEE Trans. Aut. Contr.*, v. 48, n. 12, pp. 2277–2284, 2003.

[48] LEI, H., LIN, W. “Universal output feedback control of nonlinear systems with unknown growth rate”. In: *Preprints of the 16th IFAC World Congress*, Prague, Czech Republic, July 2005.

[49] AHRENS, J. H., KHALIL, H. K. “Closed-Loop Behavior of a Class of Nonlinear Systems Under EKF-Based Control”, *IEEE Trans. Aut. Contr.*, v. 52, n. 3, pp. 536–540, 2007.

[50] PEIXOTO, A. J., OLIVEIRA, T. R., HSU, L. “Global tracking sliding mode control for a class of nonlinear systems via variable gain observer”, *International Journal of Robust and Nonlinear Control*, pp. 177–196, 2011.

[51] PEIXOTO, A. J., HSU, L., COSTA, R. R., et al. “Global Tracking Sliding Mode Control for Uncertain Nonlinear Systems Based on Variable High Gain Observer”. In: *Proc. IEEE Conf. on Decision and Control*, pp. 2041–2046, New Orleans, LA, USA, 2007.

[52] AHRENS, J. H., KHALIL, H. K. “High-gain observers in the presence of measurement noise: A switched-gain approach”, *Automatica*, v. 45, n. 4, 2009.

[53] PRASOV, A. A., KHALIL, H. K. “A nonlinear high-gain observer for systems with measurement noise in a feedback control framework”, *IEEE Transactions on Automatic Control*, v. 58, n. 3, pp. 569–580, 2012.

[54] KHALIL, H. K. “Analysis of sampled-data high-gain observers in the presence of measurement noise”, *European journal of control*, v. 15, n. 2, pp. 166–176, 2009.

[55] BALL, A. A., KHALIL, H. K. “High-gain-observer tracking performance in the presence of measurement noise”. pp. 4626–4627. IEEE, 2009.

[56] RICHTER, H., SIMON, D. “Robust tracking control of a prosthesis test robot”, *Journal of dynamic systems, measurement, and control*, v. 136, n. 3, 2014.

[57] WINTER, D. A. *Biomechanics and motor control of human movement*. John Wiley & Sons, 2009.

[58] VAN DEN BOGERT, A. J., GEIJTENBEEK, T., EVEN-ZOHAR, O., et al. “A real-time system for biomechanical analysis of human movement and muscle function”, *Medical & biological engineering & computing*, v. 51, n. 10, pp. 1069–1077, 2013.

[59] ANDRIEU, V., PRALY, L., ASTOLFI, A. “Asymptotic tracking of a state trajectory by output-feedback for a class of non linear systems”. In: *CDC*, pp. 5228–5233, New Orleans, LA, USA, 2007.

[60] KALIORA, G., ASTOLFI, A., PRALY, L. “Norm Estimators and Global Output Feedback Stabilization of Nonlinear Systems With ISS Inverse Dynamics”, *IEEE Trans. Aut. Contr.*, v. 51, n. 3, pp. 493–498, 2006.

[61] ANDRIEU, V., PRALY, L., ASTOLFI, A. “High gain observers with updated gain and homogeneous correction terms”, *Automatica*, v. 45, n. 2, pp. 422–428, 2009.

[62] PEIXOTO, ALESSANDRO J, D. R. M. F., RICART, I. “Prosthetic Legs Output Feedback Control via Variable High Gain Observer”, *American Control Conference (ACC)*, pp. 1102–1107, 2019.

[63] IOANNOU, P., SUN, J. *Robust Adaptive Control*. Prentice-Hall, 1996.

[64] KHALIL, H. K. *Nonlinear Systems*. Prentice Hall, 2002.

[65] SONTAG, E. D., WANG, Y. "On characterizations of the input-to-state stability property", *Systems & Contr. Letters*, v. 24, pp. 351–359, 1995.

[66] WARNER, H. E. *Optimal Design and Control of a Lower-Limb Prosthesis With Energy Regeneration*. Tese de Mestrado, Cleveland State University, 2015.

[67] LEE, J., MUKHERJEE, R., KHALIL, H. K. "Output feedback stabilization of inverted pendulum on a cart in the presence of uncertainties", *Automatica*, v. 54, pp. 146–157, 2015.

[68] SICILIANO, B., SCIAVICCO, L., VILLANI, L., et al. *Robotics: modelling, planning and control*. Springer Science & Business Media, 2010.

[69] SCHWARTZ, M. H., ROZUMALSKI, A., TROST, J. P. "The effect of walking speed on the gait of typically developing children", *Journal of Biomechanics*, v. 41, n. 8, pp. 1639 – 1650, 2008. ISSN: 0021-9290. doi: https://doi.org/10.1016/j.jbiomech.2008.03.015. Disponível em: <http://www.sciencedirect.com/science/article/pii/S0021929008001450>.

[70] KHALIL, H. K. "High-Gain Observers in Nonlinear Feedback Control", *2008 International Conference on Control, Automation and Systems*, pp. xlvii – lvii, 2008.

[71] DIB, A., FARZA, M., M'SAAD, M., et al. "High gain observer for sensorless induction motor", *IFAC Proceedings Volumes*, v. 44, n. 1, pp. 674–679, 2011.

[72] NUNES, E. V., HSU, L. "Global tracking for robot manipulators using a simple causal PD controller plus feedforward", *Robotica*, v. 28, n. 1, pp. 23–34, 2010.

[73] LORÍA, A. "Observers are unnecessary for output-feedback control of Lagrangian systems", *IEEE Transactions on Automatic Control*, v. 61, n. 4, pp. 905–920, 2015.

[74] KHALIL, H. K. *High-gain observers in nonlinear feedback control*. SIAM, 2017.

[75] KHADEMI, G., MOHAMMADI, H., RICHTER, H., et al. "Optimal mixed tracking/impedance control with application to transfemoral prostheses with energy regeneration", *IEEE Transactions on Biomedical Engineering*, v. 65, n. 4, pp. 894–910, 2017.